Shaw, Martin Fraser (2012) *Modelling the time-series of cerebrovascular pressure transmission variation in head injured patients.* PhD thesis.

http://theses.gla.ac.uk/3287/

Copyright and moral rights for this thesis are retained by the author

A copy can be downloaded for personal non-commercial research or study, without prior permission or charge

This thesis cannot be reproduced or quoted extensively from without first obtaining permission in writing from the Author

The content must not be changed in any way or sold commercially in any format or medium without the formal permission of the Author

When referring to this work, full bibliographic details including the author, title, awarding institution and date of the thesis must be given

Glasgow Theses Service
http://theses.gla.ac.uk/
theses@gla.ac.uk

# Modelling the Time-series of Cerebrovascular Pressure Transmission Variation in Head Injured Patients.

Martin Fraser Shaw

*M.Sci, University of Glasgow*

Submitted in the fulfilment of the requirements for the

Degree of Doctor of Philosophy

School of Medicine: Clinical Physics

College of Medical, Veterinary and Life Sciences


University of Glasgow

March 2012

*In memory of Dr Michael Daley (1942 - 2010)*

# Abstract

Cerebral autoregulation is the process by which blood flow is maintained over a changing cerebral perfusion pressure. Clinically autoregulation is an important topic because it directly effects overall patient management strategy. However accurately predicting autoregulatory state or even modelling the underlying general physiological processes is a complex task. There are a number of models published within the literature but there has been no active attempt to compare and classify these models. Starting with the hypothesis that a physiologically based model would be a better predictor of autoregulatory state than a purely statistically based one has led us to investigate approaches to model comparison. Using three different models: a new mathematical arrangement of a physiological model by Ursino, the Highest Model Frequency (HMF) model by Daley and the Pressure reactivity index (PRx) statistical model by Czosnyka, a general comparison was carried out using the Matthews correlation coefficient against a known autoregulatory state. This showed that the Ursino model was approximately three times as predictive as both the HMF model and the PRx model. However, in general, all of the models predictive accuracies were relatively poor so a number of optimisation strategies were then assessed. These optimisation strategies ultimately were formed into a generalised modelling framework. This framework draws on the ideas of mathematical topology to underpin and explain any change or optimisation to a model. Within the framework different optimisations can be grouped into four categories, each of which are explored in the text of this thesis:

- Model Comparison. This is the simplest technique to apply where the number of models under examination are reduced based on the predictive accuracy.

- Parameter restriction. A classical form of optimisation by constraining a model parameter to cause a better predictive accuracy. In the case of both the HMF and PRx we showed between a two hundred and six hundred percent increase in predictive accuracy over the initial assessment.

- Parameter alteration. This change allows for related parameters to be substituted into a model. Four different alterations are explored as a surrogate measure for arterial-arteriolar blood volume the most clinically applicable of which is a transcranial impedance technique. This latter technique has the potential to be a non invasive measure correlated with both mean ICP and ICP pulse amplitude.

- Model alteration. Allows for larger changes to the underlying structure of the model. Two examples are presented: firstly a new asymmetric sigmoid curve to overcome computational issues in the Ursino model and secondly a novel use of fractal characterisation which is applied in a wavelet noise reduction technique.

The framework also gives an overview of the autoregulatory research domain as a whole as a result of its abstract nature. This helps to highlight some general issues in the domain including a more standardised way to record autoregulatory status. Finally concluding with research addressing the requirement for easier access to data and the need for the research community to cohesively start to address these issues.

# Contents

# List of Tables

# List of Figures

# Acknowledgement

Firstly I would like to thank and remember Dr Michael Daley (1942-2010) for his advice on this extensive topic and especially for his generous donation of the main dataset. Without which the initial stages of this work would have been a lot more difficult. He will be missed.

Secondly I would like to thank Dr Ian Piper, my supervisor, for his many suggestions, constant support and the subtle reminders of things that needed to be done during this research. I am also thankful to Prof John Kinsella for his guidance through the early years of chaos and confusion.

I would also like to thank those that volunteered to help me collect both the normative impedance data: Paul and Clare and to the vets and clinical support for the experimental impedance studies: Prof Eddie Clutton and all the veterinary anaesthetists and Prof Ian Whittle for his neurosurgical expertise.

Finally, I wish to thank the following: Stephen and Kevin (for the fun and games that is life), Del (for his friendship and suggestions) *and* of course my parents (for believing enough to not pester me about when this work would be finished).

To everyone else thanks for keeping me sane enough to think the mad thoughts.

Glasgow, Scotland Martin Shaw

October 8, 2011

# Definitions / Abbreviations

$C_{IC}$ intracranial compliance.

$Z$ impedance.

**ABP** arterial blood pressure.

**AIC** Akaike information criteria.

**ANOVA** analysis of variance.

**AR** autoregulation.

**ARMAX** autoregressive moving average with exogenous inputs.

**AUC** area under the ROC curve.

**BP** blood pressure.

**CARNet** cerebral autoregulation research network.

**CBF** cerebral blood flow.

**CBFV** CBF velocity.

**CPP** cerebral perfusion pressure.

**CSF** cerebrospinal fluid.

**CVR** cerebrovascular resistance.

**FPI** fluid percussion injury.

**GCS** Glasgow coma scale.

**GOS** Glasgow outcome scale.

**GOSe** extended Glasgow outcome scale.

**HMF** highest modal frequency.

**ICP** intracrainial pressure.

**ICU** intensive care unit.

**IMPACT** international mission for prognosis and clinical trial design in TBI.

**MAD** median absolute deviation.

**MAP** mean arterial pressure.

**MBM** minute by minute.

**MCC** Matthew's correlation coefficient.

**PRx** pressure reactivity index.

**ROC** receiver operating characteristic.

**SONAR** storage of normalised autoregulatory results.

**TBI** traumatic brain injury.

**TBW** total body water.

**TCD** transcranial doppler ultrasonography.

**VM** Valsalva manoeuvre.

**WBI** whole body impedance.

**WMMT** wavelet modulus maxima transform.

# Chapter 1

# Introduction

Intensive care management of critically ill patients is one of the most expensive health care costs to hospitals. Estimates vary but costs of at least £1000 per day per bed are common [28]. One nurse to one patient nursing care is a major part of this cost but so too are the capital equipment and consumable costs of the intensive care physiological monitoring, laboratory and imaging investigations.

Continual developments in medical technology mean that intensive care units (ICUs) are routinely monitoring more physiological parameters and improvements in hospital IT infrastructure allow more of this data to be archived as part of the patient record. However, despite these advances in technology for acquiring data, the complicated nature of such multiple time-series data makes it difficult to interpret and use clinically in the acute management of the patient.

The application of mathematical modelling to detect specific events such as loss of cerebral blood flow autoregulation or to predict clinical outcome and length of intensive care stay have been investigated in a number of specific patient populations. Although some success has been achieved with time-series modelling in specific disease domains, there has not been a systematic study comparing different modelling approaches within a given population of patients nor whether some of the more robust models show efficacy across different intensive care patient populations.

Cerebral autoregulation is the process by which cerebral blood flow is maintained constant over a varying cerebral perfusion pressure, and it is important to the treatment and outcome of traumatic brain injury (TBI) patients. The non-surgical management of patients with TBI focuses upon the prevention of secondary insults such as drops in blood pressure (BP) or increased intracrainial pressure (ICP). The latter (raised ICP) is of particular concern as increases in ICP will decrease cerebral perfusion pressure (CPP = BP - ICP) and can lead to decreases in cerebral blood flow (CBF), ultimately leading to ischemia and cell death. Cerebral autoregulation is a physiological mechanism that maintains CBF constant in the face of changing cerebral perfusion

pressure (CPP) although it can become impaired following brain injury. PET [108], SPET [36] and Xenon-CT [17] can be used to measure CBF and autoregulatory status but these methods do not lend themselves to frequent measurement of autoregulation in patients that are physiologically unstable and where there is a significant clinical risk in transferring them from the intensive care unit. Howells et al, developed a Bayesian Advanced Neural Network (BANN) model and showed that the slope of the mean arterial pressure (MAP) to ICP relationship could be used as a classifier for choosing whether therapy should be targeted at either raised ICP or reduced cerebral perfusion pressure [39]. The work by Howells is suggestive that if autoregulation is normal, therapy should be targeted for CPP. CPP therapy is based on increasing BP by using pressors which, if autoregulation is present, will cause a reflex cerebral vasoconstriction, thus a decrease in cerebral blood volume which will lower ICP and improve CPP. Conversely if autoregulation is impaired, therapy should be targeted more towards raised ICP since targeting CPP by raising BP will just increase ICP further if the cerebral vascular bed is acting in a pressure-passive manner. Currently, there is considerable clinical interest in using an index of autoregulation in the management of raised ICP and reduced CPP and to this end it is an extremely important area of study and has generated a number of mathematical models to predict the state of the autoregulation process. Approaches used include linear [69] and non-linear regression models [69,70], spectral analysis [15,16,50], transfer function analysis [11], cross correlation function analysis [22,23], impulse response analysis [72] and the application of neural networks [39,67].

Over the last fifty years the understanding of the mechanisms underlying the delivery and maintenance of adequate blood flow to the brain has advanced significantly, no more so than in the subject area of understanding the mechanism underlying this process: cerebrovascular pressure autoregulation.

There are, in my view, three main developing areas in the autoregulatory field: those

of physiology and anatomy, mathematical modelling and statistical analysis and lastly physical measurement and detection of events.

The amalgamation of developments in physiological, mathematical and physical event detection is probably a key step to better care for and our understanding of head injury. However, to be able to perform this task elegantly and efficiently each of these subject areas will have to complement each others strengths. One simple approach to this problem would be to develop a mathematical model for the physiological systems and then adapt it to be used as a predictive measure of the physical events under question. This would then balance the known clinical domain knowledge with any advancements in the scientific modelling and event detection fields. Thus with this general approach in mind a review and summary of the literature in this field will be required.

## 1.1 Literature Review Methodology

To reduce the likelihood of omitting key papers in this literature review, a systematic approach to defining a structured search method was applied and tested [85]. This methodology used an automated cyclic search approach which was based on the previous results. A tailored search string was crafted to maximise the initial search which showed an 80 percent increase in the applicability to the search subject as evaluated by four set criteria: Audience, relevance, currency and reliability. The process then will go on to search again looking for other papers by the authors and keywords used in the titles of the original search. This search cycle would then repeat for a specified number of iterations, which was three in this case. Then all of these results were stored and cross referenced in a database.

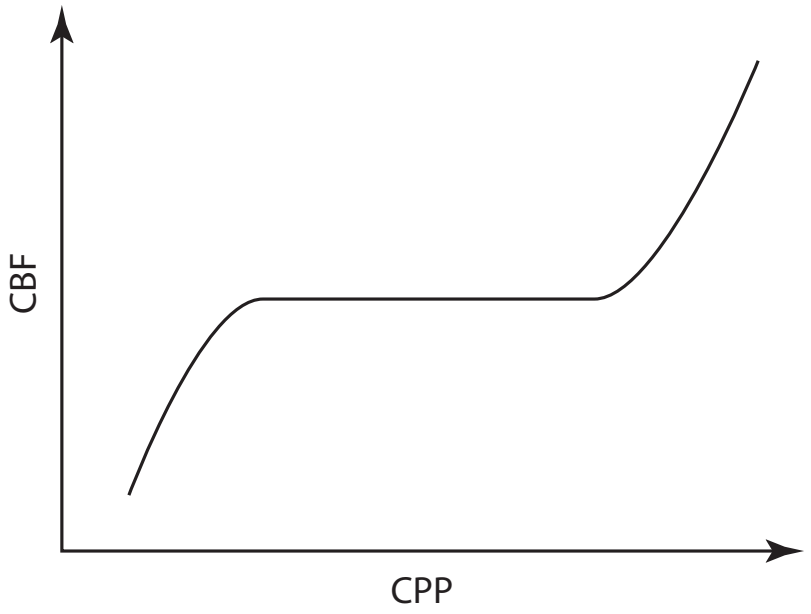


Figure 1.1: Classical autoregulatory curve of CBF vs CPP.

## 1.2 Autoregulation

Autoregulation, no matter where in the body it is found, can be thought of as the mechanism preventing change of blood flow through an organ as the pressure perfusing the arteries in the organ is varied. Autoregulation occurs between certain perfusion pressure limits and if the pressure drops too low or rises too high, autoregulation fails and organ perfusion is compromised. So, at low pressures the perfusion drops and at high pressures excessive flow occurs. More specifically cerebral autoregulation can be thought of as the process by which cerebral blood flow (CBF) is maintained relatively constant over a given cerebral perfusion pressure (CPP) range. Which is illustrated in figure 1.1.

The optimal CPP range quoted throughout the literature is a varying target, that is sometimes a little less sometimes a little more [21, 98], but it is normally quoted as between $60 - 160 mmHg$ [60].

### 1.2.1 Cerebrovascular and cardiovascular systems.

To better understand this concept it is useful to consider the basic anatomy of the circulatory system and that of the cranial space. There are five types of major blood vessels in the body and these are arteries, arterioles, capillaries, venules and veins [60]. The main differences between the types are size and direction, the arterial system takes blood from the heart through the body and the venous system returns blood back to the heart. While the arteries are larger than the arterioles which in turn are larger than the capillaries. A similar step size change happens in the venous system with the capillaries being the smallest and the venules being larger and finally the actual veins being the largest of these types [98].

These two systems generally meet in two places [60], firstly in the capillary beds and secondly in the arteriovenous anastomoses. The capillaries are the smallest of the five blood vessel types and play a vital role in the cardiovascular system. They provide the ability to allow fluid and gaseous diffusion from the blood to the surrounding tissue as well as being a connecting channel between the arterial and venous sides. Capillaries are usually to be found clustered into networks known as capillary beds [98] and can also be coupled with the second type of connection: the anastomosis [60]. The arteriovenous anastomoses are a larger conduit between the arterial and venous sides of the circulation than a capillary and therefore would allow for more blood to flow across the boundary. This anatomical feature can be important for the overall control of flow when coupled with that of a capillary bed.

The basic anatomy of an arterial or venous vessel is similar to one another. Each can be thought of as having three main sections the tunica intima, tunica media and tunica externa [60] with varying connective tissues between each (Figure 1.2).

The arterial structure starts with the lumen which is the space the blood flows through then immediately superficial is the first section which in major arteries is composed

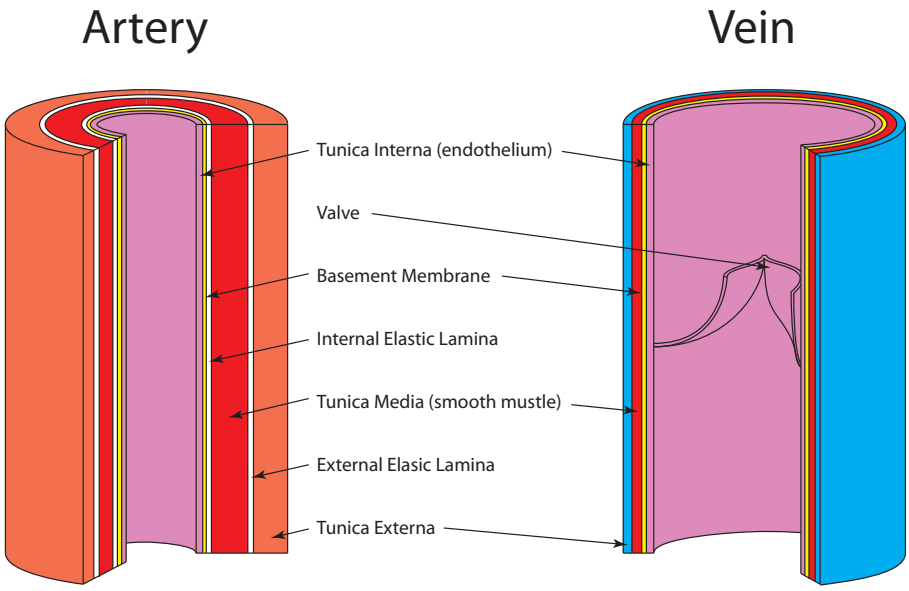


Figure 1.2: Cut away diagram of both an artery and a vein.

of the endothelium layer, the basement membrane and an internal elastic lamina. Endothelial cells in the inner most layer provide a surface which reduces turbulence in the flow of blood through the lumen and thus allowing further flow for the same amount of work [98]. The basement membrane and internal elastic lamina provide strength and resilience for tissue stretching and contracting [60] and the elastic lamina is a fibreous boundary between the tunica intima and the tunica media.

The tunica media is composed of a smooth muscle layer and the external elastic lamina. The smooth muscle is responsible for active change in diameter of the vessel which plays a crucial role in the regulation of blood flow and change in downstream pressure. It is this layer that varies the most over all the five vessel types [98] with the major arteries having the most smooth muscle whilst the capillaries having none and the rest of the vessel types varying in between these two extremes. The external elastic lamina, much like the internal is a fibreous connective boundary layer between the tunica media and the tunica externa.

The tunica externa is the outer most layer of the arterial structure and consists of both

collagen and elastic fibers. These both help to protect the artery and anchor it to the surrounding tissues [98]. Overall the arterial structure provides both strength from the tissue layers and precise control over lumen diameter during either reduction, which is known as vasoconstriction or expansion which is known as vasodilation.

The venous structure has some distinct features over that of the artery. They normally have less smooth muscle than an artery of a similar size and the connective tissues is not as thick which means in general that the vein has less structural strength than an artery. This can be seen easily on inspection where an artery will tend to keep its circular shape, a vein will deform [60]. The endothelial layer of a vein has more contractility than that of the arterial system . This is best observed during vasoconstriction of an arterial vessel where the endothelium will tend to compress into folds which does not happen on a venous endothelium layer. However the most distinctive feature separating the two systems, is the addition of valves in the lumen of some of the large peripheral veins. The valves stop gravity causing the back flow of blood to the capillaries as a result of the pressure in the venous system can be as low as 10% of arterial pressure [60].

Let us now look closer at the anatomical complexities of blood vessel organisation in the cranial space. The brain's blood supply is provided by four main arteries: the left and right carotid arteries and the left and right vertebal arteries. These vertebral arteries then join together into the basilar artery on the surface of the pons and finally traverse up the brainstem and before joining with the carotid arteries [60]. This structure is known the circle of Willis (Figure 1.3).

The joining of carotid and vertebral arteries provides a redundancy to the cerebro-system in that any occlusion which may occur in one branch will be compensated by a reciprocal increase in flow from the other branch [49]. However the circle of Willis is incomplete anatomically in about fifty percent of people [21] so this "built in" redundancy may not be relied upon.

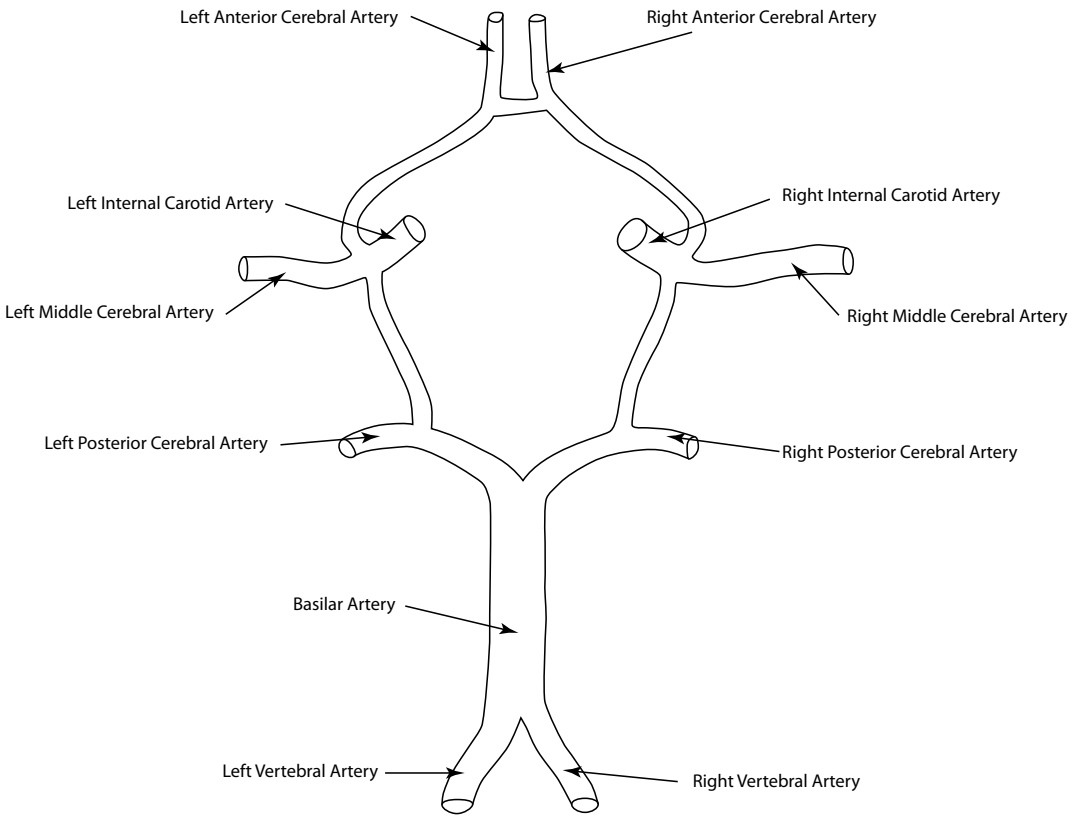


Figure 1.3: A schematic diagram of the circle of Willis. Detailing the major arteries involved

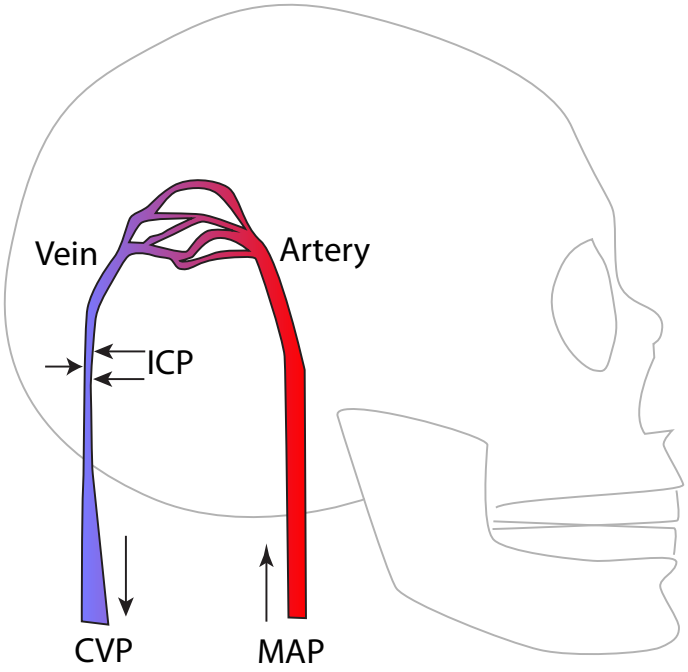


Figure 1.4: A schematic diagram of the skull. Detailing the inflow and outflow of blood and external influences.

The brain is contained with the skull which is a ridged box and this influences some of the flow and pressure dynamics. As the circulatory system is contained in a rigid container the arteriovenous pressure gradient is subject mainly to the greatest of the extra-vascular pressures which is intracranial pressure [21], figure 1.4. This ultimately leads to the conclusion the cerebral perfusion pressure is mainly driven by the arterial blood pressure (ABP) which has been influenced by the intracranial pressure, that is mathematically expressed as $CPP = ABP - ICP$.

### 1.2.2 Mechanisms underlying autoregulation

The current literature suggest there are three processes that can influence the regulation of blood flow. These are: Myogenic effects, Metabolic effects and Neurogenic effects.

### Myogenic

This mechanism proposes that the smooth muscle in the vessels has the ability to contract in response to any stretch that is caused by an increased intravascular pressure [21]. It has been shown that the smooth muscle depolarises when exposed to stretching causing the muscle to contract [49]. The time course for the myogenic response has been recorded at between $10s$ and $2mins$. This reflex generally holds up to direct visual scrutiny under a pial artery window technique [21] and as such has most weight in the literature as the primary mechanism underlying autoregulation.

### Metabolic

There is evidence that the active metabolising cells that surround the arteries can release vasoactive substances that can cause vasodilation. This is to ensure that the tissue has a good supply of oxygen ($O_2$) and any metabolising products like carbon dioxide ($CO_2$), hydrogen ions ($H^+$) and lactate are removed from the tissue [49]. In other vascular systems there is some evidence that hypoxia, depriving a tissue of its supply of $O_2$, and hence lowering its partial pressure for $O_2$, $pO_2$, can cause a vasodilatory response [98]. However in the cerebrovasculature the partial pressure of arterial $O_2$, $paO_2$. has to fall to below $60mmHg$ before there is a measurable response. This adds evidence that cerebral autoregulation occurs in response to a direct change in $O_2$ content and not $paO_2$ changes because of the nature of the haemoglobin oxygen disassociation curve at the partial pressures indicated [21].

A number of metabolites could play a part in metabolic based autoregulation with the main substances being listed in Table 1.1.

The dominant metabolic process is that of carbon dioxide diffusion which causes vasodilation via $H^+$ production in the cerebrospinal fluid by action of carbonic anhydrase [49]

| Metabolic factor | Comment |
|---|---|
| Adenosine | This is a vasodilator and there is evidence that it increases as $paO_2$ falls [21] |
| $CO_2$ | This has an important role in blood flow regulation [49]. It has also been shown that partial arterial pressure of $CO_2$ ($paCO_2$) has a distinct effect on flow [98]. |
| $H^+$ | An increase in $H^+$ shows a decreasing $pH$ and this normally causes vasodilation. However in the cerebrovascular system there is mixed evidence for this effect [21]. |
| Lactic acid | This is linked to the $pH$ of the system however it again has mixed evidence for being involved in the metabolic mechanism [21]. |
| Endothelial Derived Relaxation Factor (EDRF) | This is probably a chemically bonded version of Nitric Oxide ($NO$). Which is a known vasodilator [60]. |

Table 1.1: The main metabolic factors that could play a role in CBF regulation.

via the following reaction:

$$CO_2 + H_2O \xrightarrow{CarbionicAnhydrase} HCO_3^+ + H^+$$

**Neurogenic**

The third underlying mechanism for autoregulation is a neurogenic one. There is neuronal control of the cerebrovascular system from autonomic innervation involving mainly two processes, a baroreceptor or a chemoreceptor reflex.

The baroreceptor measures the amount of stretch in expandable organs in the body [60]. It is a likely candidate sensor however it has been shown that the reflex loop between the baroceptor and the central nervous system can be severed without the loss of autoregulation [21].

A chemoreceptor measures changes in the levels of $O_2$, $CO_2$, $pH$ in the cerebrospinal fluid (CSF) and blood [60]. If the peripheral chemoreceptors are disconnected the cerebrovascular responsiveness is not effected by either hypoxia, hypercapnia or increased $CO_2$ [21]. This is not quite as clear cut as the baroreceptor response because there is

evidence that the chemoreceptors in the medulla oblongata do perform some control over the blood flow to the brain as a secondary function. This means that if an increase in $CO_2$ is detected in the CSF the chemoreflex will cause a vasodilation in the cerebrovasculature resulting in an increase in cerebral blood flow and an increase in oxygen delivery.

These two sensory based control mechanisms do play a large role in regulatory control in other parts of the body. The ability to inhibit both of these processes and still leave autoregulatory responses intact is the main reason that it is less likely to be the main cause for cerebral autoregulation.

While all of these mechanisms have merits I suspect it is likely that it is a combination of all three that will ultimately be at the root of the cerebral autoregulatory phenomenon. There are a number of physiological models for cerebral autoregulation in the literature and the most widely accepted [21, 66] has cerebral autoregulation delivered by appropriate dilation or constriction of the cerebral blood vessels through a combination of mainly the metabolic and myogenic mechanisms [49, 60].

### 1.2.3 Cerebrospinal fluid dynamics and ICP

Any discussion of cerebral autoregulation would be incomplete without looking at the dynamics of cerebrospinal fluid (CSF) and how it interacts with ICP. Below is a brief description of a physiological model of this system and its implications for autoregulation.

As previously mentioned, the brain is housed inside a rigid cranium and is surrounded by cerebrospinal fluid which is considered a Newtonian or non-compressible fluid. The CSF itself is produced from the arterial blood supply via the choroid plexus of the ventricles in the brain which circulates round the cranial space where it is eventually absorbed again across the arachnoid villi and lateral lacunae of the large cerebral

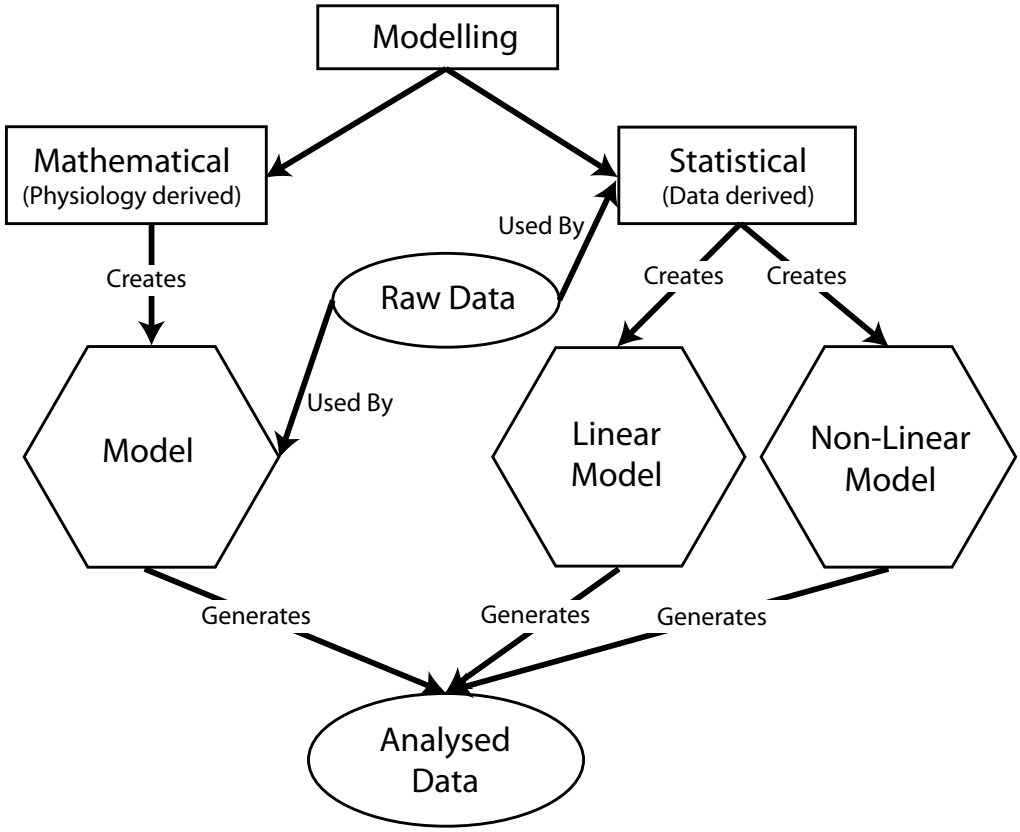


Figure 1.5: Overview of the different types of model and their commonalities

sinuses enroute to the venous circulatory system [60]. It is this balanced production and reabsorption mechanism that is the initial starting point for the Marmarous 1978 [58] paper on the dynamics of CSF. This model took an analytical approach to investigating how changes in the CSF volume affect ICP and produced a mathematical model which described the space in physiological terms. This model is especially important as it has become the basis for other autoregulatory models.

## 1.3 Modelling

There have been a number of modelling approaches used in the literature which can be broadly classified (Figure 1.5) between purely mathematical or statistical and computational.

With a purely mathematical model you would start with a number of assumptions about the system itself and generate a model and only going back to real world data to define the detail of the model. With a statistical or computational model you would start with real world data and generate a model using any one of a number of techniques. In Panerai et al's [66] review of the literature of cerebral autoregulation he classifies each of the modelling approaches purely by type and whether they operate on static or dynamic cerebral autoregulation. This I feel is an over simplification as it misses the genuine advantages of one general class of model over another. A purely mathematical model will always give you insight into the underlying system, whether it is that the model is accurate and the underlying system can generally be assumed to follow your modelled system or that the model is wrong so the underlying system must be different. A statistical model will only give information on the collected data, whether it fits or not, and from that you have to make assumptions on what that means for the underlying system.

There is prevalence in the literature towards statistical or computational modelling purely for the reason most model fitting studies are performed with existing collected data. This does not mean, however, that these studies are subordinate to the mathematical approaches as there are a number of accurate predictive computational models in existence.

Statistical models described in the literature range from the easily calculated but inaccurate at modelling the underlying system, like most of the linear regressions techniques attempted; to the effective but complex modelling approaches using nonlinear equations or Bayesian neural networks.

### 1.3.1 Simple Linear Regression Models

Most studies initially attempted simple linear regression techniques, for example Lam et al [51] proposed a simple measure of dependency of CBF on CPP, or mean ABP in the absence of CPP, in which he proposed a threshold of the correlation coefficient r = 0.5 for the separation between normal and absent autoregulation. This was an oversimplification of the actual system, although easy to evaluate and understand. There are a number of variations on this theme, papers of note using a similar technique would be the Czosnyka M. et al's Pearson Product-Moment correlation papers [23, 24].

A Product-Moment correlation indicates the strength of a relationship between two variables that are assumed to be measured on an interval or ratio scale. It can also be called a moving average correlation if more than two datasets are involved. In his 1996 paper, Czosnyka defined a Mean index or Mx as a correlation between the time averaged mean flow velocity in the middle cerebral artery and CPP. This was shown to have a good link to clinical outcome as measured by the Glasgow outcome scale (GOS). In his 1997 paper a Pressure Reactivity index or PRx is defined using the correlation coefficient between 40 consecutive samples of values for ICP and ABP averaged over a period of 5 seconds. this was found also to correlate well with outcome in traumatic brain injury patients. However in Kirkness et al's [48] paper they found that if they tried to generalise this result to acute brain injury which included both TBI and other cerebrovascular pathology then the result did not follow. On further investigation they were able to show that the effect in the cerebrovascular pathology group was not significant but they were able to reproduce the original finding with the TBI group.

In Panerai et al [66] there is a suggestion that the absolute values of the correlation do not provide a reliable threshold for clinical decision making. A classification criterion based both on the significance (p-value) and slope of the regression has been proposed

in Panerai et al [71] and was shown to provide a more predictive measure. This would tie in with the findings in Kirkness et al's [48] paper which shows that the statistical significance of the relationship between PRx and Outcome in the cerebrovascular pathology group has to be considered when using the PRx model.

Most of the linear regression approaches work on what could be classed as static cerebral autoregulation, that is evaluation of cerebral autoregulation performed under steady-state conditions: a measurement of CBF is obtained first at a constant baseline ABP and constant CBF, followed by another (steady-state) measurement that is taken after the autoregulatory response to a manipulation of ABP has been completed. The Czosnyka [23] paper is one of the few that have tried their approach with dynamic cerebral autoregulation. Dynamic cerebral autoregulation testing uses the rapid drops in ABP caused by the release of, for example, thigh mounted blood pressure cuffs, as an autoregulatory stimulus and compares ABP and CBF velocity (CBFV) during the autoregulatory process. Cerebral blood flow velocity responses are usually measured with a noninvasive transcranial doppler ultrasonography (TCD) method introduced in Aaslid et al [1].

In Tiecks' [97] paper, he compared two linear models: one for static autoregulation and one for dynamic. The static model being compared is the index of static autoregulation (sARi) which is defined to be the percentage change in cerebrovascular resistance (CVR) divided by the percentage change in CPP:

$$sARi = \frac{\%\Delta CVR}{\%\Delta CPP} \tag{1.1}$$

Where mean ABP replaces CPP in cases where ICP is negligible or unavailable [61]. The dynamic model used was the dynamic autoregulatory index (dARi) which is defined [1] to be

$$dARi = \frac{\frac{\%\Delta CVR}{\%\Delta T}}{\%\Delta ABP} \tag{1.2}$$

Both indices were shown to be highly correlated.

### 1.3.2 Complex Non-Linear Modelling

Nonlinear modelling is one way to overcome the limitations of the simplistic nature of the linear model. Nonlinear is a rather catch all term for any higher order differential modelling techniques.

In the comparative review [66] of linear and nonlinear models a number of techniques were used including a second order differential model proposed by Tiecks [96] and a moving-average approach using Volterra-Wiener kernels. Volterra-Wiener kernels stem from a functional analysis technique to classify nonlinear systems [83]. Both modelling approaches were found to significantly improve model accuracy for the same segment of data used to estimate model parameters with the linear equation which is attributed to the second order components in the nonlinear system. The main draw back of this approach found was that you can not accurately extend the second order component onto another section of data and have it accurately predict the nonlinear nature of that section. So from this point of view nonlinear analysis has a lot to offer as a more accurate real time detector as it can accurately model given data but not as a predictor because given a previously derived model the system breaks back down to its linear components when applied to another dataset.

One of the other common non-linear analysis techniques used is “frequency domain analysis”. This is a phrase which represents a number of methods which all have a central theme of representing a waveform by plotting the amplitude of its constituent components against their frequency. In general when frequency domain analysis is discussed the method most used is Fourier or fast Fourier analysis, or the associated method of transfer function analysis. Fourier analysis being a branch of mathematics concerned with the decomposition of time series data in to its component wave

parts using fourier transforms. In Birch [10] Fourier analysis is used to extract the phase difference between the fundamental components of cerebral flow velocity and ABP. This phase difference was used to show a significant reduction in phase lead of velocity over ABP with hypercapnia and a highly significant increase in phase lead with hypocapnia. It was proposed that these changes could be used as an indicator of cerebral autoregulatory state.

In Reinhard [78] the detection of autoregulatory state with phase shift was shown to be possible in patients with carotid artery stenosis. The paper itself was mainly concerned with using the detection of autoregulation as a better method of assessing hemodynamic impairment than the more standard CO2 reactivity method but it was also shown that the phase shift method during Valsalva manoeuvre (VM) correlated well with the autoregulatory slope index (ASI) introduced in Tiecks [96].

The other main frequency domain analysis method, transfer function analysis, is generally used to investigate the relationship between the input and output of a linear time-invariant system. The technique has been used effectively to model cerebral autoregulation within a constrained frequency range [109] and that the transfer function phase and gain can be used as a characterisation method for dynamic cerebral autoregulation [79].

However there is a draw back to using these frequency domain analysis techniques which are based on Fourier transform. There is an assumption that the signals are stationary, that is the mean and standard deviation of the periodic signals do not vary under time shift. This however is often not the case as many physiological signals are non-stationary but reflect transient changes in the physiological state [68]. This assumption about the non-stationary nature of the signals may have an effect on the results obtained from an analysis although the potential error has not been thoroughly assessed [14].

There is now a trend in the literature to use computers to implement models which are becoming too complex to model by hand. This is especially so of artificial neural network modelling.

Artificial neural networks (ANN) are essentially a computer program that has a number of nodes or artificial neurons which are connected together to process an input function. The nodes can be dynamically altered by the provision of data thus training the network to accurately process any input data. With enough training accurate models which have been constrained by the boundaries of the provided data can be produced.

This technique has been used to successfully model the dynamic relationship between ABP and CBFV. It was shown that there was a significant improvement in this modelling approach over transfer function analysis but not of the normal time series techniques used [67].

### 1.3.3 Mathematical Modelling.

The difference in classification of techniques between mathematical or statistical may be subtle as all the previously mentioned models have rather complex mathematics at their core, however the insight they provide on any situation is based purely on the data used to develop them. A purely mathematical model should be derived without the need for interaction with the main data, beyond the environmental constraints of the system. That is any intrinsic properties of the model itself which come from domain knowledge used to construct it.

In the literature the best example of a purely mathematical model would be compartmental models. A compartmental model is best described as a flow model where one or more entities are being transferred between compartments according to a set of flow rules. As an example to illustrate this figure 1.6 shows a one compartment model with a total of substance $z$ in the system at time 0 of $z(0)$ and the amount of $z$ in the

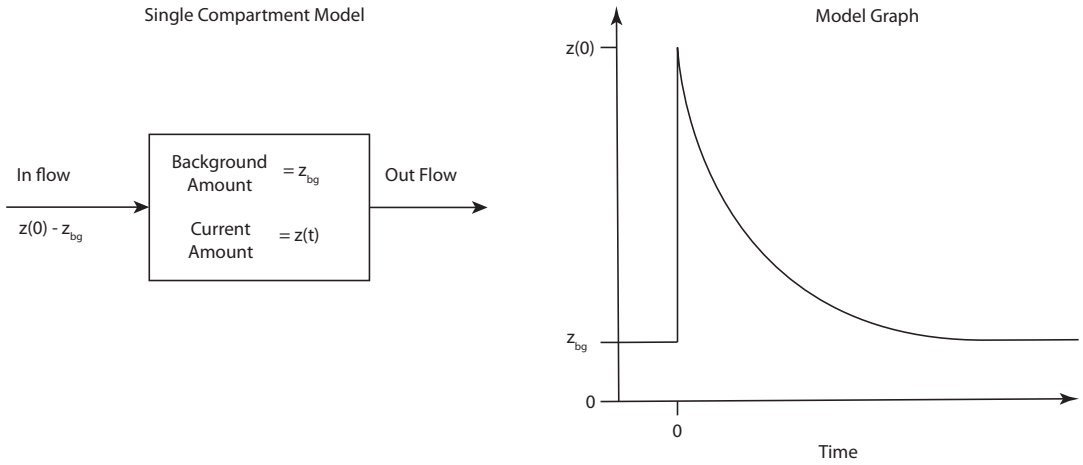


Figure 1.6: A basic one compartment model and a graph of its mathematical model of amount of $z$ in the compartment vs time.

compartment, which has a background value of $z$ equal to $z_{bg}$, at time $t$ can simply be modelled by an exponential decay curve (Equation 1.3).

$$z(t) = z_{bg} + (z(0) - z_{bg}) \exp(-kt) \tag{1.3}$$

The number of compartments and the complexity of the rules can be thought of as defining characteristics of the model. These types of model are used prevalently in pharmacokinetics to model drug behaviour [3, 94, 95].

One of the first uses of this approach was to model a near complete system of craniospinal dynamics [100, 101]. This was however too complicated to be used clinically [102]. This model or the general technique was used as the basis for a number of other papers which tried to focus more on cerebral hemodynamics.

There have been trends in the literature over the optimal number of compartments for such a model to use. For example three compartments were used in Czosnyka's [22] model of the cerebrovasculature. Then four compartments were used in the models described by Ursino [100], Kadas [47] and Gao [32] subsequently increased to eight by

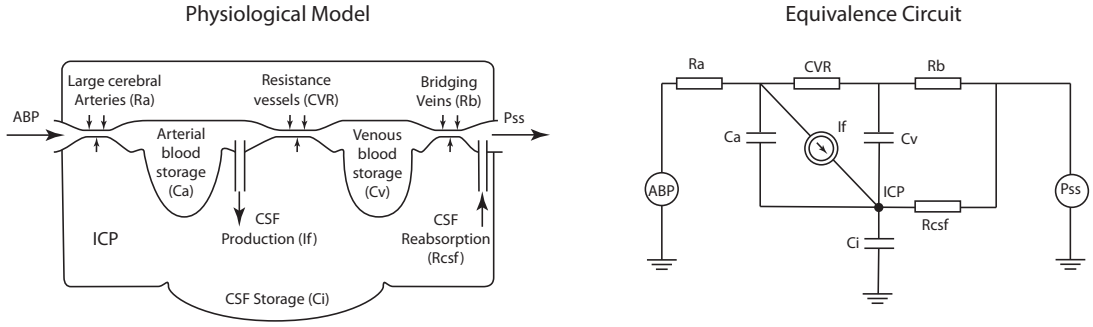


Figure 1.7: A three compartment model of cerebrohaemodynamics and its electronic equivalence circuit.

Ursino [103] and Banaji [7]. An illustration of these types of model can bee seen in figure 1.7. This is the Czosnyka three compartmental physiological model on the left as well as a circuit diagram which is an electronic equivalent model on the right. This electronic model is normally easier to understand and convert into a set of mathematical equations which describes both of these models. As such many of the models above are represented by them in their respective papers.

The main paper in this group is Ursino's 1997 [102] paper. The model itself is a cut down version of his earlier work in craniospinal dynamics [100,101], making that model much easier to understand and use. The model itself is a two compartment model which includes simulation of the hemodynamics of the arterial-arteriolar cerebrovascular bed, CSF production and reabsorption processes, the nonlinear pressure-volume relationship of the craniospinal compartment and a standard Starling resistor mechanism for the cerebral veins. Using this model Ursino shows a number of positive outcomes including an accurate representation of the CBF against CPP autoregulatory curve, in both states of intact and failed autoregulation. There is also, uniquely, evidence of b-waves being present in the model if you create the correct environment with the models defining constants. B-waves are periodic waves with a frequency of between 0.5 and 4 oscillations per minute which are manifested clinically in patients exhibiting a low

compliance state. These b-waves, from the modelling view point, show instability of the mathematical system and demonstrate from a physiological point of view that there exists a set of environmental minima which if met will cause b-waves.

The Kadas et al [47] model is similar to the Ursino 1997 model with one general difference, that being the flow resistance at the capillary-artery compartmental boundary is a function of the pressure and not a constant. This modification showed that a constant flow between the artery and capillary compartment could be maintained by a flow resistance which is directly proportional to the pressure difference between the two compartments. Oscillatory flow is re-established in the model at the capillary-cerebrospinal fluid and capillary-venous interfaces. There has been no direct comparison of both the Ursino and Kadas models to see which one better represents real patient data.

The last of the four compartmental models [32] takes a slightly different approach to defining the compartments. Each compartment is used, like the models before, to control CBF. However each compartment is made up of an increasing number of parallel vessels instead of the normal classical physiological model of the previous papers. The model itself accurately predicts the cerebral autoregulatory CBF/CPP pressure curve along with upper and lower limits as well as slopes. The model itself however is limited to only discussing autoregulation as, unlike the previous models, it isn't initially based on physiology.

Most of these models have only looked at the physical effects and the general flow between the compartments. They have largely ignored the biochemical interactions in the system. Banaji et al [7] goes some way to addressing this omission. The main compartmental model is based on the later Ursino et al paper [103] and it has been extended to include a vascular system including a chemical transport and interaction model. The model has been shown under a set of preliminary simulations to accurately model the CBF - CPP curve which implies that the new biochemical model hasn't had an adverse effect on the original physiological model of Ursino's. However, despite the

increased complexity introduced, it is still possible to generate predictions of a number of physiological quantities associated with the original data from a patient.

In general all the models, either mathematical or statistical, in the literature give an adequate way of assessing the state of cerebral autoregulation in a patient. Out of the two types, the mathematical models provide more information about the underlying mechanism under investigation.

## 1.4 Hypothesis

My working hypothesis is that by adapting a purely mathematical model into a predictive index for cerebral autoregulation will give greater insight into the underlying physiology and be a more accurate predictor compared with statistical models.

### 1.4.1 General Approach to Testing the Hypothesis

1. Initially assessing the mathematical model of Ursino et al in his 1997 paper, assess if the autoregulatory index generated from the Ursino mathematical model is either predictive or not against gold standard data with known autoregulatory state.

2. Develop an approach for ensuring a fair comparison of the derived index against widely accepted statistical models

3. Identify weaknesses in both the Ursino mathematical model and the test data-set and investigate approaches to addressing the limitations.

4. Consider the design of a prospective multi-centre study using the model found to be most accurate at predicting the current experimental and clinical data.

### 1.4.2 Experimental approach

Using a previously developed compartmental model of Ursino et al [102] a predictive variation on this has been developed. This variation shall first be validated using the high resolution animal data set with known autoregulatory state donated by the late Michael Daley [26]. The Daley data is a 6 piglet multi-channel recording with a gold standard measure of cerebral pressure autoregulation function using a cranial window technique which allows monitoring the diameter of surface blood vessels, before, during and after physiological challenges. This validation will be carried out by running the model on the data and checking to see the amount of correlation between the actual measured autoregulatory state and the predicted one.

Once validated the Ursino mathematical model will be compared to the other more accepted statistical modelling methods of autoregulatory prediction. Each of these models will be compared, not only against the new model but against each other. The Daley data would be used again for all model comparisons. From the model predictions, a measure of correlation will be calculated between the test model and the new Ursino variant model, also between the test model and the Daley dataset autoregulatory state information. This approach should place the new model in context with the other existing models.

The main intention of mathematical or statistical modelling is to improve clinical understanding of the underlying patho-physiology and aid clinical management decisions. With this in mind any given model will have to be accurate with not only the high resolution experimental data but also with glsMBM vital signs data which is the resolution most typically captured and available in the clinical setting. To assess this, there are a number of good quality minute by minute (MBM) datasets available for testing the new models upon [13].

## 1.5 Research Plan

During my research, it was not always clear where the next step would take me. To those who read this thesis they too may be wondering if there was a plan? Hind-sight is a wonderful thing and only having completed the research is it clear to me now where I have travelled and why. This brief section attempts to provide a view of the forest.

**Chapter 2:** As a mathematician, Ursino's mathematical model was immediately attractive as the base from which to start. My interest in model comparison drove me to rearrange the Ursino model to yield an index of autoregulation as the main output. In so doing, a number of parameters in the final equation clearly were not practical to measure clinically. A few approaches were looked at to produce surrogate measures to replace these key parameters, some more practical than others. However, those found to be more practical were limited by the dataset so a venturi-flow model was used as a compromise surrogate to at least allow a model comparison to proceed.

**Chapter 3:** Three models were compared: Ursino's mathematical model with two statistical models (Czosnyka's PRx and Daley's HMF). The startling poor performance of all the models tested led to approaches to optimisation with a subsequent 10 fold improvement in performance in some of the models.

**Chapter 4:** The limitation of the Venturi-flow model remained an issue and so the use of mutli-frequency transcranial impedance was investigated in both experimental animal models and clinically as a potential surrogate for $C_a(t)$ (arterial-arteriolar compliance) in the guise of intracranial compliance ($C_{IC}$). The application of impedance to the re-worked Ursino model was investigated.

**Chapter 5:** There remained a considerable variation in all the model outputs and in particular the Ursino model clearly showed that the variance in the autoregulatory

index was a better fit to the dataset than the mean value. So at this point I investigated the application of Fractal Methods to study the inherent variation and fractal nature of these types of dataset. One resulting benefit being the development and use of wavelets for filtering the dataset and how it can be used to improve the re-worked Ursino model.

**Chapter 6:** Having developed an understanding of several models of autoregulation, their relative performance and their limitations, it would be remiss to not assess their performance on a clinical dataset and especially to study their correlation with clinical outcome. This proved to be feasible as I had access to the BrainIT group [13] dataset, which is a unique multi-centre dataset of minute by minute physiological monitoring data which also included a measure of clinical outcome in the form of the Glasgow Outcome Scale (GOSe) at 6-months post-injury.

**Chapter 7:** Some "out of the box" musings on a general framework for autoregulatory model comparison and model space definition: the study of Topology.

**Chapter 8:** What has become clear is that any model comparison results are only as valuable as the quality of the data upon which they are tested. My "Gold-Standard" piglet dataset was the best available to me at the time, but clearly also had limitations in terms of size and noise. The study of cerebral autoregulation in patients with brain injury is not a new field and has many practitioners, each of whom have their own datasets in their own non-standard format. Having been encouraged to see what the BrainIT group have achieved in the realm of standardising and sharing general intensive care data from patients with brain injury, I thought I might try to test the feasibility of a similar model in the field of autoregulation research. My goal being fairly modest in trying to gain access to a number of other autoregulatory datasets so that I could ascertain if my general model comparison framework could be validated in other datasets and found useful by other groups. The response to the call of our inaugural

meeting of the Cerebral Autoregulation Research Network (CARNet) truly was unexpected and seems to have caught the interest of a large group of researchers from 15 countries including USA, Japan, Australia, Canada, China and of course Europe. The network is young and it remains to be seen whether it succeeds or flounders, but in starting this network - I have at least given myself access to a number of other datasets for testing the utility of my autoregulatory comparison framework.

# Chapter 2

# Description and the mathematical reworking of the original Ursino model.

## 2.1 Introduction

Using the Ursino et al [102] model a predictive variation of this model has been calculated. This earlier model was chosen instead of the more recent [100] model as it is mathematically less complex. This yielded a model equation containing parameters that were not readily measurable in a clinical environment. Research was undertaken to identify and develop surrogate measures of these variables more practical to measure clinically. This initial predictive model has been calculated by fully assessing the original model and simplifying the dependent variables, where it was possible, then rearranging this for the autoregulatory index parameter. This gives a model with an output measure for autoregulation dependent on a set of clinically measurable physiological variables. This new model will be assessed using the gold-standard Daley data [26] and other prospectively collected datasets. The rearranged model contained two parameters not readily measured clinically, thus approaches are described to develop alternative parameters to estimate these variables with a view to providing a re-worked mathematical model that can be practically compared with a range of statistical data driven models.

## 2.2 Aims

The main aim of this chapter is to provide a detailed assessment of the construction of the reworked Ursino model. It will investigate the issues surrounding a direct mathematical reworking of the original model including the application of this new revision in the real world. This will culminate in a basic assessment of the model against a retrospectively collected experimental dataset.

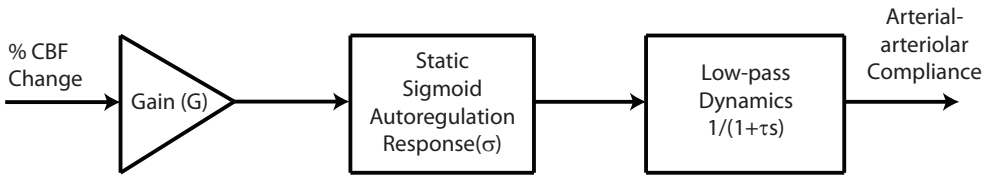


Figure 2.1: The main components of cerebral autoregulation according to the Ursino Model.

## 2.3 Basic description

Ursino's original model is a two compartment model which includes: hemodynamics of arterial-arteriolar cerebrovascular bed, cerebrospinal fluid production and reabsorption processes, the pressure volume relationship of the craniospinal compartment and a starling resistor mechanism for cerebral veins. The paper uses this model to explore a number of situations including the effects of arterial hypotension on ICP, the ICP response to a protracted cerebrospinal fluid (CSF) infusion and finally the instability of ICP dynamics when there is raised CSF outflow resistance and decreased intracranial compliance. Autoregulation in the model can be thought of as a combination of three processes affecting arterial-arteriolar compliance for a given percentage change in CBF (figure 2.1).

The first process is the autoregulatory gain, the next is the static sigmoidal shaped autoregulatory response function and the last component is a low pass transfer function. The maximum autoregulatory gain ($G$) is defined by the slope of the static autoregulatory curve at its centre point. Ursino's paper goes on to give the range of values for $G$ to cover normal healthy cerebral autoregulation through to those with impaired cerebral autoregulation.

It is from this autoregulation gain parameter that the new model is derived as this

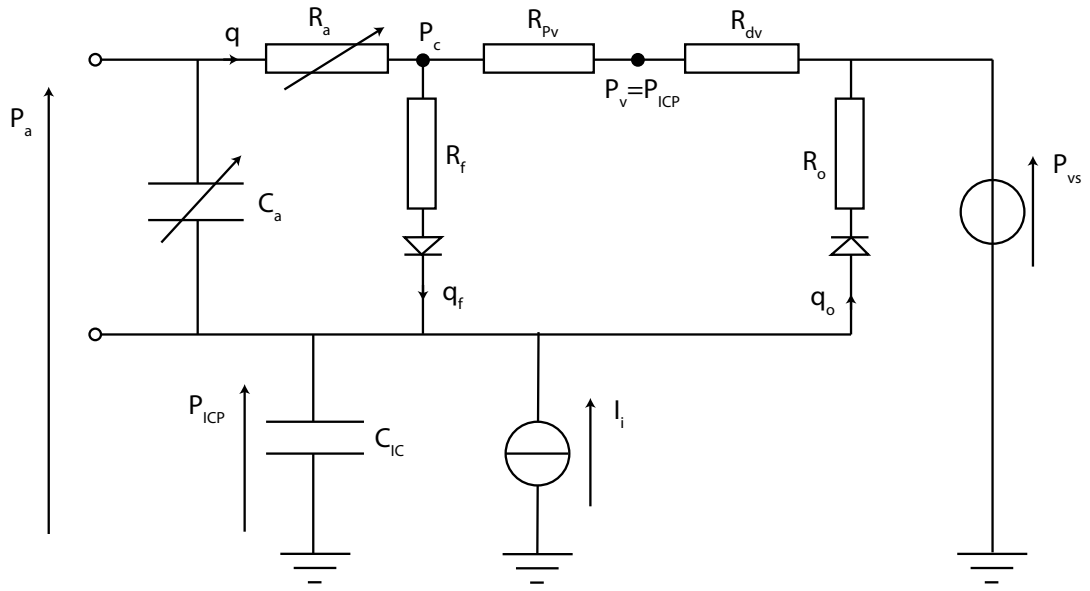


Figure 2.2: The original physiological model. The parameters used in this model are: Firstly the pressures where $P_a(t)$ is the arterial blood pressure, $P_{ICP}(t)$ is the intracranial pressure, $P_C(t)$ is the capillary pressure and $P_{CPP}(t)$ is the cerebral perfusion pressure. Secondly the compliances $C_a(t)$ the arterial-arteriolar compliance and $C_{IC}$ the Cerebral Compliance. Thirdly the resistances in the system $R_f$ the cerebrospinal fluid formation resistance, $R_{Pv}$ the proximal venous resistance, $R_{dv}$ the bridging vein resistance and $R_o$ which is the CSF Out flow resistance. Fourthly the flow rates measurable in the system beginning with $q(t)$ which is the cerebral blood flow rate, $q_f$ the CSF inflow rate, $q_o$ the CSF outflow rate and $I_f$ a CSF infusion rate. Then finally $V_a(t)$ the arterial-arteriolar volume and $R_a(t)$ which is the arterial resistance.

gain parameter $G$ is essentially a continuous index for cerebral autoregulation so with this in mind Ursino's original model has been reworked to predict $G$.

## 2.4 Summary of the mathematical reworking

The original mathematical model is based on the physiological equivalence model in figure 2.2. The mathematical formulae derived from this model have been manipulated, as can be seen in appendix A, to give a direct output of $G$. This will allow continuous

measurement of the autoregulatory state. This is shown below.

$$G(t) = \frac{-\log\left(\frac{-2\Delta C_a P_{CPP}(t)^2}{H(t)} - 1\right)\Delta C_a q_n R_f R_{Pv}}{4((R_{Pv}+R_f)(P_{ICP}(t)-P_C(t))+q_n R_f R_{Pv})}$$

Where

$$H(t) = (2C_{an} - \Delta C_a)P_{CPP}(t)^2 - \left(2\tau\frac{d}{dt}V_a(t) + 2V_a(t)\right)P_{CPP}(t) + 2\tau V_a(t)\frac{d}{dt}P_{CPP}(t)$$

and $\Delta C_a$ differs based on the sigmoid case split.

$$x(t)\begin{cases} < 0 \Rightarrow \Delta C_a = \Delta C_{a1} \\ > 0 \Rightarrow \Delta C_a = \Delta C_{a2} \end{cases}$$

This means that as $x(t)$ changes the value of $\Delta C_a$ it will switch from $\Delta C_{a1}$ to $\Delta C_{a2}$ or vice-versa. This form (equation A.28) of the reworked Ursino model has two main impediments to direct use in most clinical settings.

## 2.5 Remaining issues with the reworked model and how they can be addressed

As mentioned in the introduction of this chapter, before we can use the re-worked Ursino model, two model parameters which are not practical to measure in a clinical environment must be estimated by other variables. This section describes a number of approaches to achieve this step. The first issue concerns the measurement of $V_a(t)$ and because of equation A.1: $C_a(t)$, both of these properties are difficult to measure accurately at the bed space. So a surrogate value will need to be calculated to estimate the dynamic change in these variables. The second is the general problem with the case based asymmetric sigmoid caused by the discontinuity at the inflection point on

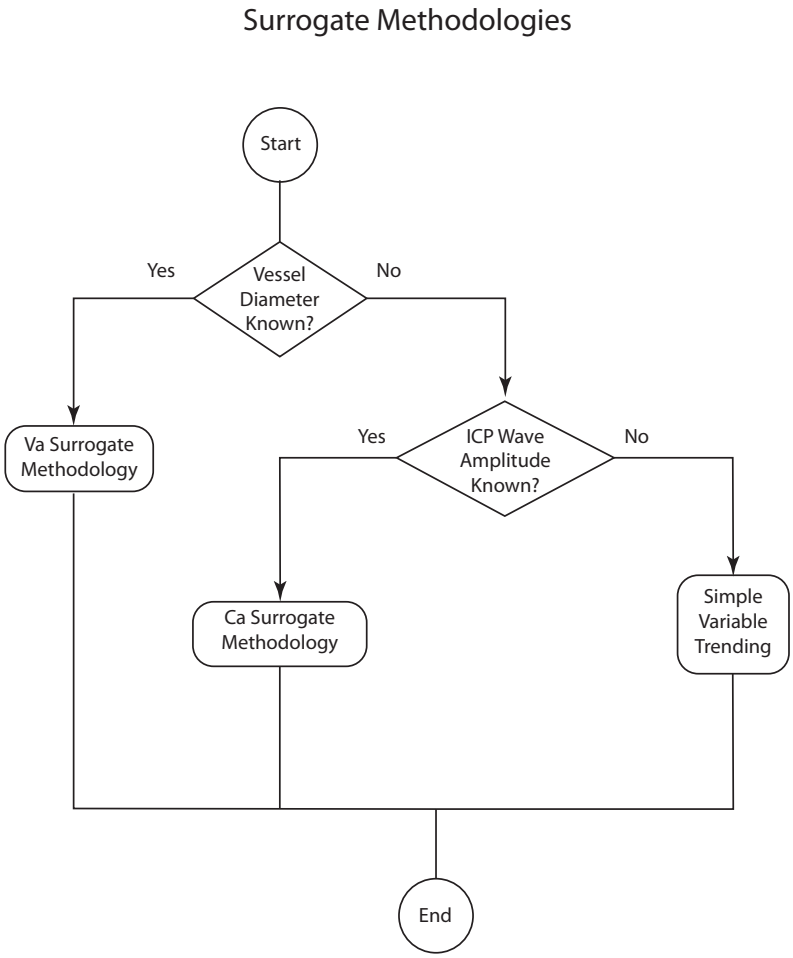


Figure 2.3: A flow chart showing the influence knowledge of vessel diameter and/or ICP wave form amplitude has on the chosen surrogate methodology

the sigmoidal curve (see figure B.4).

### 2.5.1 Surrogate values for $V_a(t)$ and $C_a(t)$

In all subsequent analyses of the model a surrogate value for either arterial-arteriolar volume or arterial compliance has been used. Which method out of the following was chosen was based solely on applicability to the dataset being used. The flow chart of decisions made in this regard is shown in figure 2.3.

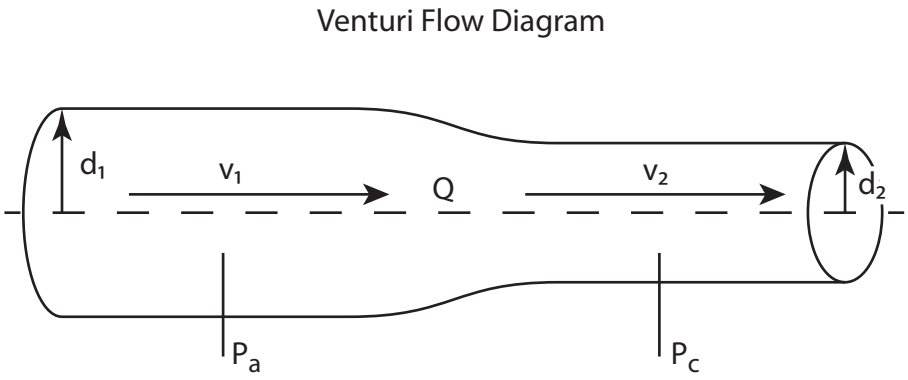


Figure 2.4: A basic venturi flow model. With $P_a$ being the arterial-arteriolar pressure, $P_c$ being the capillary pressure and $Q$ is the flow rate. Then $v_1, v_2$ are the flow velocities in their respective areas and $d_1, d_2$ are the diameters of the tube at either end as well as a change between each in the centre.

**Surrogate for** $V_a(t)$

One approach to estimating $V_a(t)$ is based upon the venturi flow effect [9]. Any fluid flowing through a tube will experience a change in pressure when moving from one diameter size into another, figure 2.4. This technique is normally used to find the flow rate of the fluid but it can also be used to estimate the volume in the system. Bernoulli's principle states that on a horizontal reference plane, with respect to gravity, the pressure in a fluid filled system and the velocity of that fluid are balanced so that as one increases the other must decrease and vice versa. Mathematically speaking this can be expressed as equation 2.1 where $\rho$ is the density of the fluid, $p$ the pressure, $h$ is the height above the reference plane which in this case is 0, $g$ is the gravitational constant, $\bar{v}$ is the velocity of the fluid and $k_s$ is the system constant.

$$\begin{aligned} k_s &= \frac{\bar{v}^2}{2} + gh + \frac{p}{\rho} \\ &= \frac{\bar{v}^2}{2} + \frac{p}{\rho} \end{aligned} \tag{2.1}$$

Since $k_s$ will be the same for any distinct part of the system this can be used to equate these parts which in this case are either side of the constriction in the venturi system. If this is rearranged we end up with equation 2.2.

$$P_a(t) - P_C(t) = \frac{\rho}{2}(\bar{v}_1^2 - \bar{v}_2^2) \tag{2.2}$$

Consider the fluid dynamics continuity equation which is centred on the idea that inflow equals outflow so with a constant density fluid the total flow rate in one part of the system is the same as in another. The basic definition of volumetric flow rate is velocity multiplied by the cross sectional area, $Q = \bar{v}A$. These two facts combine to with equation 2.2 to give equation 2.3.

$$P_a(t) - P_C(t) = \frac{\rho}{2}\left(\left(\frac{Q}{A(d_1)}\right)^2 - \left(\frac{Q}{A(d_2)}\right)^2\right) \tag{2.3}$$

Where the $A(d)$ function is the classical area of a circle in terms of the diameter and where $d_1$ and $d_2$ are the diameters of the arteries and arterioles.

$$A(d) = \frac{1}{4}\pi d^2. \tag{2.4}$$

Then if we solve equation 2.3 for flow $Q$ we get

$$Q = \sqrt{\left(\frac{2(P_a(t) - P_C(t))}{\rho}\right)}\frac{A(d_1)}{\sqrt{\left(\left(\frac{A(d_1)}{A(d_2)}\right)^2 - 1\right)}} \tag{2.5}$$

substituting equation 2.4 into this and letting that equal the flow equation A.3 from Ursino's original paper

$$q(t) = \frac{P_a(t) - P_c(t)}{R_a(t)}$$

and then solving for $R_a(t)$ we get

$$R_a(t) = \frac{\sqrt{\frac{8(d_1^4 - d_2^4)}{d_2^4}}(P_a(t) - P_C(t))}{\pi d_1^2 \sqrt{\frac{P_a(t) - P_C(t)}{\rho}}} \tag{2.6}$$

Then equating this to the arterial resistance from the paper, equation A.2

$$R_a(t) = \frac{k_r C_{an}^2}{V_a(t)^2}$$

and then solving for $V_a(t)$ we get equation 2.7.

$$V_a(t) = \pm \frac{C_{an} d_1 \sqrt{2\pi k_r (P_A(t) - P_C(t)) \sqrt{\left(\frac{8(d_1 - d_2)(d_1 + d_2)(d_1^2 + d_2^2)}{d_2^4}\right)\left(\frac{P_a(t) - P_C(t)}{\rho}\right)}}}{(P_A(t) - P_C(t)) \sqrt{\left(\frac{(d_1 - d_2)(d_1 + d_2)(d_1^2 + d_2^2)}{d_2^4}\right)}} \tag{2.7}$$

This method is only practical when there can be a direct measurement of these diameters which in reality will only be in experimental animal models such as that used in the cranial window pial artery model used by Daley et al [27]. Although this approach may seem to be merely an academic exercise it may be worth considering in the future should clinically practical methods for estimating a representative arteriolar diameter become available, possibly based upon high resolution ultrasound imaging. Therefore other more clinically applicable methods were also sought.

**Surrogate for $C_a(t)$**

To find surrogate parameters that could be used here that have a good enough fit to the model and don't introduce much noise, it is worth exploring the relationship between arterial-arteriolar compliance and intracranial compliance. Going back to Ursino's original paper it describes the intracranial compliance ($C_{IC}$) as a function of

arterial-arteriolar blood volume ($V_a(t)$) as shown in equation 2.8.

$$\frac{\mathrm{d}}{\mathrm{d}t}V_a(t) = C_{IC}(t)\frac{\mathrm{d}}{\mathrm{d}t}P_{ICP}(t) + \frac{(R_a+1)P_{ICP}(t) - R_{Pv}P_a(t)}{R_f(R_{Pv}+R_a)} + \frac{P_{ICP}(t) - P_{VS}}{R_O} \quad (2.8)$$

The general solution to this equation for $V_a(t)$ is found by integrating equation 2.8 and is shown in 2.9.

$$\begin{aligned} V_a(t) =& \frac{1}{R_fR_OR_{Pv} + R_aR_fR_O}\int\Bigg((R_fR_OR_{Pv} + R_aR_fR_O)C_{IC}(t)\frac{\mathrm{d}}{\mathrm{d}t}P_{ICP}(t) \\ &+ (R_fR_{Pv} + (R_a+1)R_O + R_aRf)P_{ICP}(t) - R_OR_{Pv}P_a(t)\Bigg)\,\mathrm{dt} \\ &- P_{Vs}R_fR_{Pv}t - P_{Vs}R_aR_ft + V_{a0} \end{aligned} \quad (2.9)$$

Now from equation 2.9 we can see that $V_a(t)$ changes in proportion to the integral of $C_{IC}(t)$ which is both time dependent and a intracranial compliance dependent upon the arterial-arteriolar volume. As an illustration of this consider a static compliance in which the system will not deform with time so that the only effect on volume will be how long a fluid flows into the system, much like filling a cup with water. If however the compliance changes in a linear fashion then as fluid flows into the system the system also changes to increase in size, so both the contained volume of fluid and the system's overall volume is changing. This would be like filling a balloon or in our case a vasodilating artery and arteriole.

We also know from equation A.1 that $V_a(t) \propto C_a(t)$ so this would give the following relationship

$$C_a(t) \propto \int C_{IC}(t)\,\mathrm{dt} \quad (2.10)$$

The approach taken here is to use a measure of total intracranial compliance and then relate that back to arterial compliance via equation 2.10. It is a well known fact, particularly from the work of Avezaat and Van Eijndhoven [4,5], that there is a relationship

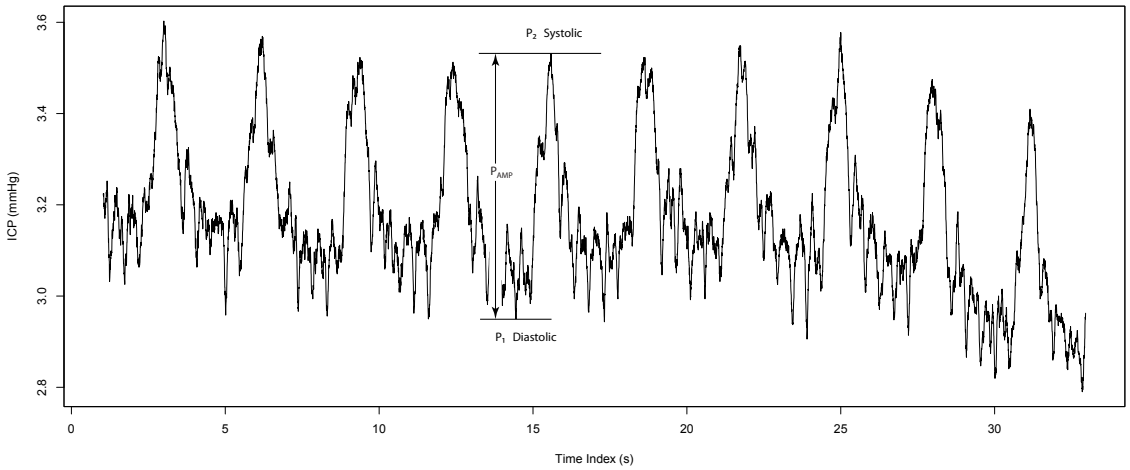


Figure 2.5: Diagram of an ICP wave trace with the diastolic level $P_1$ and systolic level $P_2$ marked to allow the amplitude of the waveform $P_{AMP}$ to be calculated.

between the intracranial pressure pulse amplitude and the total compliance of the system [77]. The dependence of ICP upon intracranial volume ($V_{IC}$) and the compliant properties ($\frac{1}{E_1}$) is described in equation 2.11. Using this form with an exponential scaling factor to simulate the relationship

$$P_{ICP}(t) = P_{eq}e^{E_l V_{IC}(t)} + P_0 \tag{2.11}$$

Using an exponential inequality for any $a > 1$ we have $x^a > 1 + a(x-1)$. If the ICP wave amplitude is $P_{AMP}$, as shown in figure 2.5 , then

$$\begin{aligned} P_{AMP} &= P_2 - P_1 \\ &= P_{eq}\left(e^{E_l V_2} - e^{E_l V_1}\right) \\ &> P_{eq}\left((1 + E_l V_2(e-1)) - (1 + E_l V_1(e-1))\right) \\ &> E_l P_{eq}(e-1)(V_2 - V_1) \end{aligned} \tag{2.12}$$

this effectively means that $P_{AMP}(t) \propto E_l$ assuming $V_2 - V_1$, considered as the intracranial cerebral pulse volume, remains constant. Then coupling this with the fact that $C_{IC} = \frac{1}{E_l}$ and the relationship between $C_a(t)$ and $C_{IC}(t)$ gives a basic arterial-arteriolar

compliance of

$$C_a(t) \propto \int \frac{1}{P_{AMP}(t)} \mathrm{dt} \tag{2.13}$$

and therefore an arterial volume, with reference to equation A.1, of

$$V_a(t) = k_{IC}(P_a(t) - P_{ICP}(t)) \int \frac{1}{P_{AMP}(t)} \mathrm{dt} \tag{2.14}$$

Where $k_{IC}$ is a constant of proportionality. Thus, using this approach based upon measuring the ICP pulse amplitude, both $C_a(t)$ and $V_a(t)$ can be estimated.

#### Other methods for estimation

The least accurate models of $V_a(t)$ are the ones only based on equation A.1 that make assumptions that $C_a(t)$ is constant and only using $P_{CPP}$ as a trending agent or similarly has to assume $V_a(t)$ is constant itself. With any of these other methods of estimation it becomes a question of how much inaccuracy is acceptable with respect to introducing noise into the model. Where possible both of these methods have been avoided in the use of the model unless explicitly stated.

### 2.5.2 Asymmetric sigmoid

Ursino's original sigmoid curve was asymmetric and initially proposed as two functions which worked on separate cases of the parameter set. However when re-engineering the methodology this dual function had a tendency to become unstable in the simulation at the crossover point of the two sets so a new asymmetric sigmoid function was devised to overcome this limitation (appendix B). Using this new asymmetric sigmoid function B.8 in the place of equation A.11 we would then end up with the following version of

Ursino's model. Starting from equation A.10 we get

$$G(t) = \sigma^{-1}\left(\frac{\tau\frac{d}{dt}V_a(t) - \tau C_a(t)\frac{d}{dt}P_{CPP}(t)}{P_{CPP}} + C_a(t)\right)\frac{1}{x(t)}$$

However because of the numerical nature of the solution to this inverse sigmoid, as has been detailed in appendix B, producing a clean mathematical formula here is impossible. To find the inverse value the algorithmic function only needs the modification shown in equation 2.15 to convert it from a function in $y$ to one in $t$.

$$y = \frac{\tau\frac{d}{dt}V_a(t) - \tau C_a(t)\frac{d}{dt}P_{CPP}(t)}{P_{CPP}} + C_a(t) \tag{2.15}$$

Then you would just solve for the roots of the equation and transform that into the inverse sigmoid value.

## 2.6 Testing the feasibility of the model.

### 2.6.1 Daley experimental dataset

The main data set for all of the initial analysis was donated by Dr Michael Daley from a previously carried out set of animal experiments. As this dataset did not have to be created from scratch this allowed a faster start to the analysis portion of this thesis however as the rudimentary analyses were being carried out a number of questions started to arise over what experimental manipulations were present in the data. It became clear quite quickly that a deeper understanding of the provenance of the data were needed. To this end a trip was arranged to spend a week with Dr Daley in his lab and learn how the data were collected and to better understand the experimental protocol.


Figure 2.6: An example of the experimental set up used in the recording of the piglet dataset.

### Basic animal preparation

The dataset consists of six healthy piglets which range in weight from between $1.5kg$ to $3.3kg$ with the average being $2.35kg$. They all received the following standardised set up, firstly both ketamine and acepromazine were given intramuscularly to initially anaesthetise the animal. Secondly they were then intubated and mechanically ventilated at rate between eight and twenty four breaths per minute. A $2cm$ diameter opening was cut over the left parietal cortex and a cranial window was then placed and sealed with dental acrylic, mock CSF was then infused below the window. A video camera is set up over the window so that the vessel diameters can be recorded during the experiment. Lastly the tip of a fluid percussion injury (FPI) apparatus was mounted on the skull over the exposed dura of the right parietal cortex and is sealed in place. During the course of the experiment $pCO_2$, $pO_2$, $pH$ and haemoglobin levels were monitored and these were used to assess and maintain ventilation so that the animal remains physiologically stable. The temperature of the animal was also monitored and was kept steady between $38°C$ and $39°C$. The full experimental set up can be seen

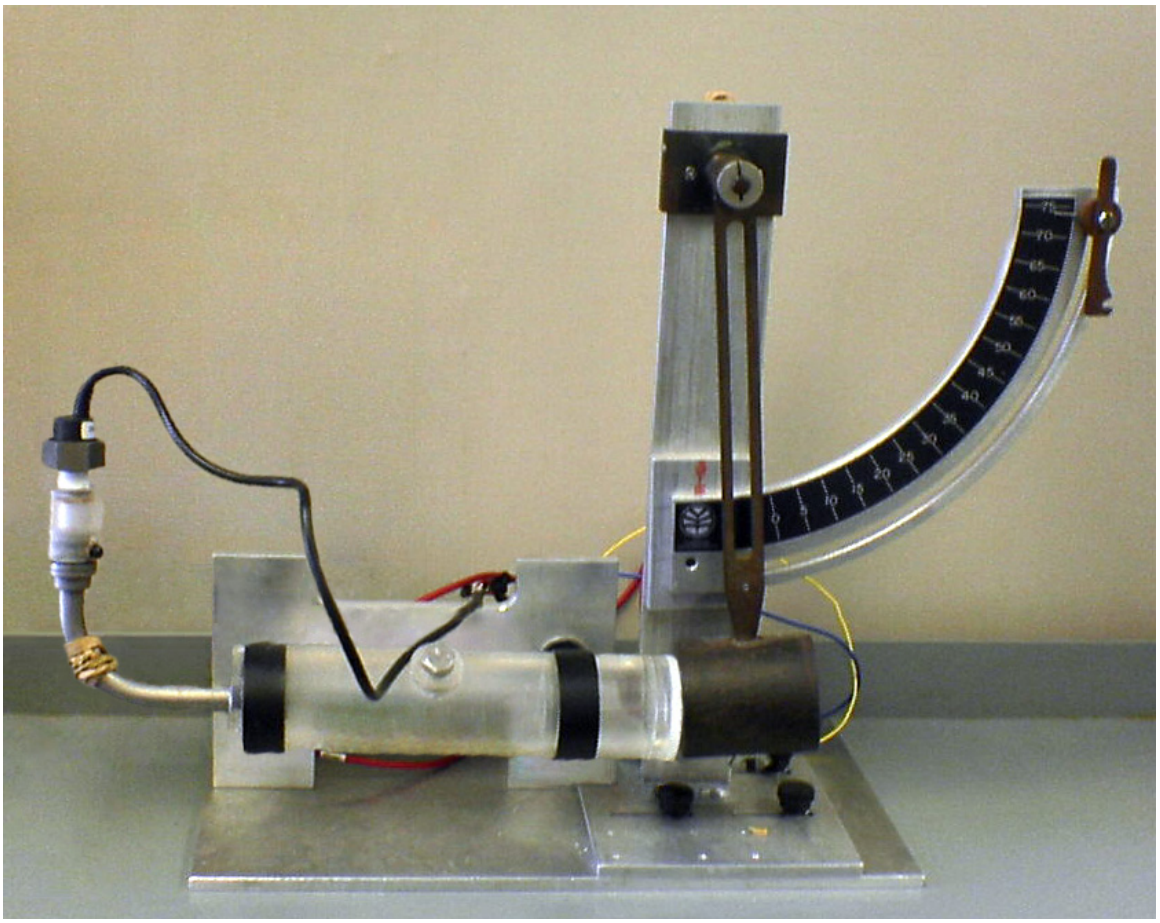

Figure 2.7: A picture of the fluid percussion injury equipment used to used in the injury model.

in figure 2.6.

**Fluid percussion injury.**

The equipment used to simulate a traumatic brain injury has been validated in a study by Shibatal [88]. It is essentially a water cannon which projects a fluid, in this case a 0.9% saline solution, in a controlled manner at a specified area. The equipment can be seen in figure 2.7. The force is supplied by a weighted pendulum which swings and strikes a syringe plunger. This then pushes the fluid out of the system via the tube and effect nozzle at the end. For this dataset the pressure exerted on impact is approximately $3.55 \pm 0.88$ bar.

With any injury model there is a question over how much impairment can be considered global and how much any focal component of the injury will affect the overall global measurement approach. The FPI is considered a diffuse type injury model as when the pressure is released at the focal point of impact, the pressure wave will radiate out through the brain parenchyma and as it is being performed in a closed environment, in this case the skull, this means the pressure disturbance will be relatively quickly and evenly distributed throughout the brain tissue. Certainly the brain pathology seen with this type of TBI model shows marked similarities to that observed in patients presenting with diffuse TBI. Thus it is reasonable to assume that the injury model deployed produces predominantly features typical of a diffuse brain injury.

However, one should also consider that with this type of injury model, there will be a varying degree of impairment between blood vessels on the surface which have more exposure to the affects of this travelling pressure wave front and any vessels that are located more deeply within the cerebral matter. This degree of variability however will not prevent the impairment of these vessels as larger pial and sub-cortical vessels are all close to a fluid-filled compartment which will rapidly transmit the pressure wave front.

**Artery diameter measurement**

The cranial window and the cranial window video is used primarily to measure the pial artery diameters as an indication of the overall autoregulatory state in the system. For example a pressure passive increase in pial vessel diameter is an indication of autoregulation impairment. The measurement of the actual diameter from the video was done by hand using the marked scale from the cranial window recording. Ten consecutive values for an artery were taken and the average value used. A raw still photo from a video can be seen in figure 2.8.

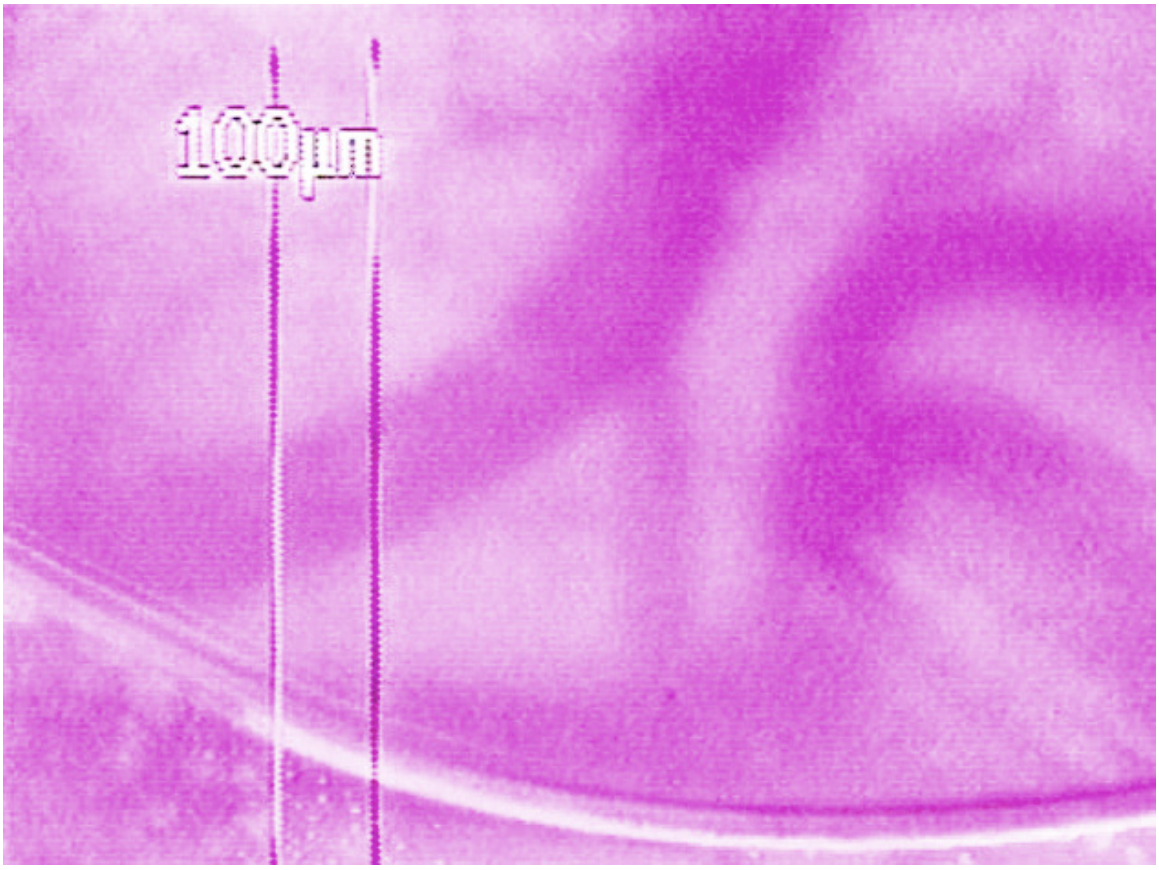


Figure 2.8: A sample video frame from which the artery diameter can be measured. The scale, in this case $100\mu m$, is overlayed on the recording by the camera.

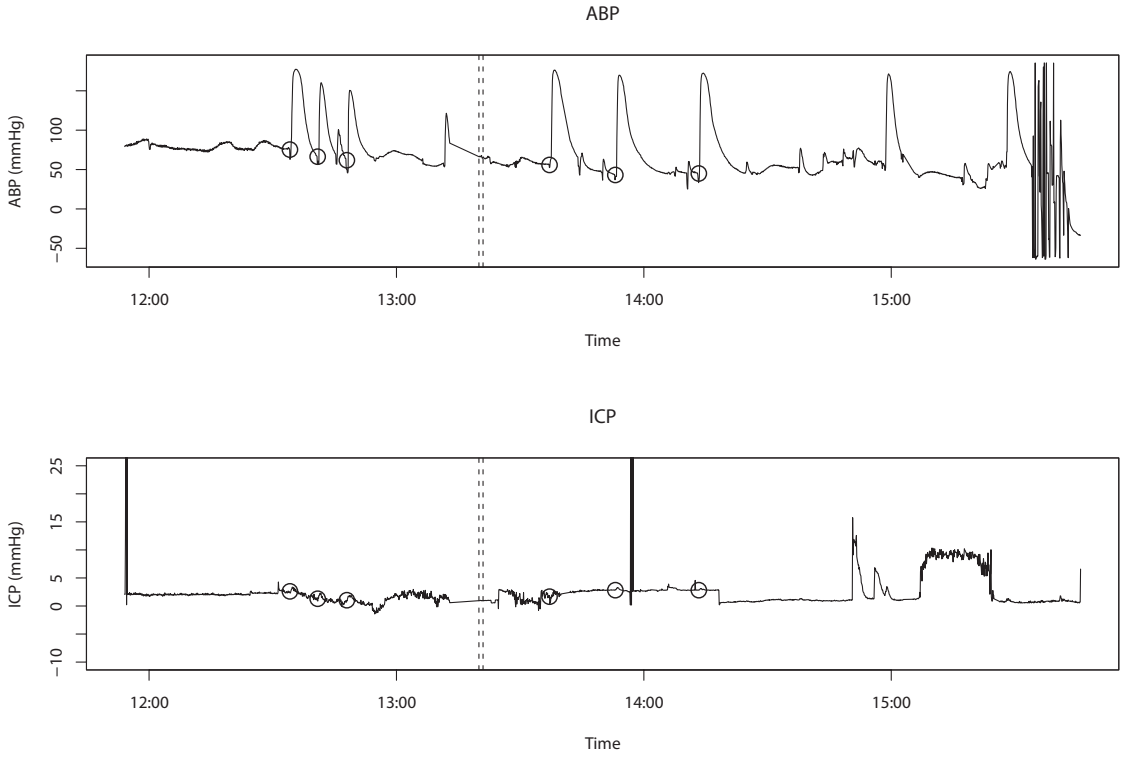


Figure 2.9: A representative raw dataset from a single piglet with both ABP and ICP traces. Dashed line indicates the fluid percussion injury and the circles indicate detected BP challenges.

### Experimental manipulations

Some of the main routine issues with this type of dataset include: basic flushing of the arterial line to keep it patent after blood samples and movement artifacts. Two manipulations of the experimental animals resulted from two different physiological challenges to the animal. Firstly norepinephrine infusion was given to increase the ABP and secondly 5% $CO_2$ was added to the inspired gases to effect the ICP through stimulating $CO_2$ reactivity. The norepinephrine was administered via infusion over a period of five minutes and the $CO_2$ was given over ten minutes.

**Data collection**

This is a high resolution data set with recording of ICP and ABP sampled at $250Hz$. Figure 2.9 gives a sample from one piglet's data of a set of ICP and ABP traces before and after fluid percussion injury also showing blood pressure challenges. Finally, using the cranial window preparation allowed the pial vessel diameters to be measured before and after BP challenge as well as before and after fluid percussion injury.

### 2.6.2 Feasibility study

Before going on to perform a definitive model comparison study between the re-worked Ursino model and several statistical models, it was necessary to initially test the feasibility of the re-worked model on real data. This feasibility study was then performed in a representative animal dataset drawn from the Daley six piglet database. During the course of testing this model which included the new asymmetric sigmoid curve and the venturi effect $V_a(t)$ estimate, it was observed that it has very good temporal discrimination and this is probably because of the dynamic approach it uses with the time measurement within the model. This of course is a double edged sword as the sampling rate between time points changes as the model changes with it to incorporate this new information. If the frequency of the collected signal is increased then the number of points over the same length of time increases and because the gain of the model will essentially predict a one to one relationship with the sampling rate there will be more predictions for the autoregulatory state over the same period of time. Since it is known that autoregulation of the system is itself a dynamic process which is constantly changing, then the predictions of $G$ will reflect this, however this increased variability can often obscure larger picture of overall autoregulatory state by making the dataset noisier. To reduce the model noise, two summary measures were calculated as moving averages of both the mean and the variance averaged over a fixed time window. All of

| Model Summary Measure | P-value |
|---|---|
| Basic model | 0.09 |
| Moving Average | 0.06 |
| Moving Variance | 0.03 |

Table 2.1: P-values for each t-test of the different model summary measures

the moving windows were calculated with a 1 minute window which was approximately 0.5 percent of the total time series length. Figure 2.10 shows an example segment from the time-series data-set of a single animal over which the model, and the two summary measures, were calculated. To initially assess each of these measures against one another the dataset was taken and was split into before FPI and after FPI and twenty points were sampled from each group. Using the known autoregulatory state assessed using the pial artery window methodology these groups can be broadly generalised into intact autoregulation before the injury and impaired autoregulation after. So which ever summary measure shows a difference between these randomly sampled groups in a Students t-test would give the best chance at detecting a good model. Table 2.1 shows the results of evaluating the t-test for each measure. To highlight this figure 2.11 is a box plot of the before and after fluid percussion injury groups per summary measure. It can be seen that the variance is the better predictor of the autoregulatory state. This makes sense physiologically because a cerebral vessel will dilate or constrict appropriately in response to changes in cerebral perfusion pressure so one would expect the system to be more unstable or variable.

The last point that needs to be addressed before the model can be used in the wider setting is how is autoregulation actually predicted from the numeric variance. To help answer that a receiver operator characteristic analysis was performed using the previously calculated testing data. The level above which the test subject would be considered to have an impaired autoregulatory status was varied and the false positives and true positives were recorded. The results led to using a cutoff level of 0.0074. Anything below this has intact cerebral autoregulation and anything on or above it impaired.

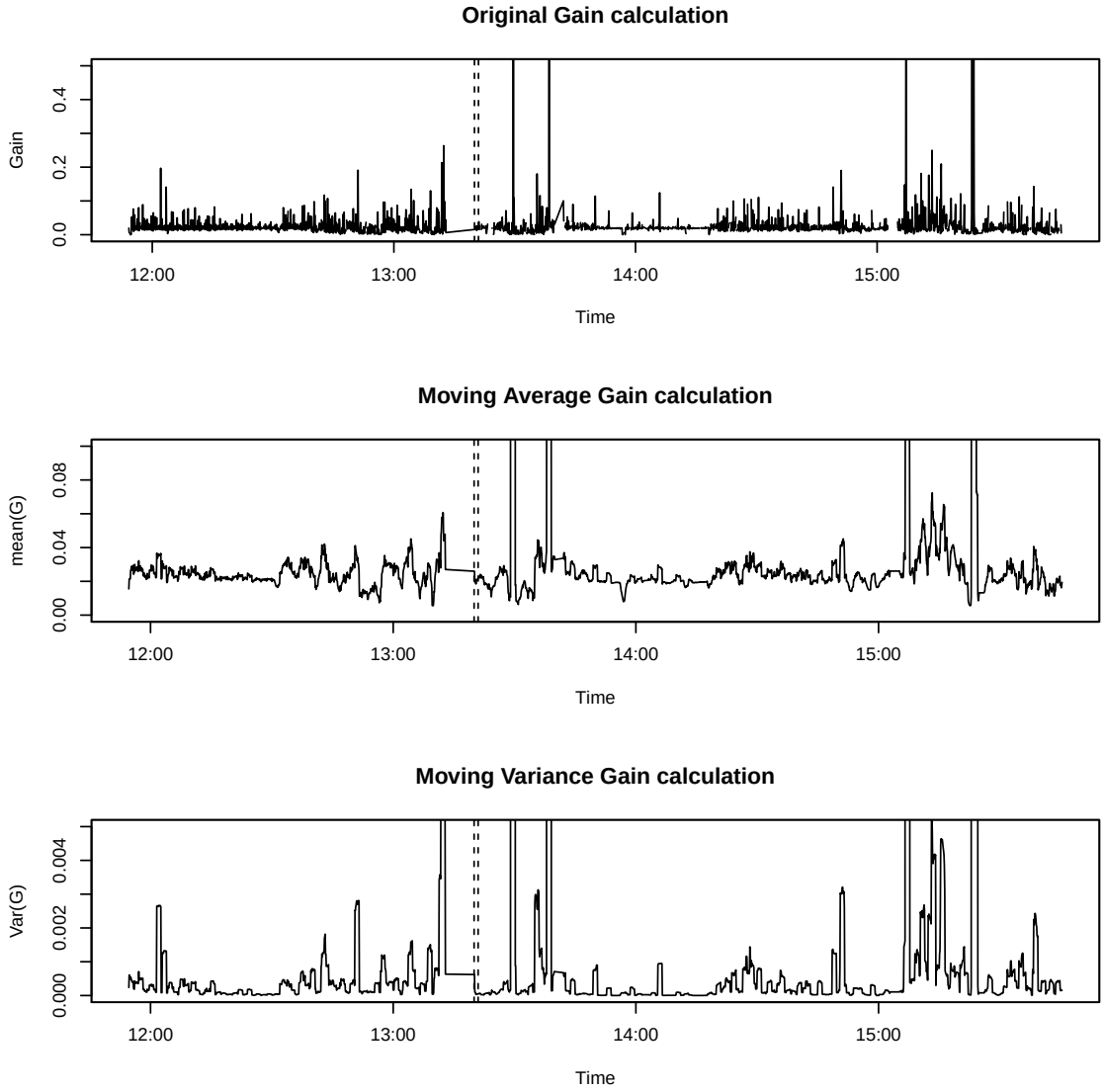


Figure 2.10: Three plots of a single animal showing the output of the three summary approaches: Firstly the original $G$ then the moving average $G$ and finally the moving variance $G$. The autoregulatory impairment is shown as a vertical dashed line. With each subsequent approach it can be seen there is visibly less variability "noise" in the trace.

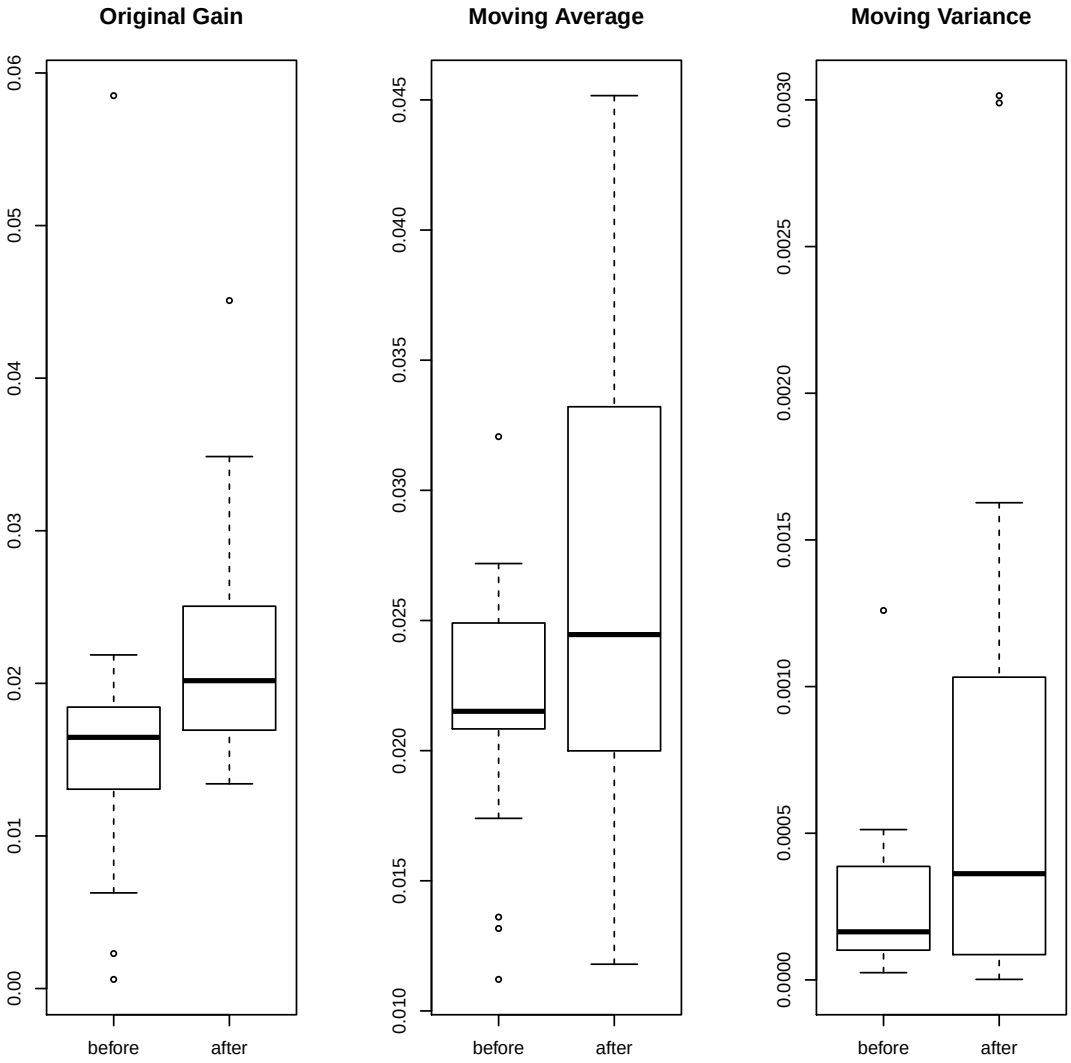


Figure 2.11: Box plots of each summary measure approach illustrating the difference in distribution between before and after FPI. With the circular point showing the outlying data points in the sample.

## 2.7 Conclusion

All of the aims which were detailed in section 2.2 were obtained and they raise the following notable observations: The re-worked Ursino model for cerebral haemodynamics provides a good base to build upon for creating a clinically practical mathematical model of cerebral autoregulation. This process was not without its hurdles to overcome which includes the estimation of arterial-arteriolar blood volume and the presence of a case based sigmoid function which is mathematically unstable. These issues have been addressed by: firstly deriving a new sigmoid function which was continuous at all points which solves many of the problems with the original. Secondly the use of several surrogate measures for model parameters to deal with the estimation problem of arterial-arteriolar volume were explored. In the absence of a method for direct or indirect measurement of these surrogate parameters, a Venturi-flow model as a pragmatic solution for working with the available data has also been derived. The model was then explored and a summary measure based upon variance appears to be a better predictor of outcome compared to the basic model or an average based summary measure. Finally the level for deciding on the autoregulatory state was found.

# Chapter 3

# Comparison of Autoregulation Models

## 3.1 Introduction

Literature on approaches to comparing these types of models, in terms of their relative accuracy, is sparse. This deficiency could be attributed to the difficulty in direct comparison of different model types; such as comparing physiological models that include known autoregulatory parameters with other models that focus primarily on generating an indexed autoregulatory status using a "black box" approach regardless of the underlying physiology.

Another difficulty concerns the lack of high quality data upon which to compare models. Without high frequency "gold standard" data on autoregulatory status, any model could be placed at a disadvantage during such a comparison. Furthermore a major problem in model comparison concerns the range of tests that can be used for comparison and the choice of test is key to the meaningful comparison of the models.

As an example, Signorini et al [90] conduct an analysis of secondary insults (eg arterial hypertension or raised intracrainial pressure (ICP)) from a physiological data set obtained from patients with traumatic brain injury (TBI). For their model comparison they used the Hosmer and Lemeshow goodness of fit test statistic. This test, although superficially a good choice for the comparison, has been shown in Hosmer et al's later paper [38] to be flawed in that the comparison outcome is dependent on the size of the deciles that are initially chosen which could cause the comparison and analysis to be biased. The later Hosmer-Le Cessie "omnibus lack of fit test" has more power and doesn't have any of the former's initial problems about the arbitrary binning of probabilities. This test may yield a better chance at more accurate model comparison. This illustrates a growing problem when choosing a test, in their case for a logistic regression, that as the problem complexity increases, the chance of incorrectly analysing the data also increases.

The above discussion indicates that advancement in this area of research will need to

have these problems overcome. One approach which could be proposed would be to perform the comparison on a related statistic but not necessarily one which is originally generated by any of the models. For example, by taking two models, one of which outputs a direct measure of autoregulation via an index and a second model which outputs a time series trend for intracranial pressure, both of these could generate a third statistic to a known value for autoregulation. This then could be used as the basis for direct comparison of the models.

### 3.1.1 Study aims

This chapter reports on the results of our application of this approach to autoregulation model comparison focused upon three models:

1. Pressure Reactivity indeX (PRx) [22]

2. Highest Modal Frequency (HMF) [27]

3. Reworked Ursino [102]

Each model will have a normalised autoregulatory parameter generated to ease comparison and a common high resolution data set will be used to ensure all model comparisons are not biased by data sampling rate. The analyses leading to best choice for model comparison statistic and finally a method for optimising the data window size to yield the best performance of a given model for estimating the status of autoregulation is also reported. Models will be compared in terms of performance at detecting baseline autoregulation status from a dataset generated from an experimental model of autoregulation disruption using pial vessel imaging before and after fluid percussion injury. This dataset has been described in detail in chapter 2. Models will also be compared against each other as well as before and after application of our data window size optimisation method.

## 3.2 Methods

### 3.2.1 Models

#### Reworked Ursino model

Ursino's original model is a two compartment model which includes: hemodynamics of arterial-arteriolar cerebrovascular bed, cerebrospinal fluid production and reabsorption processes, the pressure volume relationship of the craniospinal compartment and a starling resistor mechanism for cerebral veins. It is from this autoregulation gain parameter that the new model is derived. The gain parameter $G$ is essentially a continuous index for cerebral autoregulation. With this in mind Ursino's original model has been rearranged in chapter 2 to predict $G$.

There are however two issues which have been addressed by using the new asymmetric sigmoid (appendix B) and estimating the arterial-arteriolar volume for the system under study via a venturi flow model. This uses the test data set which has a cranial window preparation through which the diameters for the various vessels can be used to estimate the volume in the system.

However, in a pilot study of this new index parameter $G$ [87], it was shown that the variance of $G$ changes more predictably with autoregulatory status than does $G$ itself. An explanation for this would be that when autoregulation is active there are dynamic changes to the system as a whole and hence the variance in any continuous index of autoregulation will also be large.

#### HMF autoregulatory predictor.

Using a technique called modal analysis it was found that when cerebral arterial flow regulation is intact, changes in the highest modal frequency (HMF) are inversely related

to changes in cerebral perfusion pressure. In contrast, when the arterial-arteriolar vascular bed demonstrates autoregulatory impairment i.e. cerebral blood flow (CBF) shows a cerebral perfusion pressure (CPP) dependency, changes in HMF are directly related to changes in CPP (Figure 3.1). The HMF method published by Daley et al [27] is briefly described below. HMF is calculated using an autoregressive moving average with exogenous inputs (ARMAX) method from the model of ICP dynamics proposed by Czosnyka et al [22]. Cerebrovascular pressure transmission is described by a third-order system equation relating arterial blood pressure (ABP) to ICP. The resultant difference equation from this model can then be converted to a differential equation via the following methodology. Using a Taylor expansion of three generic functions a vector space basis can be derived, then using a simple substitution onto that basis a set of functions can be derived that relate the difference to the differential of the same order. This topic is explored in more detail in appendix D. Solving those equations one can calculate the eigenvalues of the original differential. These eigenvalues are the modal radian frequencies of the cerebrovascular pressure transmission. The highest modal radian frequency is ultimately converted to HMF via division by $2\pi$. These HMF's are then grouped and a linear fit is performed. The slope of this fit is then related to the autoregulatory status in the subject.

**PRx**

The pressure reactivity index (PRx) or pressure reactivity index described by Czosnyka et al [22] is a moving Pearson's correlation between ABP and ICP. This method looks at the amount of correlation between the two variables and the decision on whether there is pressure reactivity or not is based on a pressure passive model. If the correlation is positive, ie the ICP is reacting passively with ABP then it can be assumed that the subject is not autoregulating. If the correlation is negative or near zero then

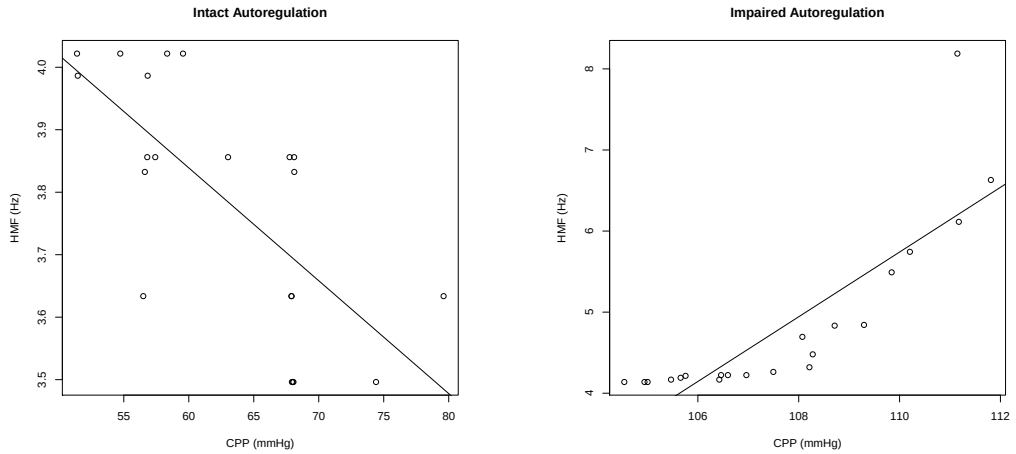


(a) (b)

Figure 3.1: Two examples of the HMF calculations for (a) Intact autoregulation and (b) Impaired autoregulation. Where the slope of the fitted line denotes the switch between predictive states.

the opposite is assumed that autoregulation is still intact and indicates that the cerebrovasculature is reacting to the change in ABP. Examples of both of these correlations are shown in figure 3.2. This has been shown to be predictive of outcome [23] and has been generally adopted as a standard of autoregulatory assessment.

### Other models

When this experiment was initially considered the plan was to compare all the above models to what was an accepted measure of autoregulation of the Bouma's methodology [12]. However during the analysis this technique turned out to be consistently at odds with most of the other models which normally had some degree of agreement between them. One of the difficulties in this area is that many of the approaches for measurement of autoregulation, such as methods using the Bouma Index, have been developed using blood flow measurement relying upon tracer clearance techniques. These methods tend to give at best spot measurements of cerebral blood flow separated over many minutes which generally have produced estimates of autoregulation which many consider to be "static" autoregulation. The methods that have been chosen for

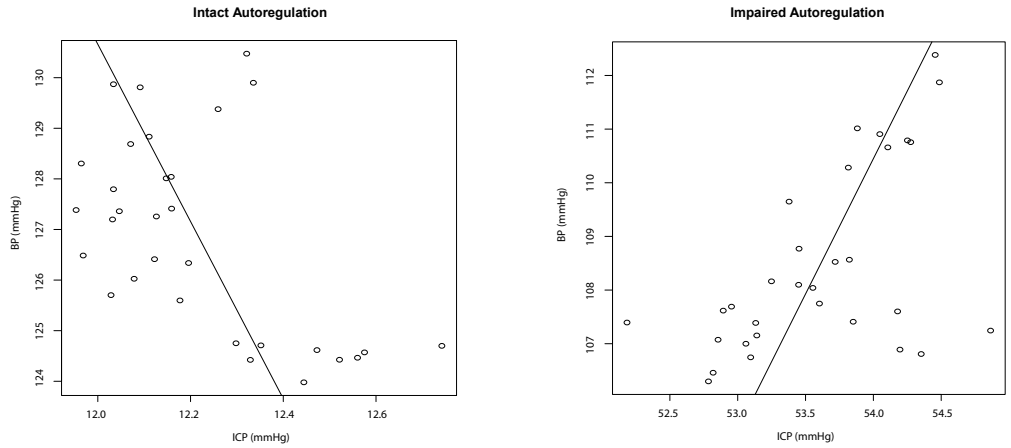


(a) (b)

Figure 3.2: Two examples of the PRx calculations for (a) Intact autoregulation and (b) Impaired autoregulation. Where the slope of the fitted line denotes the switch between predictive states

the comparison are believed to be a representative sample of the approaches used to measure "dynamic" autoregulation.

Each of these models have strengths and weaknesses associated with them with the PRx the most widely adopted surrogate measurement for autoregulatory performance in use today. It does however suffer from noise and "binning" artefact in that it is sensitive to the choice of data set size for the analysis. There have been publications that have tried to address this via a histogram methodology which is essentially a smoothing technique. The HMF methodology is more stable than the PRx however it has a reliance on higher resolution data, 250Hz sampling, to perform the analysis. The reworked Ursino model does not rely on a specific resolution of data but will predict more accurately given higher resolution sources. However that accuracy is tempered by the dynamic nature of the signal becoming noisier at the highest resolutions.

| AR Intact | AR Impared |
|---|---|
| 25 | 32 |

Table 3.1: Counts of the cumulative autoregulation states measured via the cranial window across all six piglets

### 3.2.2 Model Comparison

Across all six animals there were 57 measures of autoregulation: 25 intact and 32 impaired (Table 3.1). This dataset formed the baseline measure of autoregulation status for model comparison. Figure 3.3 is a diagram representing the analysis protocol, showing the data windows used for model input.

Firstly for the model comparison this data set was prepared differently for each model so that at the end of the process there were a similar number of calculated results for each model. Thus for the PRx the data were resampled to give a value every 6 seconds therefore giving 30 points per three minutes that the model requires. This was then run across the full data set in a moving window giving a calculation for PRx every 6 seconds. For the HMF the ARMAX process was carried out using the 250Hz data using a 150 point window then this information was used to solve the difference equation problem resulting in a HMF calculation every 0.6 of a second thus also giving a model output every 6 seconds. Lastly the modified Ursino model was just run on resampled data of six second ICP and ABP data, which in turn gave a prediction for the autoregulatory state every six seconds.

For these continuous traces for autoregulatory state, the points at the start of each blood pressure (BP) challenge were picked as points for comparison, to minimise the likelihood of system compromise from the challenges themselves. This then allows the autoregulatory prediction from each of the models to be compared to what would be the standard which is what was observed through the cranial windows before and after injury. So for example a non autoregulatory passive artery diameter change is observed with an increase in flow during BP challenge after the injury compared with

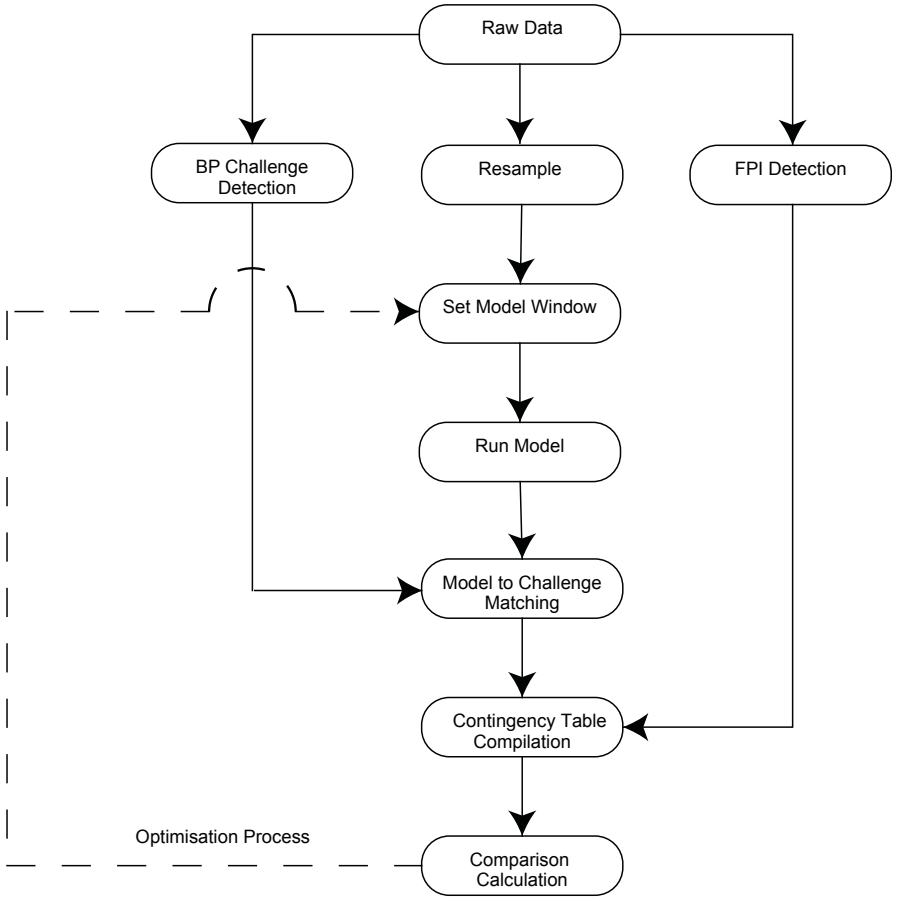


Figure 3.3: A generalised flow chart of the methodology used in the comparison of the basic models. It also shows the loop used in the optimisation stages of the process.

an "autoregulatory" pial artery contraction with decreasing flow. Initial consideration of the data in the experiment has shown that multiple challenges have a detrimental effect on the autoregulatory status of the subject which obviously affects the intact autoregulatory side more than the non autoregulating side of the tests. So for all of the comparison data only the first hour of data is selected before and after injury. With the intention this should make the testing more comparable to a binary intact versus impaired status.

### Comparison Statistic

A number of comparison techniques were considered as approaches to this analysis: Fishers exact tests, Chi-squared tests, F-measure, Matthew's Correlation Coefficient and ROC curves. The choice of methodology ultimately will be driven by the data set in use. A rigorous comparison of the methodologies was performed to narrow down and finally single out the optimal method to use as described in appendix C. From this analysis the Matthew's correlation coefficient (MCC) method has been selected as the fairest model comparison test. This is based on a simple contingency table of the frequencies of predicted against actual status.

$$M = \begin{bmatrix} T_P & F_N \\ F_P & T_N \end{bmatrix}$$

Where $T_P, T_N, F_P, F_N$ are the usual number of true positives, true negatives, false positives and false negatives respectively. The Matthew's correlation coefficient (MCC) is then calculated directly as

$$MCC = \frac{T_P T_N - F_P F_N}{\sqrt{(T_P + F_P)(T_p + F_N)(T_N + F_P)(T_N + F_N)}}$$

There are a number of ways to compare the models using the MCC with the first

presented being to base line the MCC against the known autoregulatory status via the pial artery window response to BP challenge of the piglet. This will give an MCC figure both before and after the optimisation (see below). Each of the models can also be compare against the PRx as the widely accepted standard for autoregulatory measurement thus allowing for a relative inter-model comparison to be performed. As the data set in use for the comparison has well defined observational end points they can be used as a target for optimisation.

### Optimisation

Each of the models assessed have at their core a window of data over which an analysis or comparison is occurring. For the PRx it is the amount of data used to determine the correlation function, with the HMF it is the collected data over which the slope of the line of the modal frequency change with time.

The modified Ursino model, while it has a window over which data is being processed, the model itself takes this into consideration as increasing the window would only linearly increase sampling frequency and thus merely smooth the output. Therefore lower values would result in the model prediction being more accurate where longer time windowed values will cause the prediction to deviate from the optimal value. The optimisation for this model could be considered finding the point between noisy and smoothed where the prediction is still accurate enough. However this is beyond the scope of this analysis. For these reasons the focus is on optimising the PRx and HMF models.

The optimisation itself is carried out using a quasi-Newton method [64] specifically the Broyden, Fletcher, Goldfarb and Shanno implementation in R [75]. This method maximises the determinant (Equation 3.1) of the sensitivity specificity matrix calculated

at a variable window size for each of the models in turn.

$$\mathrm{Det}(M) = T_P T_N - F_P F_N \tag{3.1}$$

The use of the determinant is merely for efficiency as there is no need to normalise this to calculate the MCC when optimising to a maximum value. The window sizes involved in the calculations are measured in the number of points used in the calculation.

## 3.3 Analysis and Results

In the case of an optimised solution to any of the models it does raise the question is the solution optimal for the number of points in the calculation or the underlying time windows those points would represent.

### 3.3.1 Optimisation of duration

To investigate this, the time base for the PRx was effectively doubled by increasing the frequency at which the original signal was initially sampled. The optimisation was then carried out again to see if an optimal solution could be found at the same number of points or at twice that which, if the latter, would show that it is the length of time which is important and not the points in the optimisation.

### 3.3.2 Modelling Time Effects

Initially a modelling analysis of variance (ANOVA) was performed to test whether the time difference measured from either start of the protocol or from time of the injury has any effect on predicted autoregulatory state of any of the models under examination. This was done by specifying a comprehensive general linear model of

| Model | AIC Weight |
|---|---|
| $Status \sim ARPred * Time * ModelType$ | 667.0304 |
| $Status \sim ARPred + Time$ | 621.7237 |
| $Status \sim Time$ | 618.8410 |

Table 3.2: Significant factors in autoregulatory status. Showing the Akaike Information Criteria weight reduction.

| Model | Baseline $MCC$ | Optimised $MCC$ | Optimised window (mins) |
|---|---|---|---|
| PRx | 0.09 | 0.25 | 66 |
| HMF | 0.09 | 0.55 | 72 |
| Ursino | 0.3 | n.a. | n.a. |

Table 3.3: Model predictive ability using $MCC$

Autoregulatory status (before or after injury) related to the interaction of predicted status, time difference and finally model type. A stepwise reduction in the model was then used to test the minimum number of factors that significantly contribute to the autoregulatory status. This analysis showed that time difference dominates in the model when run across the full time spectrum which can be interpreted as a contributory effect of the BP challenges in the assessment of autoregulation (AR) status in the model. The results shown in Table 3.2. This shows the Akaike information criteria (AIC) [2] of a set of models, which are denoted in the standard Wilkinson-Rogers notation [105], describing factors which may have a relationship to the known autoregulatory status. As the AIC becomes smaller relative to the initial model the fit to the data becomes better. If the AIC rises then the loss of that parameter would have been in error.

| Inter-model Comparison | Baseline $MCC$ | Optimised $MCC$ |
|---|---|---|
| PRx compared to the HMF | -0.55 | 0.47 |
| PRx compared to modified Ursino | -0.75 | n.a. |
| Modified Ursino compared to HMF | 0.73 | n.a. |

Table 3.4: Intermodel Comparisons using $MCC$

### 3.3.3 Model Comparison Pre-optimisation

To minimise the effect of this confounding effect of duration of BP challenge on model output, the MCC was only used on the first hour of challenge from the protocol start point. This gives the baseline comparisons as seen in Table 3.3 and inter-model comparisons as seen in Table 3.4. From table 3.3 the MCC results from the comparison between the model prediction and the known autoregulatory status were for the HMF 0.09 and the PRx 0.09 while the reworked Ursino showed an MCC of 0.3. The MCC correlation, much like the Pearson correlation $r$ value from linear regression, ranges from -1 to 1 where 1 is a perfect correlation and -1 is perfect correlation with an inverse value. The inter model comparison results from table 3.4 showed slight agreement between the HMF and the reworked Ursino model and a general disagreement between the PRx and both other models.

### 3.3.4 Optimisation Time Effects

The optimisation of both the PRx and HMF gave optimal window results of 660 and 720 points respectively. The re-optimisation of the PRx to investigate whether the solution reflected the number of points sampled or the represented the time period sampled gave a maximal model at 129 points which being double the previous number of points when sampled at twice the frequency indicates that it is the time period which is the relevant factor to optimise. This would give a final optimal value of 60 mins and 72 mins for each of those models respectively (Table 3.4). These optimal points can clearly be seen in the graphs of window size against determinant (Figure 3.4 and figure 3.5).

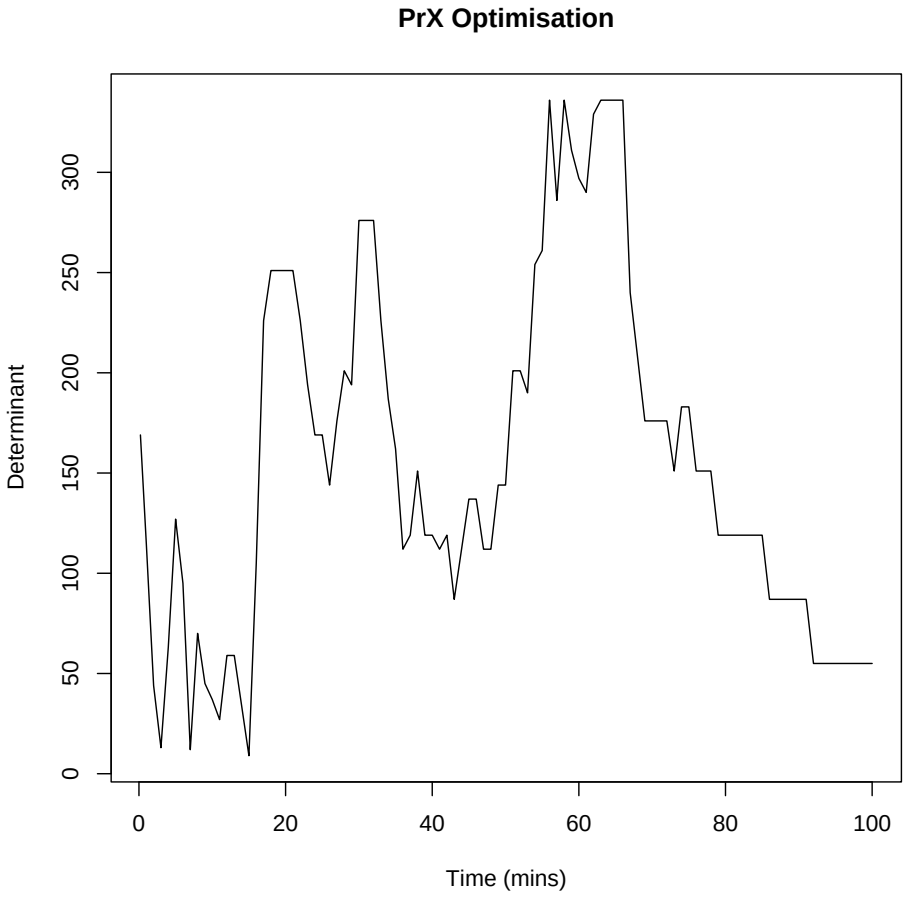


Figure 3.4: PRx model contingency table determinant vs. window size. The most optimal window size being estimated by the highest point which may not be shown on the figure due to the resolution of the plotted data.

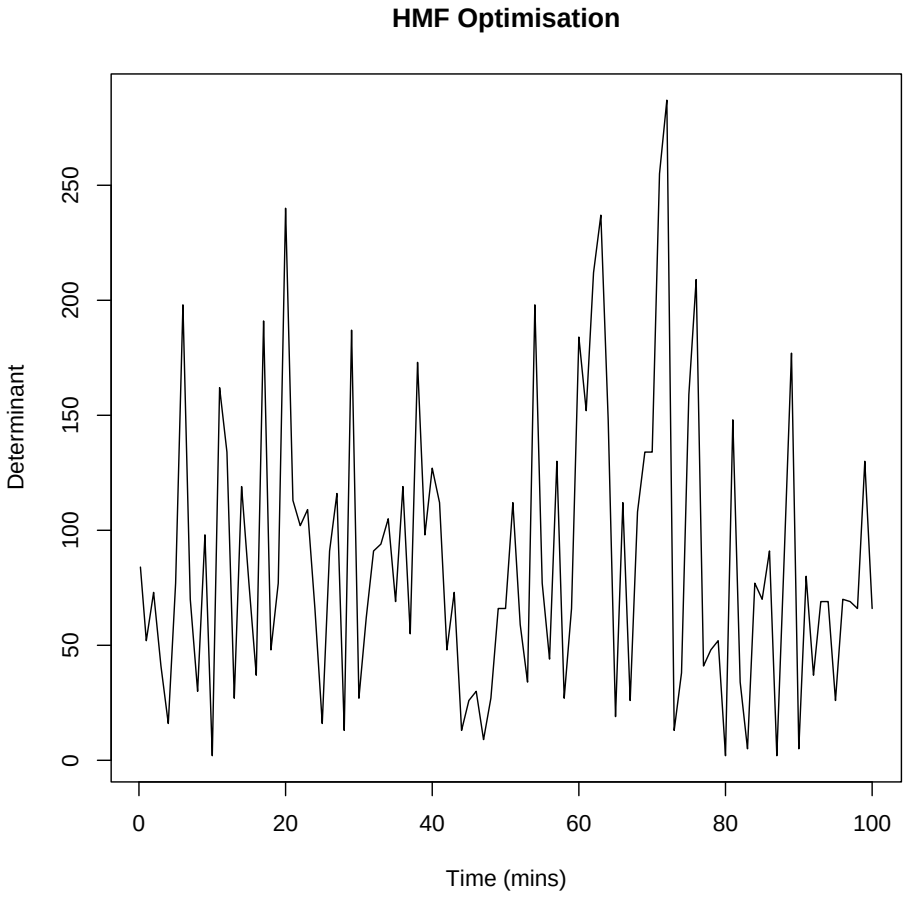


Figure 3.5: HMF model contingency table determinant vs. window size. The most optimal window size being estimated by the highest point which may not be shown on the figure due to the resolution of the plotted data.

### 3.3.5 Model Comparison Post Optimisation

Post optimisation the baseline model comparison can be seen in table 3.3 and the inter model comparison between the HMF and the PRx can be seen in table 3.4. Table 3.3 shows that the MCC for the PRx compared to the baseline known AR status is 0.25 and for the HMF is 0.55. Which if compared to the pre-optimisation values in table 3.3 shows there is between a two hundred and six hundred percent increase in predictive power after optimisation. From table 3.4 the MCC for the PRx compared with the HMF is now equal to 0.47 a distinct improvement over the initial inter-model comparison shown in table 3.4.

## 3.4 Discussion

With several models to choose from clinically, using the one which will derive the most accurate results from the vital signs data is important, and will impact heavily on the outcome and treatment plan for the patient undergoing the monitoring. The choice of model in the past has relied on what was clinically collectible and which model was in vogue at the time with no real methodology for rigorous comparison of multiple models either against a gold-standard or compared to each other. The reasons for this are easy to understand, as has been stated earlier, the general lack of a similar model output and a standardised statistical test for the comparison of models.

An important step in any comparative methodology would be standardising a data set to compare the models upon. Any data set could be used but to be fair to any model it would have to have a number of features. Firstly it has to have a known AR state so that you can definitively state whether the status is impaired or intact. Secondly it has to be of a high enough temporal resolution to evaluate all of the models, by this it is meant that if a model needs $250Hz$ data then minimally your

comparative data set would have to meet this resolution so as not to disadvantage the model under comparison. The dataset used in the study does meet these key points making it a viable candidate for the analysis however the question could be raised whether the end points used for comparison are correctly chosen. There is an accepted assumption that the each of the AR models are predicting a global measure of autoregulatory status. However, in this data set as the autoregulatory status are derived from the pial artery response recorded via the cranial window, do cover a relatively small area of observation with a small number of vessels being observed in each case. This could introduce a number of complications, firstly are the vessels under observation representative of the pial vasculature and secondly because of the small area under the cranial window, can this sample reasonably be thought of as a global measure of autoregulation. To address these points the method used to impair the cerebral autoregulation in this data set [27] should be considered. This was carried out via the fluid percussion injury model which has been used in many studies and is considered a standard experimental method for impairing AR. It has been shown to have a global effect on the physiology [88] even though in the collected data set it is monitored very locally via the pial artery-cranial window methodology. The general assumption is that the injury model is sufficient to give enough impairment to the pial vessels to be used as an analysis target. However intersubject variability including that of the vessel variability also needs to be considered [20].

Another key methodological issue is the choice of a comparison test. It is easy to lose sight of the goal of a simple but accurate assessment of the goodness of fit of the models to the data, when presented with the wide range of analysis options available in the literature to analyse the prediction data. On closer inspection however these options narrow to give a simple choice between only a couple of general analysis techniques. The first and possibly most crucial piece of information that the choice of test is based on is the output of the models, actual or surrogate, as this influences the range of tests that can be chosen. If the AR state prediction, intact or impaired, has been chosen

as the surrogate target then only tests on nominal data will be applicable as this is a dichotomous set of values. As shown in appendix C a compelling case can be made, in the case of the PRx, HMF and the surrogate $G$ parameter from Ursino's model, that model comparison using the Matthews correlation coefficient is optimal.

The application of this methodology was not without its challenges. For example the physiological dataset has missing data, artifacts and the occurrence of multiple BP challenges to assess AR status and other experimental manipulations that will reduce the amount of clean and usable data for the comparison. To address this point only the data directly preceding an AR assessment challenge was taken in order to reduce any physiological manipulation interfering with model predictions. Secondly, only data from the first hour was used to reduce sampling recovery effects after the autoregulatory impairment. This is pertinent as it was identified that AR impairment shows a clear time dependence with more intact AR assessment appearing the longer after the fluid percussion injury (FPI) they were assessed indicating that the cerebrovascular physiology gradually recovers post fluid percussion. Once these issues had been overcome the comparisons were assessed in two distinct ways: to the known AR status in each data set and also compared to each other. More specifically focusing on the comparison of each model to the PRx as this is considered the accepted AR assessment standard.

From the results of these comparisons (Table 3.3) it is easy to see that with the initial model configurations from their respective original papers, pre-optimisation, that the general predictive accuracy of all of the models are quite poor. This could be attributed in part to the data set used in respect to the inherent variability in the AR assessment using the pial artery diameter methods but also there will be variability due to choices made to try and reduce manipulation interference in the comparison data sampling. It is interesting to note how little inter model association (Table 3.4) there is between the HMF and PRx initially which does suggest that these models are predicting different

things.

As the predictive accuracy is much lower than expected for all of these models it led to the question whether the predictive accuracy of most of these models could be increased by the correct choice of window over which the data is sampled and analysed.

Optimisation relies on accurately understanding what is happening in a system and the correct choice of an optimisation target. In this case the underlying physiology of each of the piglets and the state of autoregulation. The methodology for autoregulation impairment has been shown already [88] to have a global effect on the physiology. Using this AR target, intact or impaired, it was straight forward to apply the technique of Nocedal and Wright [64] to optimise each of the models. The reason the Ursino model wasn't optimised along with the other two models is because the model in question is "temporally" independent. By that I mean it will work over any temporal resolution with the only consequence being smoothing the data set at lower resolutions. The less data you put in to the model the less data you get out of the model. So trying to increase the window size will only result in the window minimising to the same temporal resolution as the original data set as this will naturally increase the number points under consideration in the comparison and hence increase the chance of better prediction accuracy of the surrogate target. In essence this means that the variance of $G$ from the Ursino model will predict more points accurately if it has more points to work with and at its maximum that point would be a continuous estimate for the AR state. This of course is an idealised situation as there would probably be a point where there is more noise than signal at the extremely high temporal resolutions so it could decrease predictive ability at the highest resolutions.

The results from the optimisation of the HMF and PRx can clearly be seen to have had both an affect on the predictive ability of the models (Table 3.3) and the inter association of the two models (Table 3.4). One question is whether this optimal window size is defined by the number of points used for optimisation or is it related to the duration

time window fixed by the data. This was tested by rerunning the optimisation with double the sampling resolution for the PRx optimisation so it could be gauged if the optimisation result was point based or time based. With the result being that the more intuitive option of the optimisation is time windows dependent. These optimisation methods have been using the data set of the six piglets as a lumped model considering each of the piglets interchangeable with each other. To check whether this assumption was the correct, the optimisation was run again with each determinant calculated separately for each piglet and then a median value used as the maximisation end point. This approach provided a better approach for optimising, generating a maximal position which was more distinct from the rest of the trend, see figures 3.4 and 3.5. The window size however didn't deviate significantly from what was originally calculated in the first lumped determinant model.

With a methodology now in place for both model comparison and also optimisation there is a need to validate this on a second prospectively collected data set. Particularly a dataset providing a longer monitoring period post injury to allow investigation of optimisation windows beyond two hours, which was the maximum window size possible with the piglet data set. Application of single data set validation techniques like the K-fold cross validation approach frequently used in neural network training and testing wouldn't be appropriate here because of our finding that autoregulatory status is dependent on time post injury.

## 3.5 Conclusion

This work has provided a methodological approach to optimising data window size for testing models of autoregulation. A case has also been made for the use of Matthew's correlation coefficient (MCC) as a method of choice for model comparison. In the dataset we had available (Piglet data with fluid percussion injury using pial artery

visualisation), Ursino's physiological model performed best overall without any form of data window size optimisation. Post data window size optimisation only the data driven models could be compared of which Daley's HMF model showed better performance than the PRx model as a measure of the status of autoregulation. In view of the observed large variation in the autoregulation status with this dataset, further model comparison studies with other datasets and methods for testing dynamic autoregulation are warranted.

# Chapter 4

# Transcranial impedance

## 4.1 Introduction

Fifty percent of the years individuals spend with disability are caused by brain disease of which brain injury now carries an equal burden to patients as do those of cerebrovascular and depressive illness disorders [65]. The non-surgical management of patients with traumatic brain injury (TBI) focuses upon the prevention of secondary insults such as drops in arterial blood pressure (ABP) or intracranial hypertension. The latter, raised intracrainial pressure (ICP), is of particular concern as increases in ICP will decrease cerebral perfusion pressure ($CPP = ABP - ICP$) and can lead to decreases in cerebral blood flow (CBF), ultimately leading to ischaemia and cell death. Cerebral autoregulation is a physiological mechanism that maintains CBF constant in the face of changing CPP although it can become impaired following brain injury [37].

A number of indirect methods for determining autoregulatory status have been developed under these conditions which can be classed as "data driven" approaches. For example, Czosnyka et al have studied the correlation between inherent fluctuations in blood pressure (BP) and ICP deriving an index called the pressure reactivity index (PRx) which has been shown to relate to clinical outcome of patients and indirectly to the degree of autoregulatory impairment [25, 91].

The main limitations of general data driven approaches is that they rely on invasive measures of physiological time-series (such as ICP) and do not provide clinically useful information about the underlying mechanism for autoregulatory impairment which would prove useful in the appropriate targeting of medical management. An alternative to the data driven approach is to base autoregulatory status assessment upon a mathematical model of cerebrovascular fluid dynamics.

The best example of a purely mathematical model would be the class of "compartmental" models. These types of model are used prevalently in pharmacokinetics to model drug behaviour. One of the first uses of this approach in this area was to model a near

complete system of craniospinal dynamics [100, 101]. This all encompassing model however was considered too complicated to be used clinically and was later refined into a simplified form [102].

This model is only a simple two compartment model which includes: hemodynamics of the arterial-arteriolar cerebrovascular bed, cerebrospinal fluid production and re-absorbtion processes, the pressure volume relationship of the craniospinal compartment and a Starling resistor mechanism for cerebral veins. Autoregulation in this model can be thought of as a combination of three processes affecting arterial-arteriolar compliance for a given percentage change in CBF. The first process is the autoregulatory gain, the next is the static sigmoidal autoregulatory response function and the last component is a low pass transfer function. The maximum autoregulatory gain is defined to be the slope of the static autoregulatory curve at its centre point. It is from this autoregulation gain parameter that our new model is derived. The gain parameter $G$ is essentially a continuous index for cerebral autoregulation. With this in mind, Ursino's original model has been adapted to predict $G$.

However one limitation in the reworked Ursino model is that it needs a measure of arterial-arteriolar compliance which is difficult to measure in a clinical setting. In previous testing of the model this has been approximated in the past by the measurement of the arterial diameters and estimation of the volume using the physics of a venturi flow-meter [86] or a scaled version of intracrainial pressure (ICP) pulse amplitude [87].

A more direct non invasive method of measurement is required and transcranial impedance measurement is a possibility. Impedance rheoencephalography is not a new method [33]. However impedance measurements are now routinely carried out clinically as a gauge of intra and extra cellular water content across the whole body which in turn can be linked to the subjects' general well being. When this technique is applied to the cranial space the tissue impedance will depend upon intracellular swelling and the size

of the extra cellular space and so too does intracranial compliance. As there is a well defined exponential relationship between intracranial pressure and intracranial compliance there should also be a definable relationship between raised ICP and transcranial impedance.

## 4.2 Aims

This chapter aims to show the viability of a non invasive technique of measuring transcranial impedance and its relationship to ICP and ICP pulse amplitude. This will be achieved through both an experimental study in sheep and a normative study in humans. With these relationships between impedance and ICP established this provides an approach for relating a non-invasive estimate of compliance for use as a practical surrogate measure in the reworked Ursino Model.

### 4.2.1 Total body water measurement

Total body water (TBW) or whole body impedance (WBI) measurement is a measure of the ratio of intracellular to extracellular water content. To be more precise consider the circuit diagram, figure 4.1, the extracellular component is modelled by the bottom leg of the diagram and the intracellular component by the upper leg of the circuit. When an electrical signal of variable frequency is passed through a biological tissue modelled by such a circuit the signal passes mostly through the extracellular resistor at low frequencies but passes through both legs of the circuit simultaneously at high frequencies due to the reduced cell membrane reactance at higher frequencies.

If the resistance and reactance is measured and then plotted on a complex plane each of the vectors to those points will be an impedance ($Z$) reading (Figure 4.2). Cole-Cole

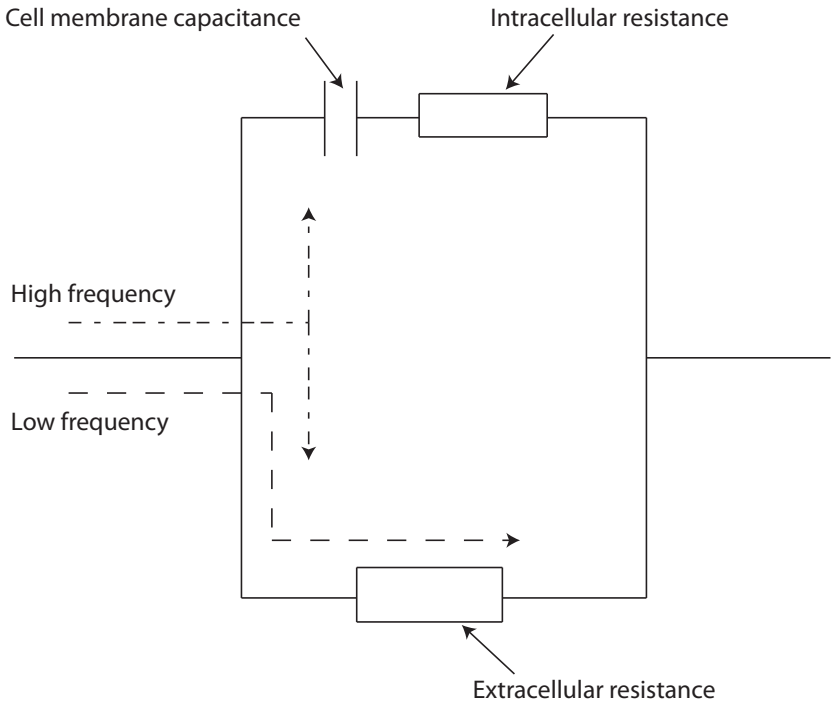


Figure 4.1: Cellular equivalence circuit for the basic path the current can take depending on the frequency of the signal.

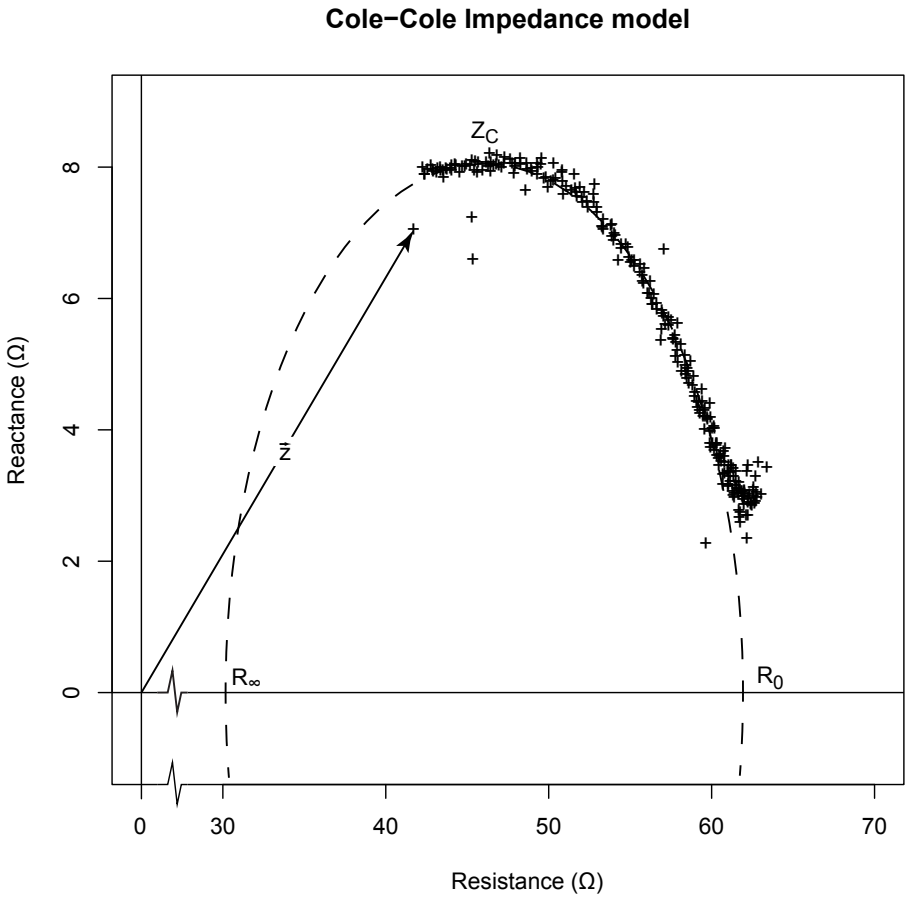


Figure 4.2: A basic example of an impedance plot with a Cole model fit. $\bar{z}$ is the vector of impedance the points where the circular fit crosses the axis are $R_0$ and $R_\infty$ respectively and the turning point of the fit is $z_c$ the characteristic impedance.

analysis [19] can then be used on these impedance measurements to estimate non-measurable features of the system. Firstly a circular fit to the data is then made and the resistance at infinite frequency, $R_\infty$, and zero frequency, $R_0$, can be estimated from the crossing points. The characteristic impedance, $Z_c$, can also be estimated from the turning point for the fit. From these values a TBW value is then calculated, normally from either $R_\infty$ or $Z_c$.

There are a number of mature technologies in clinical use which apply the above technique, Maltron Bioscan 916S [55] and the Impedimed SBF7 [43] to name two. All of the following studies have been carried out with the latter, the ImpediMed SBF7. This device has an operational variable frequency range of 3kHz to 1MHz and applies the Cole-Cole technique to calculate TBW values. This device has been assessed against a normative database with claimed accuracy close to 5% compared with direct measurement methods.

The feasibility of using this type of commercial technology for assessing transcranial impedance has been shown experimentally in a neonatal piglet model of brain tissue hypoxia, showing that transcranial impedance correlates well with both direct cerebral tissue impedance and raised ICP [53].

### 4.2.2 The main aims of the research

There are three main questions that need to be answered to give a basis for any further research into application of this methodology to be used as a surrogate measure of intracranial compliance. Firstly can a normal data range for the impedance when used “transcranially” be established in healthy normals. secondly what influence does electrode position have upon impedance in healthy normals? Lastly can evidence be provided that transcranial impedance relates to actual intracranial events?

| | |
|---|---|
| Number of volunteers | 50 |
| Gender | M = 19, F = 31 |
| Age | 21 to 64 (mean 39) |
| Height | 150 to 188cm (mean = 170) |
| Weight | 49 to 140kg (mean = 77) |
| BMI | 19 to 51 (mean = 26) |
| Head Circumference | 54 to 62cm (mean = 57) |

Table 4.1: Volunteer demographics

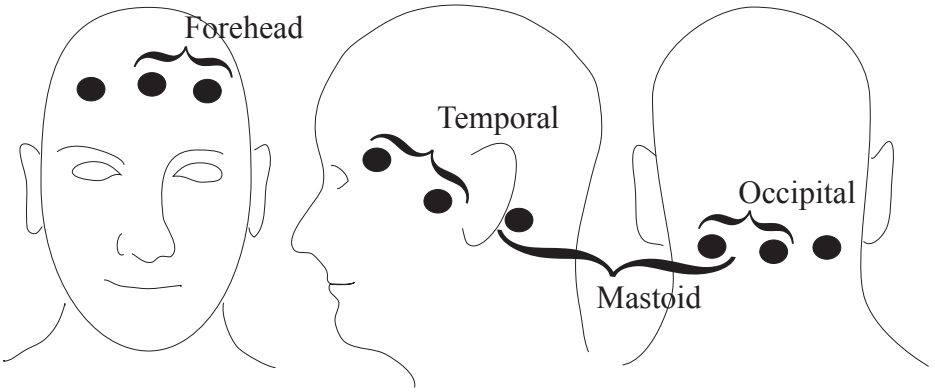


Figure 4.3: A representation of the impedance electrode positioning on the head. Two electrodes are depicted per position firstly for one end of the signal generation circuit and the second for the one end of the sensing circuit.

## 4.3 Material and Methods

### 4.3.1 Experimental protocol for the normative study

Fifty normal adult volunteers were recruited, table 4.1, with a gender split of 19 males and 31 females and an age range of between 21 to 64 with a mean of 39. On each of the volunteers the following electrodes were placed on the head, figure 4.3, for both the right and left sides at the following sites: forehead, temporal, occipital and mastoid. The skin at each electrode site was abrasively cleaned (using a gel abrasive) in order to ensure good electrode contact. All the electrodes were put in place before any measurements were taken, and no electrodes were removed until after all measurements were recorded. The volunteers details (height, weight, sex and age) were input into

the impedance device. The subject lay on their back on a bed and closed their eyes. Measurements were then taken from each pair of electrode sites: forehead to mastoid (FM), forehead to temporal (FT), forehead to occipital (FO), temporal to mastoid (TM) and finally temporal to temporal (TT). Where each measurement consisted of 20 signal sweeps from $3khz$ to $1Mhz$ in 256 steps, with total sweep time taking 40 seconds.

### 4.3.2 Experimental protocol for the animal study

#### Anesthesia

Five healthy adult female Blackface sheep were used for the experiments. They weighed between 46 and $60kg$ and were fasted overnight. Anesthesia was induced by intravenous etomidate ($0.5mg/kg$) and midazolam ($0.5mg/kg$) and the animal was intubated (Size 10.5 ETT). Ventilation was commenced with a tidal volume of $50cc/kg/breathe$ with 100% O2 and an isofluorane concentration of 1 MAC. Bilateral auricular artery cannulae were inserted for ABP monitoring, together with a saphenous intravenous cannula, see figure 4.4. Paralysis was with atracurium ($0.5mg/kg$). ECG, level of muscle paralysis and Endtidal $CO_2$, inhalational agent concentrations were all monitored continuously. Buprenorphine ($20\mu g/kg$) was given IV prior to surgery. During the experiment the animal received $10ml/kg/hr$ Lactated Ringers solution.

#### Neurosurgical Preparation

Once general anesthesia had been induced and all monitoring lines inserted and stabilised the head was positioned prone, in a semi-sitting position, with the cranium supported in a dedicated head rest. Two 21G needles were inserted into the lateral

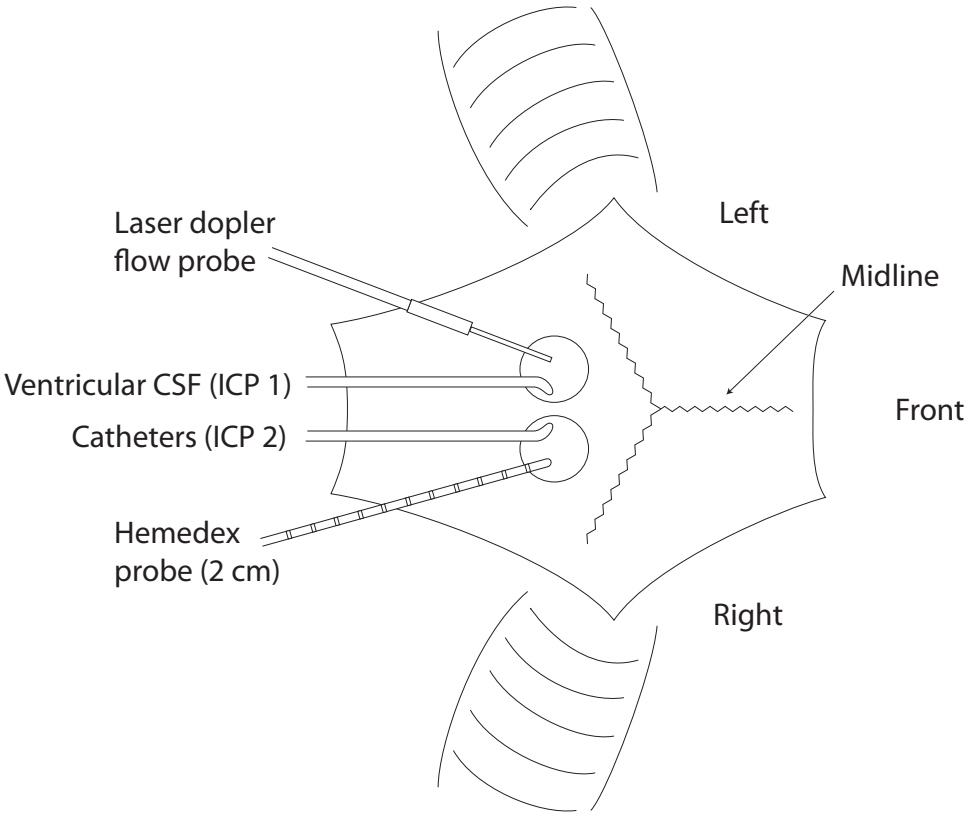


Figure 4.4: Schematic view of the monitoring preparation.

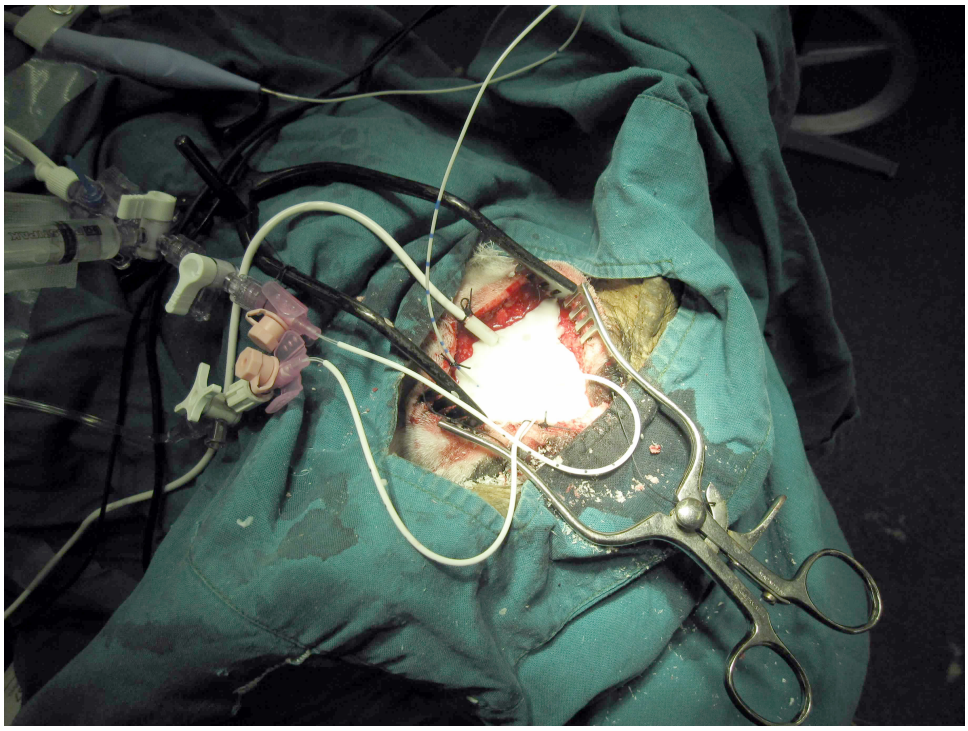

Figure 4.5: Actual view of the monitoring preparation.

side of each scalp and connected to the impedance monitor for measurement of intracranial impedance.

A midline incision was then made starting between the horns and going posteriorly $5 - 6cm$. A self-retaining retractor was positioned and the periostium elevated to display the junction of the metopic suture and the coronal suture. An 11mm burrhole was then drilled on either side of the midline (centre approximately $6mm$ lateral to midline) with one being centred $1cm$ behind the metopic suture and the other $15mm$ behind it. The dura was then diathermied and opened with an 11 blade. A dedicated ventricular catheter (Codman) was then passed into the lateral ventricle on either side. Accuracy of ventricular cannulation was confirmed by obtaining a good quality ICP waveform. A Hemedex (Codman) cerebral blood flow measuring probe was then placed in the brain parenchyma on the right side and a laser doppler flow probe on the left side through the burrholes. All monitoring lines were secured to the scalp using 2.0 Silk. The burrholes were then covered with chopped Surgicel (Johnson and Johnson) and filled with cold setting methylmethacrylate cement to make them water tight.

**ICP and arterial pressure manipulation and recording**

The arterial blood pressure was elevated using an infusion of phenylephrine ($10mg$) and adrenaline ($200\mu g$) mixed in $500ml$ normal saline. The ICP was elevated with an infusion of mock cerebrospinal fluid (CSF) into the opposite ventricular line to that used for the ICP monitor. All ABP and ICP monitoring was carried out via a Spiegelberg Compliance-Monitor CMP 27.1 instrumentation amplifier. From these monitors continuous waveform recording was carried out to a computer harddrive, figure 4.6. The experimental protocol was carried out in two distinct sections pre and post autoregulatory impairment. With the same main protocol steps being carried out in each run: Firstly readings of all monitored parameters (blood gases, ICP, ABP and $Z$) are taken and a baseline measurement of static autoregulation status via a BP

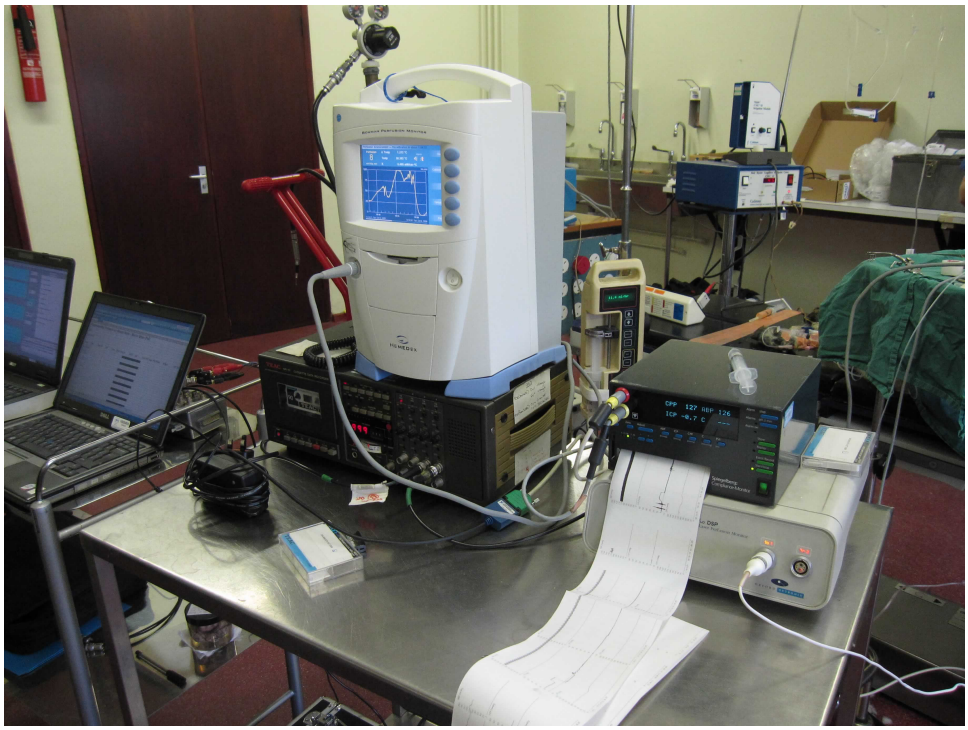

Figure 4.6: Monitoring equipment used in the study.

challenge was recorded. Then a stepped increase in ICP of $10mmHg$ was performed and all parameters measured again, this sequence was then repeated from baseline to highest achievable ICP level which was approximately $50mmHg$. Next normal cerebral autoregulation was disrupted through a period of prolonged systemic arterial hypertension ($MAP > 150mmHg$ for 10 minutes) and the main sequence of actions carried out again between an ICP of $10 - 50mmHg$.

### Removal and examination of the brain

At the end of the experiment the animal was sacrificed with a lethal dose of pentobarbital. A craniectomy was then performed and the brain removed and placed in 10% Formalin. After 48 hours fixation it was cut coronally and the parenchyma assessed for intracerebral contusion or hemorrhage, and the ventricles for evidence of any intraventricular hemorrhage. In all of the brains that were inspected post-mortem by an

| Electrode Position | Male Range | Female Range |
|---|---|---|
| Forehead to Mastoid (FM) | $65.8 \pm 15.0$ | $98.8 \pm 47.2$ |
| Forehead to Occipital (FO) | $72.7 \pm 15.6$ | $88.2 \pm 12.9$ |
| Forehead to Temporal (FT) | $60.3 \pm 16.3$ | $89.0 \pm 35.9$ |
| Temporal to Temporal (TT) | $58.2 \pm 24.2$ | $78.0 \pm 17.9$ |
| Temporal to Mastoid (TM) | $41.7 \pm 12.2$ | $70.2 \pm 55.2$ |

Table 4.2: Normative ranges (mean $\pm$ sd) for the characteristic impedance per electrode position

experienced neurosurgeon, nothing out of the ordinary was observed. These inspections while cursory and only done macroscopically by eye, were felt to be sufficient to be indicative of a viable experimental subject and hence the continued use of the dataset.

## 4.4 Results

### 4.4.1 The normative study

For this study the mean of the characteristic impedance value, $Z_c$, was taken across each of the 20 readings per electrode position per volunteer. Firstly an analysis of variance approach was applied to the data assessing the model dependence upon electrode placement, gender and whether the measurement was taken on the left or the right side of the head. This showed that there was no side to side bias in the data but there were highly significant ($p < 0.001$) influences by both gender and electrode position. Further investigation with a Tukey multiple comparison test then showed that the temporal to mastoid reading had a significantly lower mean value than the rest of the electrode placements. The gender split was then shown to have the female impedance readings higher than their male counterpart on all electrode positions. The main normative range is shown in table 4.2and illustrated in figure 4.7.

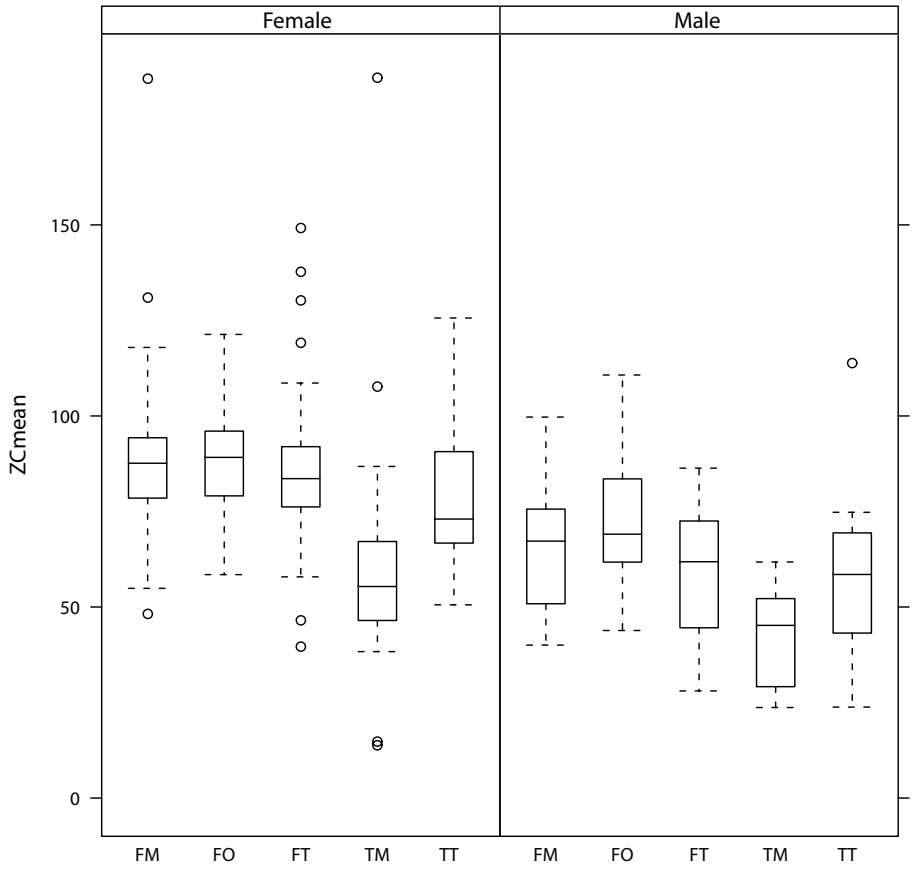


Figure 4.7: A box plot of the characteristic impedance per electrode position split by gender. The plot shows the difference in the temporal-mastoid (TM) group.

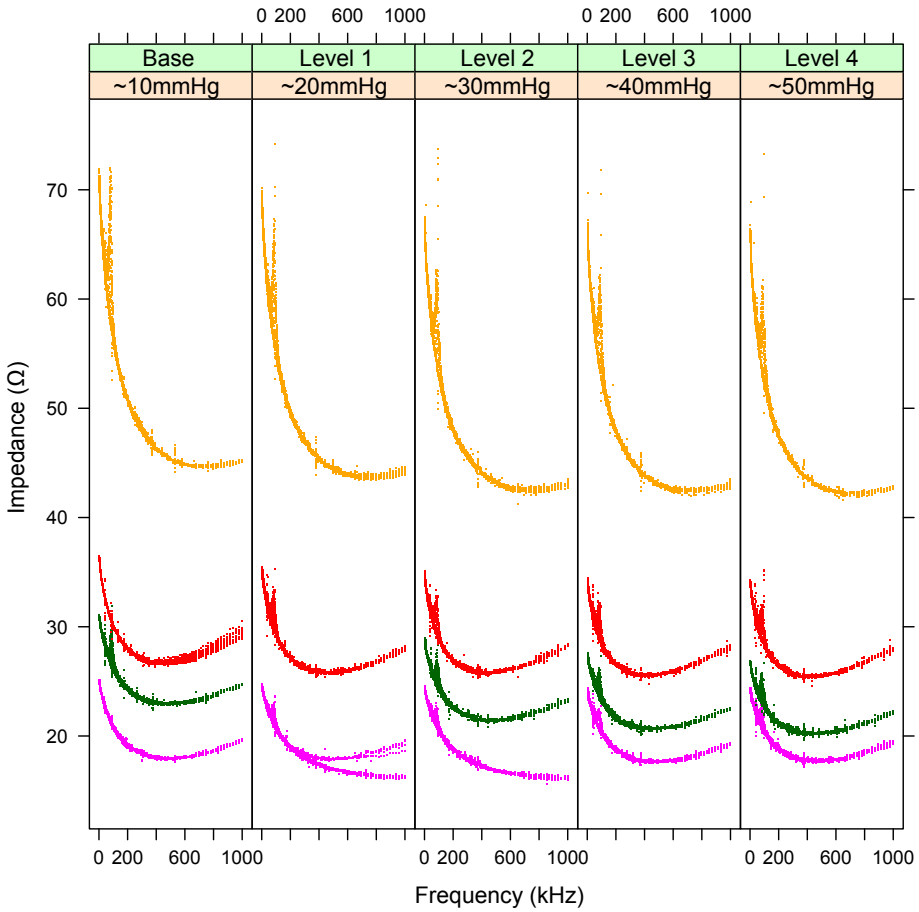


Figure 4.8: Plots per ICP level of the impedance versus frequency. Each colour represents a different animal.

### 4.4.2 The experimental study

For the animal study the data were analysed using a repeated measures analysis of variance (ANOVA) which looks at both within subject and between subject interactions in the model and accounts for any multiple sampling error that could occur. This analysis looked at the variance difference in the mean impedance value per animal per ICP step level, between $10 - 50mmHg$ in steps of $10mmHg$. The impedance values against their respective frequencies are shown in figure 4.8. This showed there was a statistically significant difference ($p < 0.007$) in these values per level. There is however a large inter animal variance in the data which is present at all ICP levels.

The absolute relationship between ICP and impedance has also been explored. To

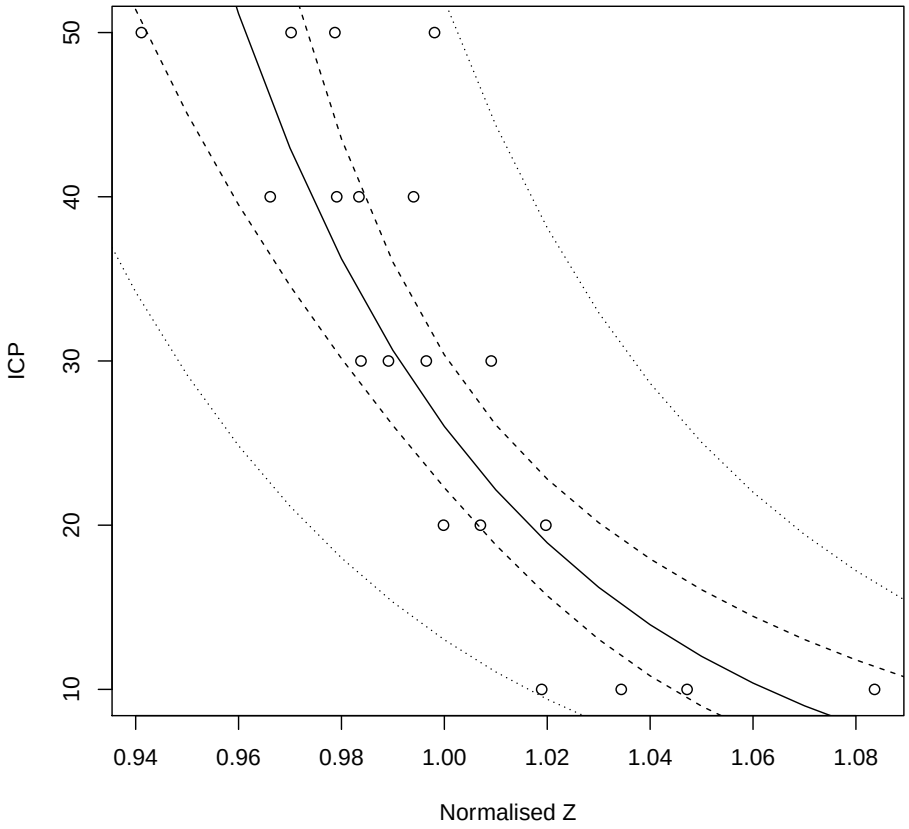


Figure 4.9: Regression plot through the mean normalised impedance per animal against ICP with confidence intervals shown as a dashed line and prediction intervals shown as a dotted line.

minimise the aforementioned variance in the data a normalisation technique was applied to the impedance data which included dividing each value by the mean of a subset of the data at the beginning of the set. This adjusts the output range of the independent experimental samples into similar ranges which can then be directly compared through adjusting the impedance for the animals baseline state. The mean value of this now normalised range was then taken per ICP level giving an overall summary for that ICP value. This was then plotted and the best fit simple exponential model $ICP = \exp(a/Z + b)$ fitted to this data, see figure 4.9. This gives an r-squared correlation of 0.7 and where $a = 16.225$ and $b = -12.967$. As can be seen in figure 4.9, there is a relatively constant set of regression limits with respect to the model, this adds

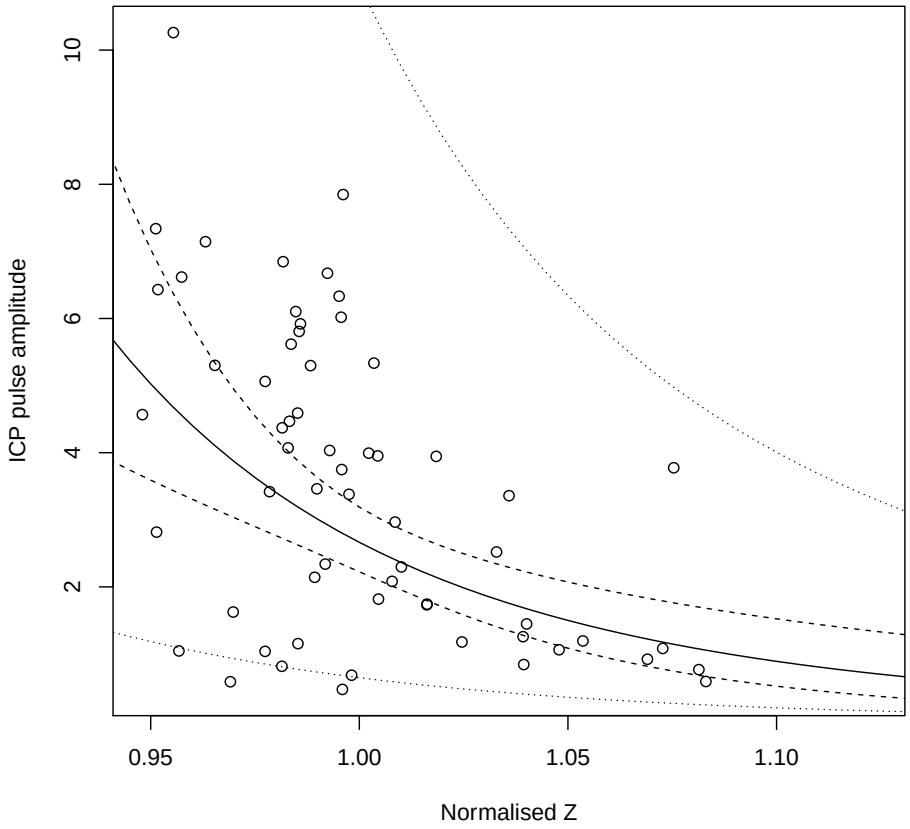


Figure 4.10: Regression plot through the mean normalised impedance per animal against ICP Pulse amplitude with confidence intervals shown as a hashed line and prediction intervals shown as a dotted line.

confidence that the model is correct for the given population and that any prediction based the collected data will follow the proposed model.

To make this result more practical the analysis was revisited, but this time the relationship between impedance and ICP pulse amplitude was studied. A similar process was carried out to the previous study where the impedance values were normalised by a division by the mean of a subset at the beginning of the data. The same model was then fitted to the data $ICP_{amp} = \exp(a/Z + b)$ which yielded $a = 12.059$ and $b = -11.079$. However the ICP pulse amplitude has more variability which results in a fit of only $r = 0.24$. This model is shown in figure 4.10 in which the variability can easily be seen in the widening predictive and confidence limits of the model.

## 4.5 Discussion

From the normative study analysis it has been shown there is a distinct placement effect for the temporal to mastoid electrode position measurement. Why this electrode pair position is so different to the others is most likely due to the current path length being considerably shorter for this electrode set compared to the other position pairs and thus more likely that more current flow is extracerebral rather than intracerebral. So in general any electrode set chosen for this type of measurement needs to have a long enough path length and by inference needs to cover a large enough part of the cranial space to ensure a stable intracerebral impedance value. This placement effect is also highlighted again in the animal study where the large inter-animal variance in the temporal to temporal electrode set is likely to be caused by placement differences. With the better understood landmarks for the human head this variance seen on the sheep should not be so prevalent in any further clinical studies.

It was also demonstrated from the normative study that there was no side-side bias which has a two fold application, firstly, by merging the left and right electrode position data, it effectively doubles our dataset per volunteer and yet keeps open the possibility to test for side to side differences due to midline shift in future studies. However, despite establishing a normative base-line for transcranial impedance these normative studies do not really answer the question whether this technique actually relate impedance to ICP and indirectly to compliance.

In the sheep study, the first of the five animals data were removed from the dataset as they were found to be physiologically unstable with an assumed infection. This made interpretation of the impedance data difficult, as all data values for this animal were a factor of 10 higher than the maximal point on all other animals. So it was deemed reasonable to exclude these outliers from the analysis. The remaining data clearly shows that there is a definable, reproducible exponential relationship between

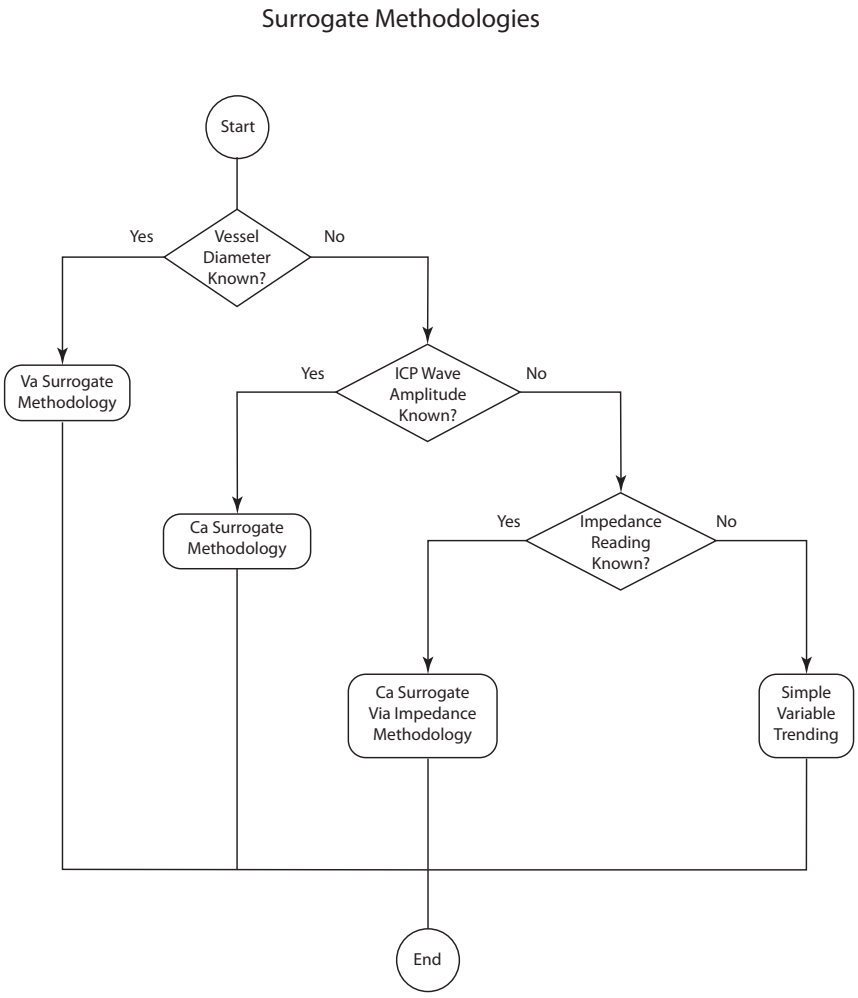


Figure 4.11: The flow chart showing the influence knowledge of vessel diameter and/or ICP wave form amplitude has on the chosen surrogate methodology now including the impedance methodology.

transcranial impedance and ICP or to a lesser extent ICP pulse amplitude. This has established the feasibility of using transcranial impedance as a surrogate measure of intracranial compliance as needed by the Ursino model. This would modify the surrogate measure flow chart, figure 2.3, in chapter 2 to be as shown in figure 4.11.

## 4.6 Conclusions

In general it has been shown that the cerebral impedance measurements are a viable and practical clinical technique and that it shows promise as a non invasive measure of ICP and its related parameter ICP pulse amplitude. A clinical study directly comparing transcranial impedance with invasive ICP will be required before a conclusive decision can be made on its use beyond the research domain. A normative range for transcranial impedance has been established, with a gender bias of higher impedance for females. Practically, any electrode positions that includes a large enough volume of the cranial space have been identified with forehead to occipital or temporal to temporal being the obvious choices. The dependence of Impedance measurement on ICP has been established and the absolute relationship between these two parameters has started to be explored. However further work is needed to identify which physical and physiological factors need also be measured to provide a more stable and robust measures of transcranial impedance.

# Chapter 5

# Pilot application of fractal characterisation and its response to change on physiological wave forms.

## 5.1 Introduction

Over the last two decades analysis techniques are moving from classical stochastic process analysis using basic statistics to more nonlinear systems or chaos theoretical based approaches which are looking at patterns in the variability of the time series. It has been shown that physiological time series exhibit complex multi-fractal properties [8]. So by designing a classification and analysis based on this nonlinear and chaotic nature of the time series we should be able to detect changes and alterations in the underlying physiological processes. To this end two different analysis scenarios were tested to gauge the feasibility of the technique, this is followed by a study of a noise reduction technique using wavelet thresholding. The first of the feasibility studies looks at the raw intracrainial pressure (ICP) wave form and characterising the fractal nature of a trending function itself based upon a windowing function of the raw waveform data over time.

## 5.2 Aims

The main aims in this chapter is to investigate a chaos based modelling technique which characterises physiological signals using a fractal summary measure and then to use this measure as an estimate of non physiological noise in the original signal allowing it to be removed via a modified hard thresholding wavelet smoothing technique. Initially the idea of fractal characterisation is defined and explored through two analyses looking at global and trending characterisation of a stable and unstable ICP signal. Then the noise reduction aspects of the chapter are assessed via comparison to a standard noise reduction technique.

## 5.3 Materials

Twenty randomly selected ICP waveforms from the BrainIT dataset [74] were studied for feasibility of the fractal analysis then the method applied to all of the Daley dataset [26] towards assessing its potential for reducing noise in the variability of the autoregulation (AR) index $G$ derived from the Piglet dataset. The R [75] statistical package was used exclusively for algorithm implementation and analysis.

## 5.4 Methods

### 5.4.1 Wavelet transforms and fractal derivation.

The main idea used in the initial analysis and fractal characterisation of the wave form leverages the relationship between the mathematical properties of a wavelet transform and a signal's localised fractal nature.

Wavelets [63] can be thought of as a time-frequency analysis technique analogous to a Fourier transform but without the inherent frequency related problems of the latter approach. This is mitigated by the fact the convolution is carried out with a scaling factor and a translational factor applied to the convolving function. Like Fourier transforms they can either be continuous or discrete the former implying that all scales are calculated the latter only integer scales are calculated. The actual transform is carried out via equation 5.1.

$$Wf(s,b) = \frac{1}{s}\int_{-\infty}^{\infty} f(x)\psi\left(\frac{x-b}{s}\right)dx \tag{5.1}$$

This is a scalable convolution with the $\psi()$ function being called a mother wavelet function and a scaled "s" and translated "b" variant of it known as a daughter function.

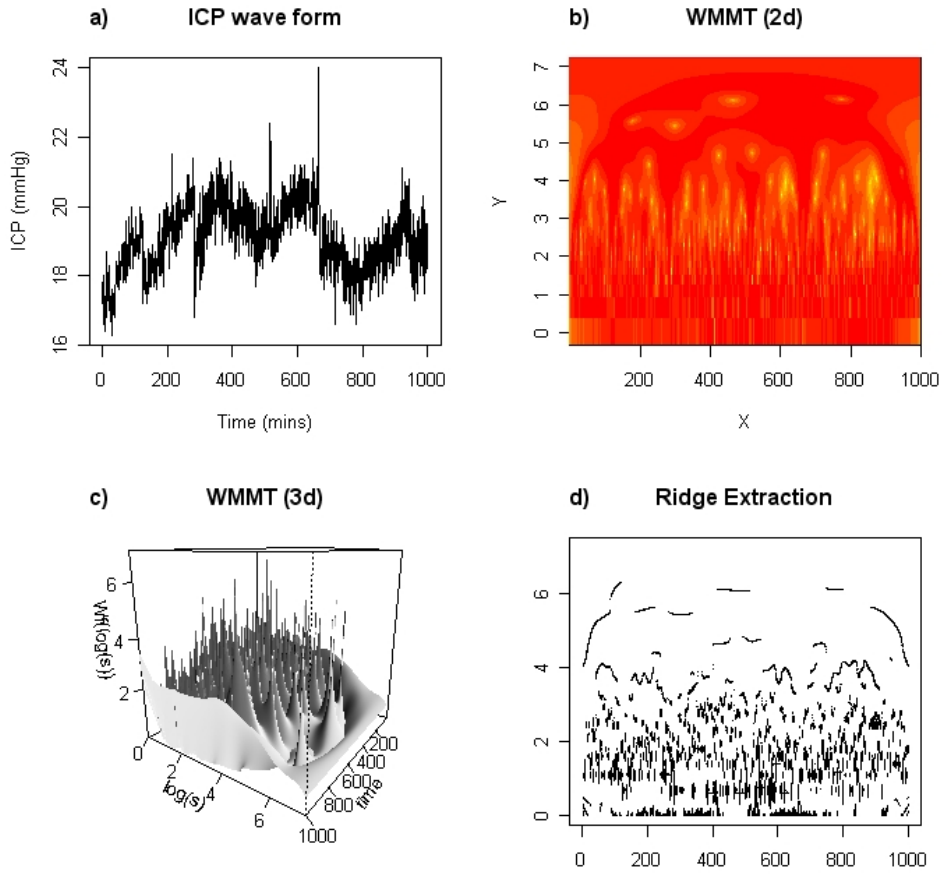


Figure 5.1: The basic stages of the characterisation technique a) Original ICP wave form, b) A 2d Wavelet Modulus Maxima Transformation of (a), c) A 3d representation of (b) and finally d) Ridge Extraction from (b) which selects the maximal points that have a discontinuous transition from those points around it.

In all of the later tests a Mexican hat wavelet mother wavelet (5.2) was used

$$\psi(p) = (1 - p^2)e^{-\frac{p}{2}} \tag{5.2}$$

which is the second derivative of the Gaussian function. Figure 5.1 is an example analysis using the above mother wavelet function on an ICP wave form.

Mandelbrot [56] defines a fractal as self similar signals repeating at different scales within the same signal. He also defines the Hurst exponent as a way of characterisation of the scaling properties of the signal that then can be thought of as an overview of the whole signal. However as we are interested in the signal on a more localised level, there

is a related value known as the Hölder exponent [84]. This essentially characterises the singularities of a signal at a single scale level. Where a singularity is defined to be a discontinuity in a signal where the differential of the signal is not continuous at that point. It can be shown that via the Taylor expansion [93] of the wavelet transform that equation 5.3 holds over the set of all singularities of the time series.

$$Wf(s, x_0) \cong |s|^{h(x_0)} \tag{5.3}$$

Where $x_0$ is the set of all singularities, $h(x_0)$ is defined to be the Hölder exponent of the singularity at $x_0$. However calculation of $h$ by using the full continuous wavelet transform is not efficient. If instead an optimised partitioning function and a counting argument [93] the "local" Hölder exponent can be calculated at a much reduced cost in time and complexity.

Firstly the wavelet modulus maxima transform (WMMT) is performed and then the ridges are extracted from this view [84]. This ridge representation of the signal is all that is required to calculate the local Hölder exponent; this should make the analysis more efficient as no redundant information needs to be processed. This form is in fact a representation of all the singularities in the signal. (Figure 5.1b, Figure 5.1d). Then by using a partitioning function, 5.4, over the set of all singularities $\Omega(s)$ at a given scale $s$

$$Z(s, q) = \sum_{\Omega(s)} Wf(\omega_i(s))^q \tag{5.4}$$

we can define the mean wavelet transform value of all singularities at that scale $s$ to be equation 5.5.

$$M(s) = \sqrt{\frac{Z(s, 2)}{Z(s, 0)}} \tag{5.5}$$

Finally, the mean Hölder ($\bar{h}$) is then calculated by solving for the slope of the straight line function 5.6.

$$\log(M(s)) = \bar{h} \log(s) + C \tag{5.6}$$

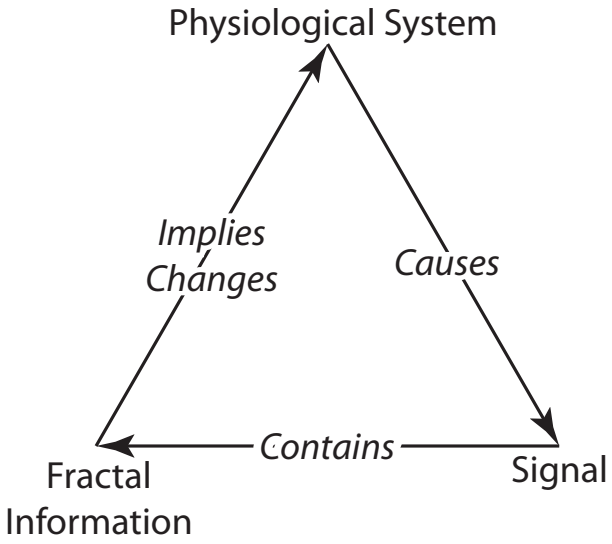


Figure 5.2: Schematic diagram of the relationship between the physiology, fractal characterisation and the signal produced.

It can then be shown [93] that the local Hölder exponent at scale s is calculated by equation 5.7

$$\hat{h}_{s_{lo}}^{s_{SL}}(s) \cong \frac{\log(Wf(s_{lo})) - \log(M(s))}{\log(s_{lo}) - \log(s_{SL})} \tag{5.7}$$

where $s_{lo}$ is the minimum scale used and $s_{SL}$ is the sample length.

This paradigm can be understood in terms that the waveform signal is caused by the physiological system and this signal contains fractal content or information which is directly related to the underlying physiology (Figure 5.2). This implies that changes to physiology will directly alter the signal and hence the information contained within. By using the above analysis techniques we gain an overview of this fractal information. To test these ideas, two general applications of the above method are presented; Firstly a global signal overview by looking at local Hölder distributions and secondly a more localised view of the data looking at the trending of the mean Hölder exponent.

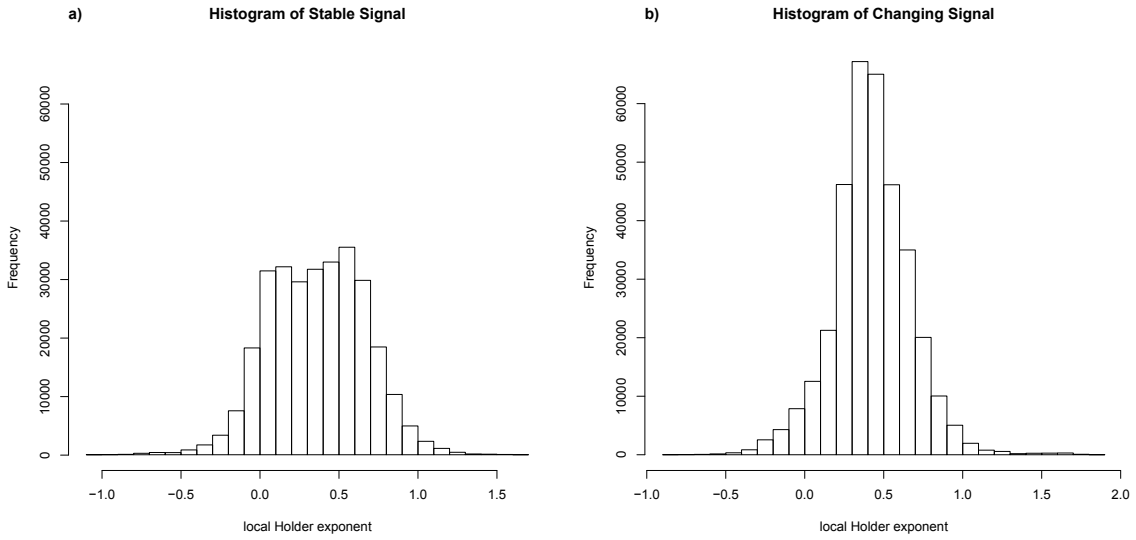


Figure 5.3: Comparison of a stable (a) and a changing (b) local Hölder exponent distributions shown over all scales.

### 5.4.2 Basic feasibility studies

This first methodology can be thought of as an overview of the waveform signals local Hölder exponent. Such a global look at the nature of the singularities of the time series should present a snap shot of the underlying physiology across the time range an approach akin to a "fingerprint" of the signal. ICP wave form data from a single patient was sampled from the BrainIT database and was split into a number of equal lengths: a "stable" segment where the signal remains relatively steady and the amplitude of the number of singularities remain low and a "changing" section, where the signal becomes more unstable and the amount and amplitude of the signal singularities increases. The local Hölder exponent calculated for each of these sections and the distribution of the local Hölder exponent was then plotted and analysed over all scales (Figure 5.3).

The second analysis technique to be applied looks at the change or trend in the mean Hölder calculation over the full time course of a signal. It can be thought of as a moving window approach, similar to a moving average, to viewing the Hölder exponents of a signal. This should represent the time course of changes in physiology of the patient. Again six ICP wave form signals were randomly sampled from the BrainIT dataset and

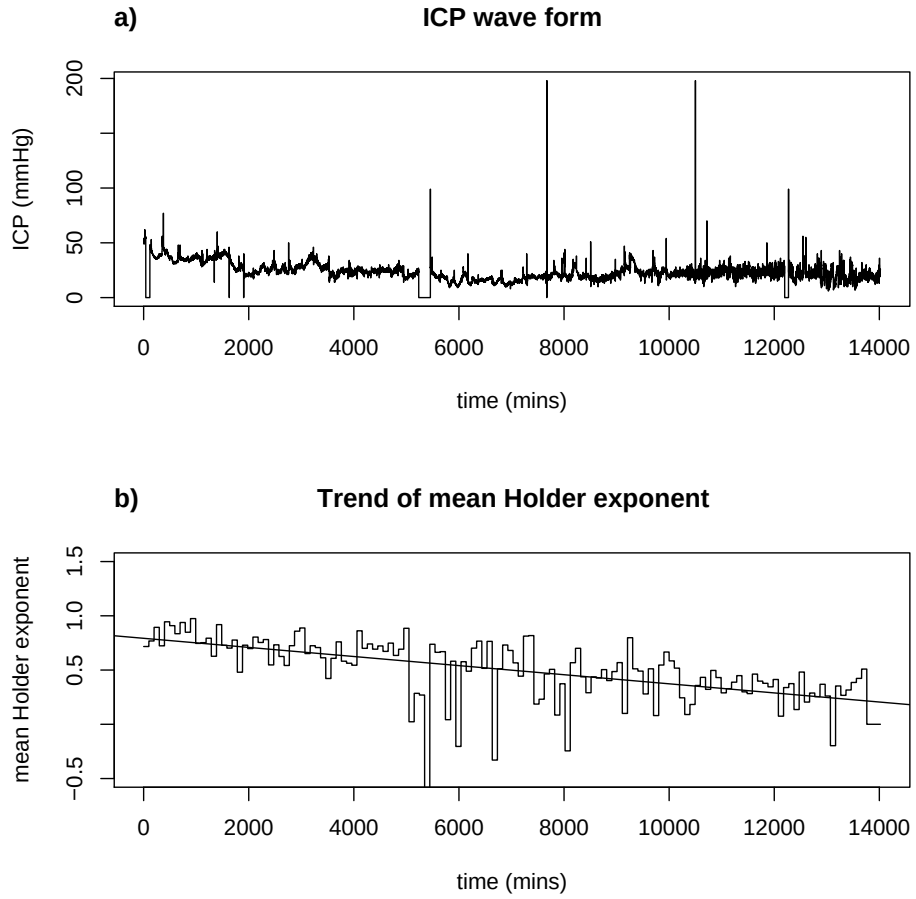


Figure 5.4: An example of an ICP signal (a) and corresponding mean Hölder exponent trend (b).

these were then cleaned and a moving data window approach was used to allow the repeated application of the mean Hölder function along the time course of the original signal. The window size used for this analysis was 200 minutes with a 100 minute overlap. The choice of this window size was arbitrarily defined by the signal length from previous testing. Once this approach was applied to the signals a linear regression was applied to give an overall trend for the calculated mean Hölder exponents (Figure 5.4).

## 5.5 Fractal characterisation as a noise estimate

### 5.5.1 Wavelet noise reduction

As the Hölder exponent is an estimate, per scale level, of the physiological content of the signal it can be used to dampen the noise using a classical wavelet noise reduction algorithm. At the heart of any wavelet noise algorithm is the wavelet transform, see equation 5.1, which decomposes a signal into a number of different scales and resolutions. Within the original signal most of the lower frequency portions of the signal will contain the overall trend of the original waveform and the higher frequency components will contain more of the noise along with any detail for the signal. When the wavelet transform is applied to the signal these frequency bands separate out and they then can be filtered individually to tackle any noise contained within. The second important fact is that wavelet decomposition transforms white, or gaussian, noise into white noise making it invariant under transform [29]. This is important if only noise is to be removed when executing the algorithm because the underlying signal will be transformed but the noise will remain the same so any removal will do so in both domains.

In general the process of using wavelets to reduce the noise in a signal typically follows these steps: Initially the noisy signal is decomposed via a wavelet transform from which the level of noise is then estimated. From this estimate a threshold is computed and then applied to the transformed signal after which it is then reconstructed using an inverse wavelet transform resulting in a signal which has had the noise component reduced [30]. The concept of thresholding is typically associated with the higher frequency components which after decomposition can readily be separated and once detected a measure (threshold) of the noise content calculated. Following this, when the signal is reconstructed, any signal above the threshold (noise) can be easily removed. When you reconstruct this altered signal there will be no noise above the threshold resulting in a less noisy signal overall without losing important physiological information.

There are two types of thresholding in common use in wavelet noise reduction. The first is hard thresholding which is what has been described previously and is essentially setting any values that are considered noise to zero before reconstruction the second is soft thresholding this is where the noise is set to zero and the signal reduced to make it continuous from the zero level boundary. This second method has application in image processing where discontinuities are easily spotted so reducing the hard change between the original signal and where the noise has been removed is advantageous in this context. However within the context of a physiological signal processing this in this way is unwanted as any reduction in the reconstructed signal will change the meaning significantly.

### 5.5.2 Noise estimation

Where fractal characterisation can play a role in this process is in the estimation portion of this algorithm. From Donoho and Johnson 1994 paper [30] the noise threshold should be calculated as equation 5.8.

$$t = \sigma\sqrt{(2\log(d))} \tag{5.8}$$

Where $d$ is the number of wavelet coefficients in the lowest frequency decomposition. This is intended to preserve the actual signal and find the level at which the correct signal degrades into noise. From Donoho et al's later 1995 paper [29] they give an estimate for the standard deviation $\sigma$ derived from the median absolute deviation (MAD)

$$\sigma = \frac{1}{k_w}\text{median}(|w_i|) \tag{5.9}$$

Where $k_w$ is constant equal to 0.6745 and $w_i$ are the wavelet coefficients again from the lowest frequency decomposition. This calculated threshold will only estimate a threshold based on the amount of information in the low frequency portion of the

signal. However the Hölder exponent may allow for a more tailored estimate of the noise across the whole signal and hence a better estimate of an optimal noise threshold. From equation 5.3 the relationship between the complete wavelet transform and the exponent can be seen, more importantly the wavelet coefficients can be generated by knowing the scale level and points of singularity within that scale. So if we firstly apply equation 5.8 to equation 5.9

$$t = \frac{1}{k_w}\text{median}(|w_i|)\sqrt{(2\log(d))} \tag{5.10}$$

Then by applying this to only the coefficients generated by calculating the local Hölder exponent from equation 5.7, and then using these to calculate a set of $w_i$ from equation 5.3, we will end up with a tailored threshold for a specific scale level based on the fractal characterisation of the signal at that scale level. This ultimately means that it can be applied over all scale levels not just the low frequency levels of the original paper. Which implies that it should cope with high frequency signals mixed in with the noise as well.

### 5.5.3 Assessing the wavelet technique against other common filtering approaches

Before carrying on with this analysis of this wavelet technique and its application to the Ursino model. It should be examined in the context of other noise reducing filters that are commonly used in signal analysis. To this end a simple comparison has been designed with a common Butterworth filter. The Butterworth filter [82] has a number of interesting properties: firstly it has a maximally flat frequency response at the point where part of the signal is retained that makes it well suited for use in noise reduction. Secondly it is easily adapted from one filter type to another, for example going from a low pass filter, that is one which allows low frequency signals to pass and removes high

| Type | Approximate Frequency ($Hz$) |
|---|---|
| Cardiac | 1.3 |
| Respiratory | 0.25 |
| Slow wave | <= 0.1 |

Table 5.1: Basic harmonic frequencies found in a normal ICP signal.

frequencies to a high pass one that is a filter that allows only high frequency signals to be retained.

To understand fully why the noise reduction comparison parameters and especially those associated with Butterworth filter are valid it is important to explore the frequency breakdown of ICP. Using a standard fourier methodology to create a periodogram for a normal ICP waveform, that is one which is at a base resting state in a healthy individual, it is expected to see a fundamental cardiac frequency at approximately $1.3Hz$ with the other major frequencies shown in table 5.1. It is commonly accepted that a physiological pressure wave is well represented by considering a maximum of 10 harmonics of the fundamental. Thus if we take a worst case of 120 beats per minute heart rate, which is $2Hz$, then to faithfully represent the blood pressure (BP) signal would require a bandwidth of $20Hz$. Assuming 5 times oversampling to avoid aliasing artifacts than a sampling rate of $100Hz$ is appropriate. As the major frequencies in the ICP signal are all less than what the butterworth filter has been designed to filter this will ensure that none of the frequency components of the original signal are lost during processing. In general filters also affect both the amplitude and the phase of the returned signal compared to the original and this generally has to also be considered. A Butterworth filter was originally created to be "maximally flat" which means that the amplitude response in the part of the signal it passes should not be affected but there will be a slight phase variance in the returned signal at frequencies close to the cutoff frequency of the filter. For the purposes of this comparison the phase response of the filter should not disadvantage it against the wavelet technique.

To examine the performance of the wavelet technique an ICP signal was extracted

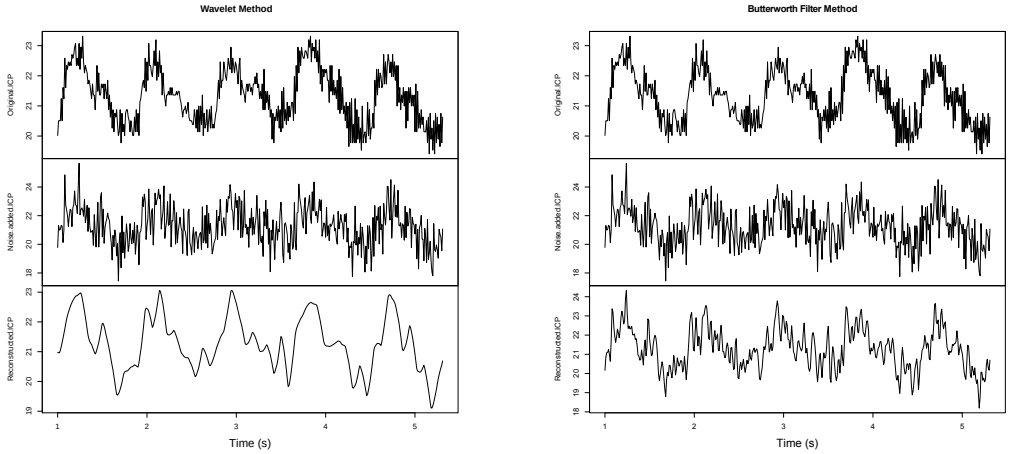


(a) (b)

Figure 5.5: Plot of the evaluation stages of the noise reduction techniques where (a) is the Wavelet technique and (b) is the butterworth filter. On the upper panel of both plots is the raw ICP signal, in the centre is the raw ICP signal with noise added finally on the lower panel is the reconstructed wave after the specific technique has been applied. Each of the techniques are assessed via comparison to the original signal.

| Noise reduction technique | Pearson correlation | Confidence Interval |
|---|---|---|
| Wavelet | 0.83 | (0.78, 0.86) |
| Butterworth | 0.75 | (0.71, 0.79) |

Table 5.2: The two noise reduction techniques correlation with the original ICP signal.

from an experimental dataset. Normally distributed random noise was generated with a mean of zero and a standard deviation of one. This was then added to the ICP sample to give a measurable and consistent amount of additional gaussian noise on the ICP trace. As this ICP signal was recorded at 100Hz and the noise was added one to one with the signal a butterworth filter was constructed to remove all noise above 200Hz. The wavelet technique will estimate the variance as shown above.

Each of the noise reduction techniques were applied to the original ICP signal and the results are shown in figures 5.5a and 5.5b. The reconstructed signals were then compared to the original ICP signal. The results can be seen in table 5.2, the wavelet techniques gave a correlation of $r = 0.83$ with a 95% confidence interval of $(0.78, 0.86)$ and the butterworth filter had a correlation of $r = 0.75$ with a confidence interval of $(0.71, 0.79)$.

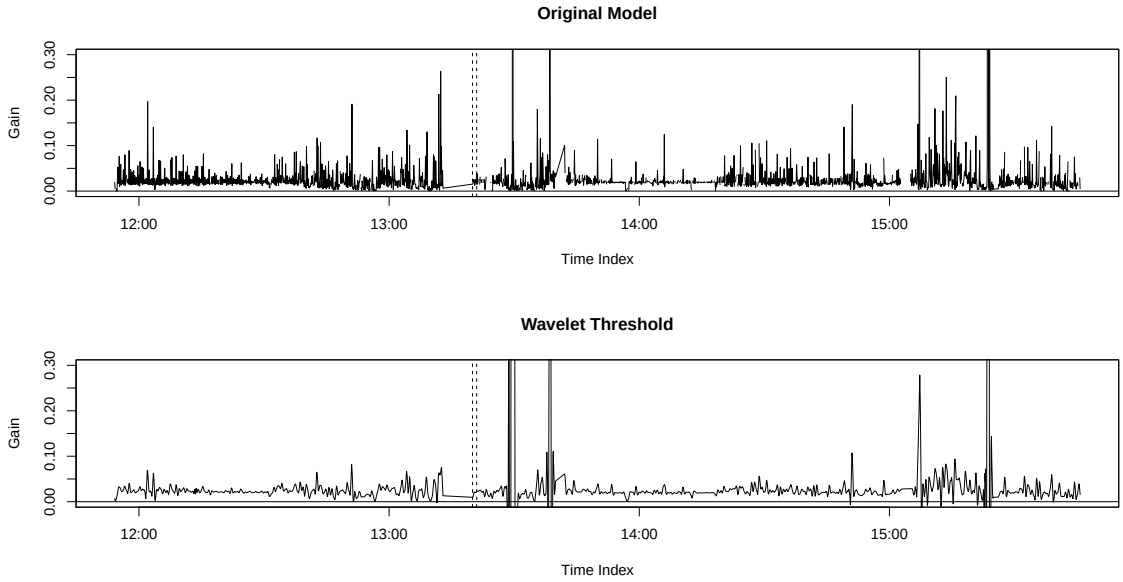


Figure 5.6: An example of the wavelet noise reduction technique applied to the reworked Ursino model.

Both of these results are quite close to one another but the wavelet technique has a slightly better correlation. This is not the only advantage this technique offers, over the Butterworth filter in addition, the fractal characterisation is fully automated. By that I mean the noise estimate is deterministic and therefore repeatable. While techniques do exist to estimate a required frequency cutoff [31] of the Butterworth filter it is normally done manually which is an issue if this technique is to be used in a more clinical setting.

### 5.5.4 Application to the reworked Ursino model

The usefulness of this noise reduction technique can be assessed by applying it to the reworked Ursino model (Chapter 2) where its ability to optimise the prediction process by suppressing the amount of ancillary noise in the output and thus allowing the actual predictions to become more prominent. Using the Hölder addition the wavelet noise reduction algorithm was applied to the Daley dataset, an example of the resulting smoothed signal can be seen in Figure 5.6. But to test this more fully, 200 random

| Model | $MCC$ | Confidence Interval |
|---|---|---|
| Original | 0.06 | (-0.04,0.16) |
| Wavelet | 0.21 | (0.11,0.3) |

Table 5.3: Predictive accuracy for both the original model and the wavelet smoothed variant.

samples were selected from the dataset, before and after autoregulatory impairment and the $MCC$ calculated for both signals and the confidence interval estimated using the Fisher's $z$ approach. The results can be seen in table 5.3.

## 5.6 Discussion

For the first analysis looking at the distributions of the Hölder exponents between a stable and unstable ICP signal, as can be seen from (Figure 5.3) there is not much if any separation in the distributions and this is representative of all samples tested. This is not totally unexpected as the differences in the ICP waveforms tested between stable and changing signals are not significantly different mathematically. These types of signals are minimally deterministic, that is they have both deterministic and random processes [76] effecting them so are less likely to have greatly different fractal "information" content. If this is the case then this technique should be then aimed at more deterministic signals such as looking at ICP B-wave activity in the ICP trend.

In the analysis on trending of the mean Hölder it can be considered to be inversely proportional to signal fractal information content. However quantification of this is difficult as we would need an independent measure of the signal stability to statistically compare it with the trend gradient. That said over all the samples tested the gradient does show a predictive ability (Figure 5.4) where it can be seen that the decreasing trend in the Hölder exponent appears to precede a marked increase in ICP instability and ICP pulse amplitude. The technique itself with the moving window application of the function needs more study to find the optimal size for the window measured and still

provide enough signal to accurately represent it with the mean Hölder exponent.

Finally, the most useful application of the localised Hölder exponent is in a noise reduction capacity. The addition of the Hölder exponent as a measure of the signal content allows for a more tailored noise reduction than the "standard" noise estimation methodologies. This can be seen in the 350 percent increase in predictive accuracy however I feel further study of this may be warranted as the confidence intervals are quite large by comparison.

## 5.7 Conclusion

It has been shown in this chapter that the new noise reduction technique which mixes the new fractal characterisation of the physiological system and a classic wavelet smoothing technique is both a viable and practical alternative to more conventional signal processing techniques. This has resulted in a 16 percent improvement over the comparable alternate Butterworth filter method and a 350 percent improvement over the base model. Overall this pilot study has only scratched the surface of possible areas in which these techniques may find application. Further research is required to study the implications of the links between the physiological systems and the fractal information content of the signals they contain. In the context of cerebral autoregulation research, fractal methods will find application in processing model output and with removing non-physiological noise from these signals.

# Chapter 6

# Analysis of a cerebral autoregulatory indices relationship with outcome in head injured patients

## 6.1 Introduction

Cerebral autoregulation, as has been stated previously, is the process by which cerebral blood flow (CBF) is maintained relatively constant over a specific cerebral perfusion pressure (CPP) range. This has been shown to have a relationship with outcome using other models of autoregulation [23] which raises the question does the reworked Ursno model relate to clinical outcome in a similar fashion?

While direct comparison of the three models (pressure reactivity index (PRx), highest modal frequency (HMF), Ursino) relationships to outcome would be preferable this is unavailable at this time due to limitations in the dataset, namely lack of the temporal resolution required to accurately execute both the PRx and HMF models, so only the reworked Ursino will be assessed at this time.

To evaluate the reworked Ursino model's relationship to outcome the performance of the new model was tested firstly, directly against clinical outcome, secondly, when combined with other clinical prognostic factors and finally to analyse its trend over time to quantify how the level of autoregulation changes temporally post-injury.

## 6.2 Aims

With any new clinical model the question will arise of whether this new parameter will add to the existing domain knowledge. To explore this, this chapter outlines work investigating the relationship between the new model output to a model of clinical outcome.

## 6.3 Methods

As was shown in chapter 3 cerebral autoregulation in the original Ursino et al's model can be thought of as a combination of three processes affecting arterial-arteriolar compliance for a given percentage change in CBF. It is from this continuous index for cerebral autoregulation $G$ that the new model is derived. With this in mind Ursino's original model has been rearranged to predict $G$. In the validation of the new model it has been found that the variance of the $G$ parameter is a closer predictor of autoregulation [87].

As with previous testing of the model the relative change in arterial-arteriolar volume has to be considered. This has been done in the past with the measurement of the arterial diameters and estimation of the volume using the physics of a venturi flowmeter [9]. This time however as there were no arterial diameter parameters available, the intracrainial pressure (ICP) pulse amplitude technique was used as an estimate for this parameter. As has been shown in chapter 2, this is a reasonable approach to consider as there is good evidence that ICP pulse amplitude relates to intracranial compliance ($C_{IC}$) and that $C_{IC}$ can be related to arterial-arteriolar volume ($V_a$).

## 6.4 Analysis

Twelve patients were sampled from the BrainIT database [73] with measurable ICP pulse amplitude, it required patient's with monitoring systolic and diastolic ICP values, and had a good spread of clinical outcome as measured by the extended Glasgow outcome scale (GOSe) [45]. This is an eight point scale, shown in table 6.1, which gives a measure of the recovery process. It is based on the earlier Glasgow outcome scale (GOS) [44] and is normally assessed via a structured questionare [106]. The GOSe has become the gold standard measurement in clinical practice for outcome measurement

| Score | Meaning |
|---|---|
| 1 | Dead |
| 2 | Vegetative state |
| 3 | Lower severe disability (completely dependent on others) |
| 4 | Upper severe disability (dependent on others for some activities) |
| 5 | Lower moderate disability (unable to return to work or participate in social activities) |
| 6 | Upper moderate disability (return to work at reduced capacity, reduced participation in social activities) |
| 7 | Lower good recovery (good recovery with minor social or mental deficits) |
| 8 | Upper good recovery |

Table 6.1: Extended Glasgow Outcome Score (GOSe) and associated meaning

in patients with traumatic brain injury (TBI). The GOSe also compares well to other scoring systems [52, 107] which are in use in this population of patients.

Using the new model, the absolute value of $G$ was calculated for the full patients monitoring time course. The data for each of the patients was then split into three equal time periods (early, middle and late) and the variance of $G$ in each period calculated. Patients were then grouped by a dichotomised GOSe ("good outcome" GOSe $> 4$ and "poor outcome" $\leq 4$). The outcome sets for the late time period were then compared to each other time period using a one sided Student's t-test. These late periods were considered as they should show the greatest accumulative effect of autoregulatory state on the outcome. This analysis was used to test if impaired autoregulation was representative of poor outcome, specifically that the mean variance was greater for poor outcome than good outcome.

Secondly the twelve patients were reanalysed with respect to outcome but in this case the time period being considered was only during the first 48 hours post-injury as this can be considered more clinically relevant. The model was then augmented to include some of the more classical prognostic factors such as age, sex, Glasgow coma scale (GCS) motor scores previously shown to influence clinical outcome (GOSe). One of the latest predictive models for outcome in a head injured population, the International Mission for Prognosis and Clinical Trial design in TBI (IMPACT) study, was used

[54, 59] and those international mission for prognosis and clinical trial design in TBI (IMPACT) parameters which were available from the BrainIT dataset for the original twelve patient dataset were included and then the outcome analysis was performed again. The new IMPACT model has a distinct similarity in the final model parameters chosen with a number of older outcome studies [18, 41, 42, 90, 92]. Out of all the parameters, age and GCS motor score on admission, were included in all models as they have a high predictive value against outcome [40]. A stepwise regression technique [104] was then applied on this model to assess how much of a contribution to the model outcome the autoregulatory index gave.

The time course of autoregulation was also looked at over the duration of stay in all patients. The length of stay was divided into ten distinct segments which will allow a consistent overview of each of the time courses. These patients were then grouped by their dichotomised GOSe thus allowing comparison of the basic trend. var($G$) was calculated for each of these sections and a median value was then taken across all patients in each of the ten time groups, giving a ten point trend of autoregulatory status over each patient.

## 6.5 Results

The general model output for all patients in the study is shown in table 6.3. With the basic demographics of the patients given in table 6.2.

The results of the first analysis (Figure 6.1a) using a one sided t-test showed that there was a significantly greater mean variance in the parameter $G$ for autoregulation in the poor outcome set compared with the good outcome set($p = 0.033$). The results of the second analysis (Figure 6.1b) using a one sided t-test showed that the mean variance wasn't significantly greater than the other time-points (p=0.871).

| Patient ID | First 48hrs var($G$) | Percentage Late var($G$) | GOSe | Outcome |
|---|---|---|---|---|
| 04027262 | 1.325984e+03 | 1.428077e+02 | 1 | poor |
| 04816150 | 1.327917e+01 | 1.039321e+00 | 8 | good |
| 16137372 | 9.197743e+01 | 2.557953e+00 | 7 | good |
| 26248362 | 3.003330e+00 | 3.042090e+02 | 4 | poor |
| 27240484 | 2.448823e-03 | 3.028827e-03 | 1 | poor |
| 38351504 | 1.851523e+01 | 8.296829e+01 | 1 | poor |
| 48355050 | 6.402678e+00 | 2.089445e+02 | 1 | poor |
| 51573727 | 4.048400e+03 | 1.908241e+01 | 1 | poor |
| 61683383 | 5.619044e+01 | 8.150098e-05 | 8 | good |
| 73684838 | 2.712204e-02 | 1.220374e+00 | 1 | poor |
| 83815161 | 8.383307e+01 | 4.652178e+01 | 5 | good |
| 84861515 | 2.074122e+00 | 2.817550e-01 | 8 | good |

Table 6.2: Summary of var($G$) for the first 48 hours and for the last third of the patients stay.

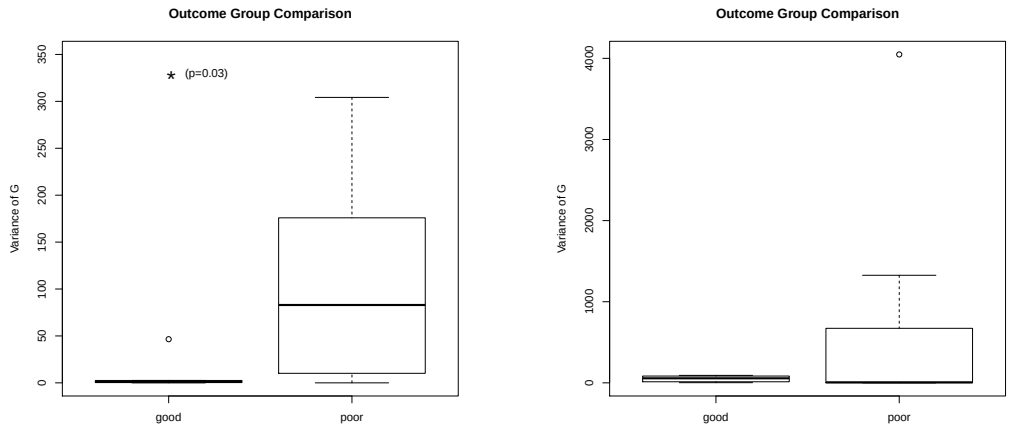


(a) (b)

Figure 6.1: A comparison of the autoregulatory index dichotomised via "good" and "poor" outcome groups in both (a) the "late" period analysis and (b) the first 48 hour analysis

| Model | AIC Weight |
|---|---|
| $Outcome \sim Age * Sex * GCSEye * GCSMotor * ARIndex$ | 22 |
| $Outcome \sim Age + GCSEye + GCSMotor + ARIndex$ | 10 |
| $Outcome \sim Age + GCSEye + GCSMotor$ | 8 |

Table 6.3: Akaike Information Criteria weight of each reduction step of the predictive model

| Step | Model Component Removed |
|---|---|
| 1 | Base Line Model (Nothing Removed) |
| 2 | $-Age : Sex : GCSEye : GCSMotor : ARIndex$ |
| 3 | $-Sex : GCSEye : GCSMotor : ARIndex$ |
| 4 | $-Age : GCSEye : GCSMotor : ARIndex$ |
| 5 | $-Age : Sex : GCSMotor : ARIndex$ |
| 6 | $-Age : Sex : GCSEye : ARIndex$ |
| 7 | $-Age : Sex : GCSEye : GCSMotor$ |
| 8 | $-GCSEye : GCSMotor : ARIndex$ |
| 9 | $-Sex : GCSMotor : ARIndex$ |
| 10 | $-Age : GCSMotor : ARIndex$ |
| 11 | $-Sex : GCSEye : ARIndex$ |
| 12 | $-Age : GCSEye : ARIndex$ |
| 13 | $-Age : Sex : ARIndex$ |
| 14 | $-Sex : GCSEye : GCSMotor$ |
| 15 | $-Age : GCSEye : GCSMotor$ |
| 16 | $-Age : Sex : GCSMotor$ |
| 17 | $-Age : Sex : GCSEye$ |
| 18 | $-GCSMotor : ARIndex$ |
| 19 | $-GCSEye : ARIndex$ |
| 20 | $-Sex : ARIndex$ |
| 21 | $-Sex : GCSMotor$ |
| 22 | $-Sex : GCSEye$ |
| 23 | $-GCSEye : GCSMotor$ |
| 24 | $-Age : GCSEye$ |
| 25 | $-Age : GCSMotor$ |
| 26 | $-Age : Sex$ |
| 27 | $-Sex$ |
| 28 | $-Age : ARIndex$ |
| 29 | $-ARIndex$ |

Table 6.4: The set of terms removed from the original model by the stepwise reduction. Where a term name is shown as standard *italic* text and $x : y$ means $x$ interacting with $y$ in the model. With greater influence being shown by a larger step number, although not enough to remain in the final model.

The next analysis results are shown in table 6.3 and in table 6.4. Using the Akaike information criteria (AIC) relative reduction weights to find the best fit showed that $Outcome \sim Age + GCSEye + GCSMotor$ was the best model. However it should be noted that from the actual reductions (table 6.4) that both the autoregulation (AR) index and the AR index's interaction with age were the last to be removed. Indicating that they have a more significant model contribution than any of the other removed parameters. However not enough contribution, on this dataset, to warrant inclusion in the final model.

Figure 6.2 shows the pilot data trending $G$ for a patient with good outcome and one with bad outcome. These autoregulatory time courses are quite variable and as such not conclusive but it is interesting to note that the overall trending may also be predictive of outcome.

## 6.6 Discussion

The first analysis was statistically significant showing that there was a good correlation between the reworked Ursino model output $G$ with clinical outcome over the later stages of stay in the intensive care unit (ICU). Though the numbers of patients analysed was small these results warrant further investigation with larger numbers of patients. When analysed by looking solely at the last third of the stay there is a strong statistical difference ($p = 0.034$) between the good and bad groups using a t-test. This suggests there is a definite temporal link with outcome via the degree by which the groups separate then diverge as the length of stay for the patients increase.

In the previous study the data were divided into three sections based on total length of stay, this of course isn't very practical in a clinical setting so the study was revisited and a more relevant time split was chosen. In general the first 24 or 48 hours post injury is considered to be the critical time window for interventions and also considered

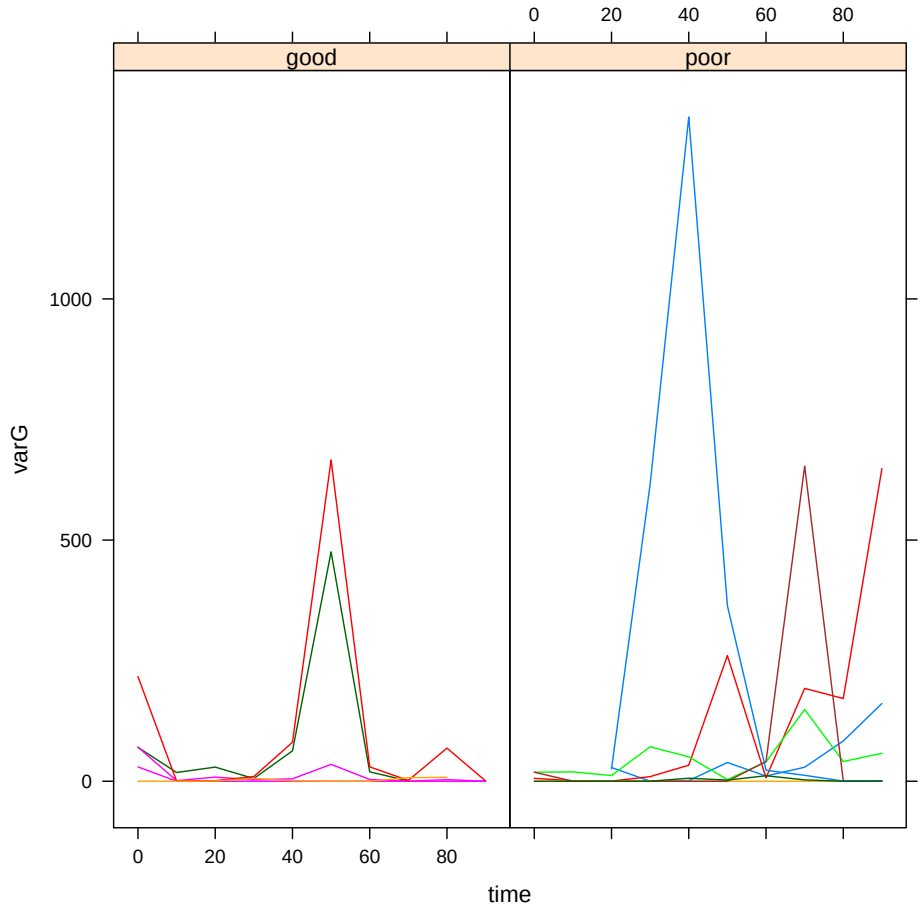


Figure 6.2: A comparison of the trend in the variability of the autoregulatory index, that is increasing instability with the percentage of length of stay which is split by outcome group.

the time period when autoregulation disruption is most likely to be present. So if the model correlated as well with outcome over this time period than the model could have greater clinical value. A Student t-test was performed between the early var($G$) and the two outcome groups ("Good", "Poor") and showed no statistical difference ($p = 0.8714$). The reworked index is statistically not an early predictor of clinical outcome, however over the whole time course of each group there appears to be a link between worsening autoregulatory state and poor outcome. This negative result may in part be due to underpowering the analysis with only 12 patients, due to the need to use ICP pulse amplitude as a surrogate measure of $V_a(t)$ surrogate.

One of the interesting analyses was to assess if this autoregulatory index contributes anything to a clinical outcome model compared to existing predictive models. To this end a model comprising of a set of known predictive variables for outcome was chosen based on the well described IMPACT model. These variables comprised of age, sex, the GCS Eye score and the GCS Motor score on admission to which was added the reworked Ursino var($G$), for the same early period in the previous analysis. An automated stepwise reduction routine was then applied. Although the autoregulation measure was dropped out of the final model, it was the last parameter to be reduced out of the model. This study, even though conducted in a small sample of patients, does seem valid as the model showed the same key parameters remaining in the model of outcome, namely age, GCS pupil and GCS Motor scores remain highly indicative of outcome. The failure for the AR index to be included is again probably because of the under powering of the study with only 12 patients. In Czosnyka's 1997 paper [23] he stated there was a distinct relationship between a negatively correlated PRx value and "good" clinical outcome ($p < 0.00001$). However the correlation between the two variables was only $r = 0.48$ showing less than half of the correlation relationship is explained by the autoregulatory status. This fact could be more evidence that a larger study is needed to show the relationship with the reworked Ursino model. It is interesting to note about the Czonsnyka result that while it can be reproduced in traumatic brain injury

populations it doesn't hold up in other neuropathology groups [48].

As has been stated at the beginning of this chapter it would have been a more complete analysis if all three models Ursino, PRx and HMF could have been assessed in this outcome study however due to a lack of high enough resolution data in the patient BrainIT dataset [74], which has a sampling frequency of once per minute, the calculation of both PRx and HMF could have been disadvantaged. However, pilot studies are in progress collecting both waveform quality blood pressure (BP) and ICP data together with the lower resolution minute by minute data with a view of comparing the efficiency of the models performance on data of different sampling resolutions. If those studies show that minute by minute data is feasible to use for the HMF or PRx model, then a more comparative analysis can be carried out.

Due to the early analysis suggesting a temporal link between the autoregulatory index's prediction of autoregulation for the "late" period and clinical outcome, time-series figures were plotted of $G$ categorised by outcome group,"Good" Vs "Poor". From these figures the time dependence can easily be seen with the "good" group var($G$) decreasing over time and the opposite being true for the "poor" outcome group. What is striking about the two group's is that the "poor" group has increasing variability of the $G$ index as time goes on whereas the good group has low variability throughout. With one notable exception around about half way through the ICU stay there is a spike in this groups variability (figure 6.2), where it is likely that these patients are being removed from sedation, woken up and tested clinically at this time to evaluate their clinical progress. These results seem to make sense intuitively, in that those patients with worse clinical outcome have increased autoregulatory variability than those with better outcome.

## 6.7 Conclusion

All outcome model studies rely on two linked processes. Firstly the model parameters will have a high enough statistical power to show that they influence the outcome parameter over noise and random error and secondly that the study has enough subject's to allow the first point to be established. In this case the study did not have enough subjects to show the relevant parameters were statistically significant. However because the autoregulatory prediction term added enough weight to the outcome for the reduction process to remove it only at the very last step, this suggests that it does influence outcome but it would need a larger number of subject's to show this conclusively. In general though the reworked Ursino model has been shown to have promise as a predictor of autoregulation and now also has been shown to be linked to clinical outcome especially when considered as part of the patient's time course.

# Chapter 7

# Topology of autoregulation

## 7.1 Introduction

The study of topology in mathematics is one of great importance as it underpins advanced set theory, differential geometry and both algebraic and complex analysis [62] but more than that it links many different and distinct topics in mathematics together. A rigorous exploration of the application of topology to the subject of autoregulation is beyond the scope of this chapter however a number of basic topological ideas will be used as a starting point for developing a framework for the process of autoregulatory model fitting and optimisation.

## 7.2 Aims

All of the previous work has been building up to the creation of a generalised framework for modelling cerebral autoregulation. This chapter will attempt to amalgamate all of the disparate threads of this work into a cohesive whole by drawing on the underlying mathematical theories of topology. More specifically the need for the definition of a set of topological spaces on which this framework can be based. Once this is completed this new framework will be applied to the existing base reworked model and this then assessed on the prospectively collected data set obtained from the impedance work described in chapter 4.

## 7.3 Topology

Topology as a subject is the study of sets and their subsets, how they interact within themselves and how each can be linked to other sets through functional mapping. A topology is also a mathematical construct, it is a combination of a set with its subsets that follow three axioms [89]:

1. Any union of subsets is contained in the topology

2. An intersection of any two subsets is contained within the topology

3. The empty and trivial sets are contained in the topology

If they do conform to this you can state that the subsets form a topology, normally denoted $\tau$, over the set. The classic example of this is the four element set $S = \{a, b, c, d\}$ and the family of subsets $\phi, \{a, b\}, \{c, d\}, \{a, b, c, d\}$. All of three rules (union, intersection and membership) can be easily verified so this family of sets is classed as a topology over $S$. It is worth noting at this point that it is not the only topology over $S$, the two other classic topologies which also hold for all sets would be the discrete and indiscrete topologies. The discrete topology being every subset on the main set and the indiscrete being only the trivial set $S$ itself and the empty set $\phi$.

On the three dimensional space of real numbers $\mathbb{R}^3$ it is more common to define the sets involved in defining a topology via a metric or distance measurement. This type of topology is know as a metric space and in the special case of using the Euclidian distance metric $d = \sqrt{\left(\vec{i}^2 + \vec{j}^2 + \vec{k}^2\right)}$ the Euclidean space or Euclidean manifold. This metric can be easily visualised as a sphere surrounding a point defining a subset of three dimensional space. This idea of a metric of course extends to that of higher dimensional spaces as well.

Once a basic set of topological spaces exist it becomes interesting to ask the question how do they relate to one another and what can be inferred from one to another. To understand this a study of functions between topological spaces needs to be conducted.

### 7.3.1 The study of functions and their relationships.

The terms “function” and “map” will be used interchangeably, even though the term map is normally used in the context of taking a subset of one space and linking it to a counterpart subset in another via a specified function. This process is also called “projection”, as in the map has projected one subset onto another. The study and categorising of functions is an expansive field within mathematics, especially so in topology however for the purposes of this discussion this shall be limited to only two concepts “homeomorphisms” and ”homotopy”.

#### Homeomorphisms

Before a definition of homeomorphism can be presented there is a need to define what a homomorphism is. Take a map $f : X \to Y$ this is defined to be a homomorphism if and only if there exists a unique $x \in X$ that maps explicitly onto $y \in Y$. The uniqueness of the map is an important thing to consider as this implies that that the function will cover the whole of the space $X$. If we then define another homomorphic map this time $f^{-1} : Y \to X$ then we will have every $x \in X$ mapping uniquely to a member of $Y$ and also every $y \in Y$ mapping uniquely to a member of $X$ [35].

Then the function $f$ is said to be a homeomorphism if and only if there exist two homomorphisms $f$ and $f^{-1}$ such that they are continuous and $f \circ f^{-1} = I_X$ and $f^{-1} \circ f = I_Y$ [62]. Where $I_X$ and $I_Y$ are the identity maps of sets $X$ and $Y$ respectively. This means that the map $f$ will be one to one between $X$ and $Y$. The term homeomorphism is used interchangeably with “isomorphism‘. This class of function is important as it means that both spaces are equivalent to each other which means any theory that holds in the first space will automatically hold in the second space because of the invariance of the spaces under the map $f$. This is normally said as space $X$ is homeomorphic to space $Y$.

Ideally all functions being applied to a topology would be homeomorphisms however this is often not to the case. Another key type of function which also preserves some properties of one space as it is projected onto another is that of "homotopy".

**Homotopy**

Instead of attempting to define a function $f$ and its inverse $f^{-1}$ to make sure all properties are mapped onto the opposite space. A set of functions $f_1, f_2, \ldots, f_n$ can be defined such that there exists a continuous transformation between $f_1$ and $f_2$ then a continuous transform between $f_2$ and $f_3$ and so on. This would mean there exists a continuous transform between $f_1$ and $f_n$. This continuous transformation between one and the other is the general idea of homotopy [89].

More formally homotopy is defined to be a map $h : X \times [0, 1] \to Y$ that is a function from the cross product of the topological space $X$ and the unit line $[0, 1]$ inclusive of 0 and 1 to the topological space $Y$ such that for an $x \in X$ there exists $h(x, 0) = f_1(x)$ and $h(x, 1) = f_n(x)$.

There can then be defined a homotpy equivalence which is defined in a similar way to a homeomorphism except that the compositions only need to be homotopic to the identity maps instead of equal to them. That is, there will exist two homomorphisms $f : X \to Y$ and $g : Y \to X$ such that $f \circ g$ is homotopic to $I_X$ and $g \circ f$ is homotopic to $I_Y$. This would mean that the topological space $X$ could be continuously deformed into the topological space $Y$. As such, many of the properties in one would be preserved in the other.

Before any investigation into how these topological concepts could be applied to autoregulation modelling an overview of the whole process should be investigated.

## 7.4 Autoregulation modelling

All of the autoregulatory models that have been looked at previously in this work have three things in common: Firstly, they all take a subset of the patient's vital signs parameters as an input to the model, secondly they all map these vital signs parameters onto a prediction for autoregulation and finally they all use a function or algorithm to perform the mapping.

These things hold true of course for any model of autoregulation not just the small sample reviewed here. These three processes can be generalised into a set of rules defining an autoregulatory model:

1. A parameter space $\mathcal{P}$ from which a subset can be chosen that will drive the autoregualtory model.

2. An autoregulatory answer space $\mathcal{A}$ which contains a representation for autoregulation.

3. A model space $\mathcal{M}$ from which a model can be picked that maps the parameter subset on the autoregulatory space $\mathcal{A}$ subset.

As all models that can map any subset of $\mathcal{P}$ onto a subset of $\mathcal{A}$ exist in $\mathcal{M}$ then there must exist a model $i$ than maps $p_i$ an existing subset of $\mathcal{P}$ onto the whole of $\mathcal{A}$ as the whole set is the trivial subset of itself. This would then be the idealised model for autoregulation, that is, the model that predicted with a hundred percent accuracy the autoregulatory state of the system under study. While $p_i$ could be the whole of $\mathcal{P}$ this wouldn't be a desirable outcome as having to know everything about the system would be impossible to obtain, if for no other reason than because of Heisenberg's uncertainty principle. This result can be tightened so that $p_i$ is the smallest subset of $\mathcal{P}$ for which the model holds true. All of this allows the generalisation of the search for the best model to be reduced to: Finding a model which maximises the subset in $\mathcal{A}$ while at

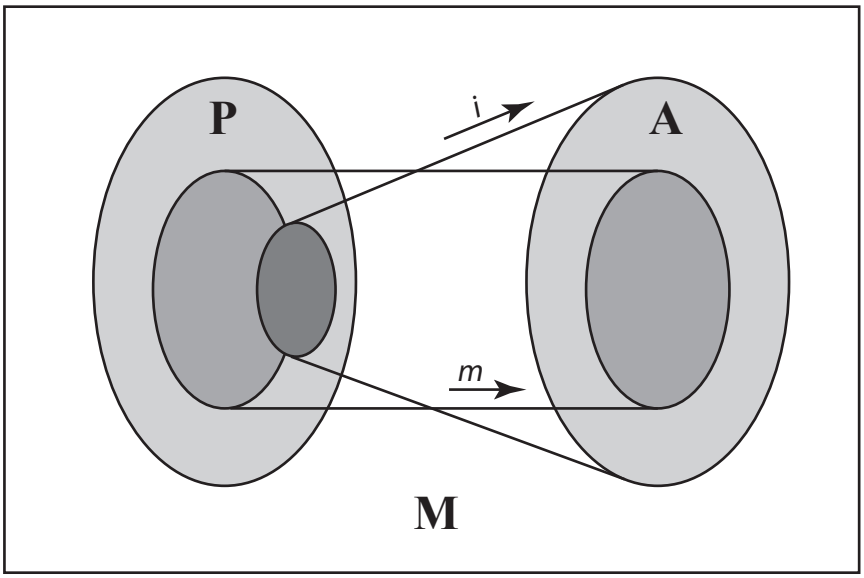


Figure 7.1: Illustration of the three spaces $\mathcal{P}$, $\mathcal{A}$ and $\mathcal{M}$ and how they relate to one another.

the same time minimising the subset in $\mathcal{P}$. This is shown in figure 7.1.

Topologies can be constructed easily for both spaces $\mathcal{P}$ and $\mathcal{A}$. As $\mathcal{P}$ is a contraction of $\mathbb{R}^n$ where $n$ is the number of vital signs parameters used in all models from $\mathcal{M}$. It has boundaries that are on the edge of the maximal ranges of each vital signs parameter. As such, a distance metric can be found to partition $\mathcal{P}$ and a topology can be created. The autoregulatory space $\mathcal{A}$ though has to be considered more carefully as if it is, in our case only a boolean answer space, that is the system is autoregulating yes or no, then only a very simple discrete topology can be crafted. If however the space is the set $[-1, 1]$ then another metric space could be constructed. This can radically alter what is possible to infer topologically and to map between.

### 7.4.1 Application of homotopy to the modelling process

Homotopy is a powerful idea, one where functions can be classified by family and type but also supports the concept that two different functions will preserve the same

topological information between the spaces if they are homotopic to each other [89]. It is with this core concept of one function being able to be transformed into another that you can start to build a framework in which functional modelling and more specifically autoregulatory modelling can be carried out.

If the changes to any model are classified in this way then small changes will be closer to the original model on the $[0, 1]$ continuous scale than any large changes which would be closer to the final model destination. On the spectrum of possible changes, simple parameter changes and substitutions would be considered small to medium changes much like any model change which results in no outward change only an internal methodological one. A model alteration that results in a large change in precision or predictive accuracy of the model would be considered a large change.

This last point of change being measured by predictive accuracy of the model should be the idea of optimisation. With this in mind the concept of topological space transformation or more specifically restriction should also be considered as the companion to homotopy of the model functions.

### 7.4.2 Application of topological space transformations to the modelling process

As has been stated before there are three main spaces involved in any autoregulatory modelling process. The parameter space $\mathcal{P}$ the model function space $\mathcal{M}$ and finally the autoregulatory prediction space $\mathcal{A}$.

Transformations to $\mathcal{A}$ have already been mentioned and maximising the amount of the space any subset covers is the desired end point of any operation performed in this framework as this will mean a large proportion of correct predictions for the autoregulatory status.

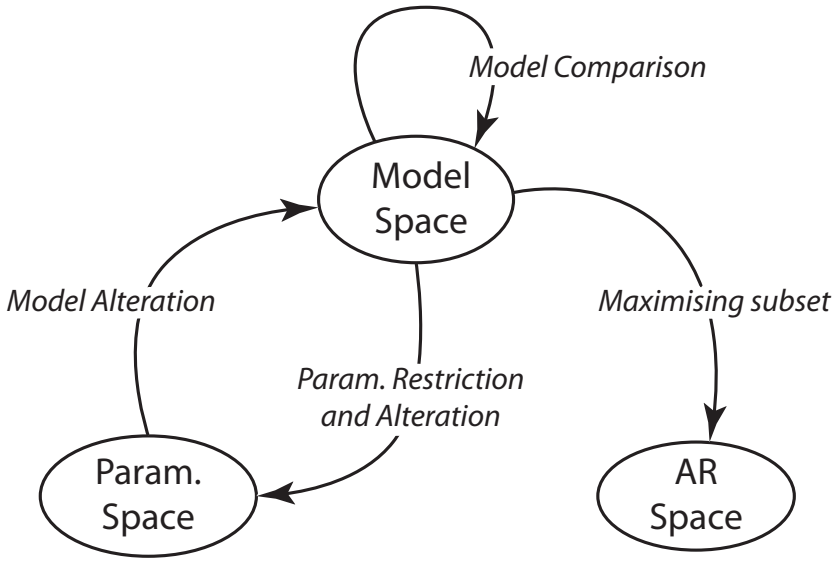


Figure 7.2: Illustration of the how various optimisation processes will interact within the three spaces.

Restrictions to $\mathcal{P}$ has also been mentioned before in the context of the amount of information that had to be collected to calculate an ideal model. This however is not the only reason to reduce the parameter space, the second being the application of classical optimisation techniques such as parameter restriction. This is where some of the parameter space is constrained to reduce the chance of selecting a non optimal value with respect to the output of the model function.

Lastly restriction to $\mathcal{M}$ has not yet been considered but it is possibly the easiest to understand. As this space contains all the potential models for autoregulation, any reduction to this space will effectively remove models from consideration. This type of restriction is normally achieved via a model comparison study and the rejection of any under performing models.

### 7.4.3 Modelling framework

If both of these ideas of homotopy of the model and transformation of the three spaces are put together a framework can be defined, illustrated in figure 7.2, with the following optimisation steps:

1. Model space restriction via model comparison techniques. This only affects the model space by reducing its size.

2. Parameter space restriction via classical parameter based optimisation techniques. This affects the dimensions of the parameter space by constraining the size of the space.

3. Parameter alteration via small to medium homotopic changes in the model parameters. This affects the parameter space by allowing parameters in the model to be changed into others.

4. Model alteration via small to large homotopic changes to the model function. This affects the model space as there is a change of one model into another.

All of these steps should only be carried so that they increase the size of the subset of the autoregulation (AR) prediction space.

Any modelling performed within the bounds of this framework could then be thought of as following a number of stages. Firstly a general model or technique would be chosen for study. Then both parameter space and autoregulatory prediction space would be defined. The model would then be assessed to give a baseline for predictive accuracy or fit. The four main optimisations in the framework should then be evaluated for use with the model (not all of the techniques could or should be applied to all models). Any which are considered feasible should then be applied in a series of steps and the predictive accuracy or fit checked again for an improvement against the baseline recorded earlier after each step.

As an example of this process the reworked Ursino model was re-evaluated using all of the applicable techniques described above.

## 7.5 Application of the full framework to the reworked Ursino model

In chapter 3 an initial model comparison technique was performed between the reworked Ursino model, the highest modal frequency (HMF) model and the pressure reactivity index (PRx) model and this showed that before any optimisation was performed the Ursino model had the best predictive accuracy out of the three models under test. A Matthew's correlation coefficient (MCC) of 0.3 versus 0.09 of the other two models. The first framework optimisation in this case would be to focus on the model which has the most potential.

### 7.5.1 Dataset preparation

Using the dataset collected in chapter 4 three measures of arterial-arteriolar compliance were calculated. Assessing all of the available options on the flowchart figure 4.11, the venturi method could not be evaluated because of the lack of an artery diameter measurement. The surrogate $C_a(t)$ parameters were initially calculated via the intracrainial pressure (ICP) pulse amplitude technique as shown in chapter 2 then subsequently with an impedance measurement technique which was detailed in chapter 4. Finally, scaled and trended ICP measurement could also be used but this represents the least viable surrogate possible and should give an indication what the models lower limits of the parameter space.

In the experimental studies described in Chapter 4, the impedance measurements were

taken multiple times per ICP step during the study and this allowed a rough trend for impedance to be defined over the whole time course which could then be referenced by the model when required.

The full dataset was re-sampled into the same time range, a model prediction performed every six seconds, as with the initial study in chapter 3 this was to minimise systematic differences in comparison between the initial comparison study and this new one. The summary measure used was a simple average of both the mean arterial blood pressure (ABP) and the mean ICP over the six second window.

### 7.5.2 Baseline model prediction

The initial reworked Ursino model was then applied to this data set and the variance of the Gain var($G$) calculated. The two periods of pre and post impairment were then separated out and two hundred points were sampled from each period. The $MCC$ method was then employed again to assess the fit between the predicted autoregulatory state and the induced state during the study.

The $C_a(t)$ has been calculated in two ways for this baseline study. Firstly with a more clinically accessible method of basic variable trending and secondly using the ICP pulse amplitude methodology. An example of each model output is shown in figure 7.3.

### 7.5.3 Framework optimisation

In general the superficial differences between the original reworked Ursino model and the framework optimised variant are minimal. Both models, the original and the framework optimised variant, are already using the new asymmetric sigmoid curve which would be considered a model alteration optimisation this is used out of necessity for a working model. There are no parameter restriction optimisations that can be

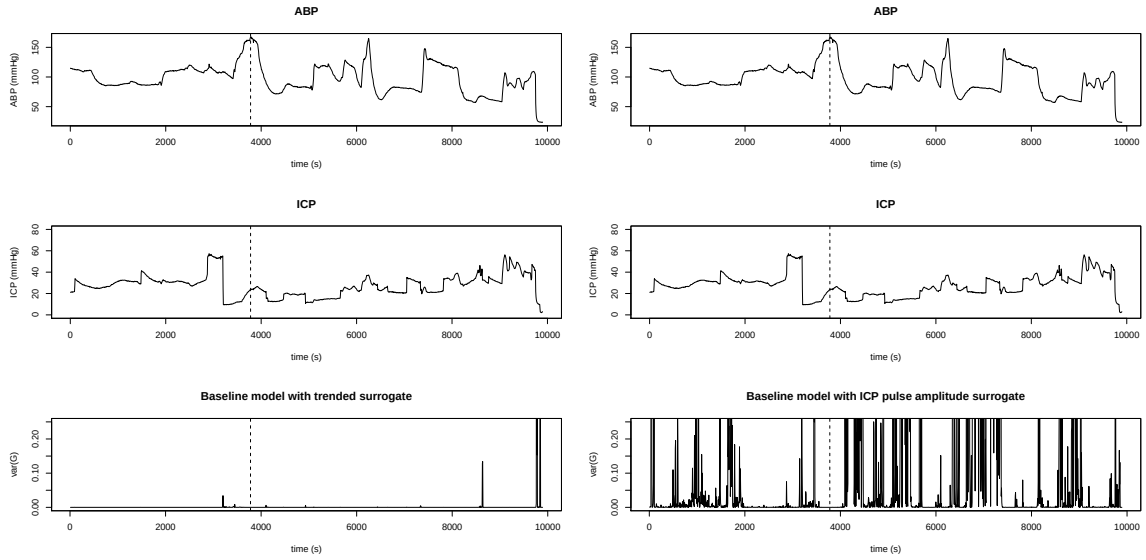


(a) (b)

Figure 7.3: Two examples of the reworked Ursino model with different surrogates for $C_a(t)$, (a) simple scaled variable trending and (b) the ICP pulse amplitude technique. The ABP and ICP waveforms are also shown and the autoregulatory impairment is denoted via the dashed vertical line. Early assessment of model performance can be seen in the better discrimination between before and after injury events comparatively between the two models.

applied here and the reasons for this have also been covered previously.

This leaves two main optimisation approaches that will be applied from the framework, parameter alteration and model alteration. For parameter alteration, the transcranial impedance measurement will be used in place of ICP pulse amplitude as a $C_a(t)$ surrogate. The fractal characterisation wavelet noise reduction technique will be applied to the Ursino model output as a model alteration approach to reduce any non physiological noise and optimise the predictive accuracy as a result. An example of this framework optimised model output is shown in figure 7.4.

Similarly to the baseline original model prediction the new model var($G$) was calculated over the dataset described above and the MCC for the autoregulatory state in both pre and post impairment periods was assessed using the same sampled 200 time points from the original baseline prediction.

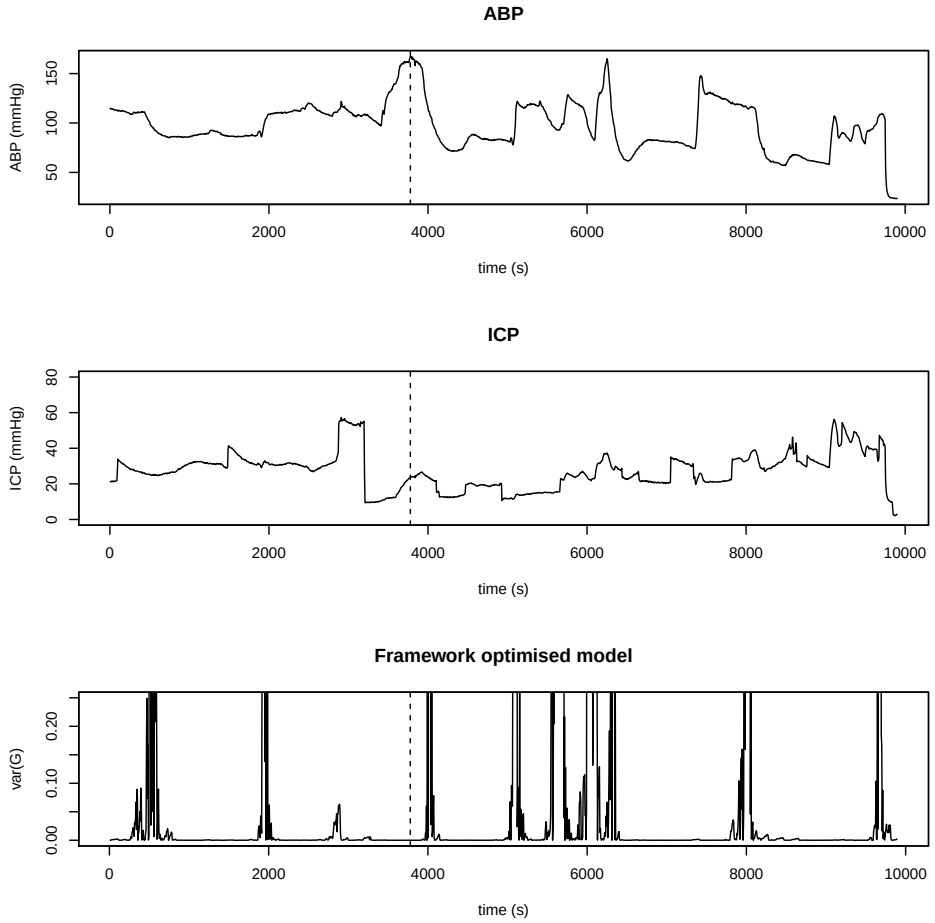


Figure 7.4: An example of the framework optimised model output shown with ABP and ICP waveforms and the autoregulatory impairment is denoted via the dashed vertical line. An early assessment of the performance can be seen in the less noisy prediction of impaired autoregulation in the lower plot.

| Model | *MCC* |
|---|---|
| Baseline Model with variable trending | -0.24 |
| Baseline Model with ICP pulse amplitude | 0.19 |
| Framework Optimised Model | 0.29 |

Table 7.1: Table showing the predictive accuracy of both the original reworked Ursino model and the new framework optimised variant.

### 7.5.4 Results

The results for the predictive accuracies can be seen in table 7.1. This shows an increase in predictive accuracy from the poorest surrogate to the normal reworked Ursino model. The framework optimised model variant then shows a 52.6 percent increase over the baseline model using the ICP pulse amplitude as the $C_a(t)$ surrogate.

## 7.6 Discussion

This framework has the potential to make it easier to perform model comparison and optimisation tasks. It also should provide a basic structure to begin to standardise the procedures used to perform these types of task not just on autoregulatory modelling but also modelling in general. This approach is not without its drawbacks however as there will need to be a more rigorous study and understanding of the topology involved if any deeper understanding of the relevant spaces is to be achieved. So far while it can be shown there are topologies over both parameter space and AR status space, are the models under study homeomorphisms? Is there a second homomorphism from the AR space back to the parameter space thus defining the spaces to also be homotopic to one another? Any assessment of these questions can only begin if the AR prediction space is understood in greater detail, and that will only be achieved if there is some consensus across the research domain as to how to record the autoregulatory status.

One thing that is clear from these basic topological definitions, is that mathematical

models based on the physiology have a better chance, over purely statistical models, of providing more information about the AR prediction space. This is because most statistical models are not uniquely defined so there will be many variations of the parameter set to give the same or similar output for the prediction. This precludes their use as a homeomorphism as an inverse function can not be defined which implies that any topology under projection with that model will never be directly equivalent to the dataset used as parameters. In this case, the best that could be hoped for is a homotopy equivalence.

The application of the topological framework has shown that you can introduce an overall improvement in a base model. This is achieved via incremental improvements not just to predictive accuracy but also to the models utility for use in a clinical setting. Which in this case is a non-invasive estimate of arterial-arteriolar compliance via transcranial impedance measurements.

However as many of the alterations applied only minimally change the model, as they are designed to be homotopically close to the original, the change in predictive accuracy is not as large as those seen in the pervious optimisation study, in chapter 3, which made use of parameter restriction.

## 7.7 Conclusion

Generally the modelling framework defined above provides an interesting methodology for improving the output of any model which, for example in the case of the Ursino model produced a 52.6 percent improvement when run on new test data. Each stage of the framework when applied to the basic Ursino model does give a marked improvement over the previous model. This demonstrates that such a structured methodology can have benefits for improving model fit and efficiency and thus should be applied before attempting to use a new model in a formal clinical setting. The topological

underpinnings of the framework enable consideration of what is needed to improve not just this specific autoregulation model but the research domain in general in particular considering how autoregulation is interpreted and recorded. When this step is completed then a much more rigorous study of this topological concept can then be carried out.

# Chapter 8

# Conclusions and further work

In summary the underlying theme of this work has been to look at modelling in a very generic manner then to specifically focus on how this can be applicable within the cerebral autoregulatory domain. The techniques that have been used are all linked through the interplay of the mathematical structures involved and it is only when you abstract these ideas do you see a larger framework that can apply to any modelling problem.

What has been proposed here is that this framework should help to improve how any system is studied and eventually modelled, in this specific case of cerebral autoregulation the model that has been focused on was the simple model published by Ursino in 1997 [102]. This model was chosen for study because of its physiological nature with the idea that because of this it should initially be a more predictive simulation of the cerebrovascular system compared with more data driven statistical models. To understand this reasoning the driving processes behind autoregulation should be explored.

The classical definition of cerebral autoregulation is the process by which blood flow is maintained over a changing cerebral perfusion pressure, however this is a property of the overall system not a directly measurable quantity. There are a number of physiological processes which play a role in cerebral autoregulation principally metabolic and neurogenic. The dominant metabolic process would be the coupling of tissue metabolism to blood flow through carbon dioxide diffusion which in turn causes vasodilation via hydrogen ion production in the cerebrospinal fluid by action of carbonic anhydrase [49]. Myogenic processes detect the increase or decrease in the transmural pressure which will in turn cause the vascular smooth muscle to contact or relax in an attempt to restore blood vessel diameter. Lastly the overall weak sympathetic processes in cerebral autoregulation are explained by the over-riding strong metabolic response that attenuates sympathetic vasoconstriction during sympathetic activation [49]. If this didn't occur then during strenuous exercise, a situation which causes sympathetic activation, cerebral perfusion would decrease [49]. It is because of this complex interplay

of different mechanisms that any attempt to design a model which does not include the physiology would initially seem to be a poor choice for predicting autoregulation accurately. To fully comprehend how these processes translate into the mathematical models of autoregulation a larger picture of the anatomy and physiology needs to be described.

The cranial space is composed of a number of layers and systems which work in unison and make it a unique challenge to devise a model that encompasses all of these diverse factors. The first dominant factor is the bone container all tissues reside within called the cranial cavity. This structure defines the system's boundaries and as such makes the modelling easier because of the simplifications that can be made. The main assumption of rigidity allows for pressures to equilibrate consistently within the space as there is no significant deformation of the boundaries. Inside the cranium sits the brain which is modelled as a viscoelastic solid surrounded by cerebrospinal fluid (CSF) which is considered a Newtonian or non-compressible fluid. The CSF itself is produced from the arterial blood supply via the choroid plexus of the ventricles in the brain which then circulates around the cranial space where it is eventually absorbed again across the arachnoid villi of the venous circulatory system.

This description lends itself well to compartmental modelling because of the clear channels of flow between the major systems involved and this is exactly the approach Ursino took in his 1997 paper. So applying this mathematical model against a data set to study autoregulation should provide better insights than merely looking for correlations between vital signs parameters which would be an example of a purely statistical approach.

The framework, described in full in chapter 7, is loosely based on the mathematical ideas of topological spaces and of generalised mappings between them. A topology is best thought about as a collection of partitions of a general set which fulfil three basic axioms. When a topology exists on different spaces, basic assumptions can then

be made on how they will behave under mapping as well as beginning to understand the underlaying multidimensional structure. With this in mind three distinct spaces have been defined one for which the model parameters or variables are discerned, this space is in the multi-dimensional space of real numbers ($\mathbb{R}^n$) where the dimension $n$ equals the number of parameters under study and is usually drawn from the vital signs patient data in the case of autoregulation. The second space is the model space where all functions for attempting to evaluate autoregulation exist and draw their input from the "parameter" space. Lastly the autoregulatory space in which all predictions for either static or dynamic autoregulation exist, this is essentially the answer space into which the models map.

This last space needs careful consideration as one of the first problems that comes to light when looking into autoregulatory modelling is there is no consensus for what the answer space should contain. The main reason for this stems back to the fact that autoregulation is a concept not a measurable entity. So for each model that has been published there is a different view onto this answer space. For example should it be based upon a boolean value [46], the simplistic "yes" autoregulation is intact or "no" it isn't, or alternatively it may be based upon a dichotomous scale [1], possibly numeric or categorical or lastly the model may be based upon some continuous scale [24]. It could be argued that a boolean values function is merely an extreme form of the dichotomised scale and that in turn is merely a continuous scale summarised via some metric which leads inevitably to the conclusion that a continuous scale is the best way to measure what is ultimately a dynamical system. However this lack of standardisation poses a significant hurdle for attempting to apply some of the frameworks suggested.

Once the concept of these three spaces (parameter, model, autoregulaory) has been understood it is much easier to visualise how interactions will effect the spaces and in turn any model under study. It also becomes obvious that because of the constraints on the three spaces there will exist an idealised model which maps some partition or

subset of the "parameter" space onto the full autoregulatory space which is considered a "trivial" partition of itself. So any question of creating a "good" model for cerebral autoregulation becomes one of maximising the mapped partition in the AR space and attempting to minimise the partition in the "parameter" space with the goal of making any model under study as equal to this idealised model as possible.

Modelling within this framework of spaces can be thought of as a five stage process. Firstly define a modelling technique you wish to study, choose a subset of the autoregulatory space which can be evaluated by some measurable end point, decide on the partition of the "parameter" space which can be recorded and then execute and evaluate the model and finally optimise the model and space partitions to improve the relationship between all of the spaces. This last step in creating any model is often skipped in much of the literature but can have a large influence on the overall effectiveness of a model and it is on this topic much of this work is devoted. There have been a number of optimisation techniques illustrated: Model Comparison, Parameter Restriction, Parameter Augmentation and Model Alteration.

Model Comparison is a classical model refinement technique that attempts to evaluate each model against either each other or against some ideal. This normally allows for the best choice of initial model and technique. The comparison needs to be structured in such a way as to not bias the analysis towards or away from any model under test. If all models are refined to output to the same autoregulatory space partition, for example no model should output ICP while others output a measure of autoregulation. The dataset used should have a sampling rate as high as any model under examination requires which is then resampled to lower rates for the remaining models and finally the statistical test needs to be balanced and easy to use with the output from the evaluations. The comparison, based on MCC of PRx, Daleys HMF index and a reworking of Ursino's 1997 model showed that the reworked Ursino Model had the greatest predictive accuracy on the dataset tested, 0.3 versus 0.09 of the other two

models. The optimisation here is the rejection of the PRx and HMF models as they have less predictive power however even the Ursino model's accuracy is not optimal. There could be a number of reasons for the lacklustre performance by all the models tested. Generally the data set which was initially used to evaluate the models has a considerable amount of noise in it created by manipulation of the animal during the experiment which of course limits the amount of usable data to all models under examination. The second criticism which could be raised here and throughout all of the analyses is that were are assessing global models for autoregulation and comparing them against what is essentially a highly focal "gold standard" measure of AR based upon pial artery diameter. The literature supports that the injury model used and the pial artery window technique are standardised and acceptable however it is not out of the question that the dataset and AR assessment method used as a gold-standard could be a contributing factor to the poor model performance. However, it is believed that the methodological approach developed in this thesis is relevant and potentially useful clinically, independently of the quality of the available dataset used for comparison. Furthermore, the predictive accuracy of all of these models are a very good illustration for the need of optimisation techniques.

Parameter Restriction is a form of optimisation where the parameter space is constrained to maximise the partition in the autoregulatory space or to put it another way to increase the accuracy of the model. Every model parameter has a range over which it can be used within that specific model and the process of parameter restriction is one that allows these ranges to become better defined. This is an automated process where the model is repeatedly evaluated against a known end point and the accuracy assessed for values within the chosen parameters range. The automated process can be as simple as trying all parameters linearly across the range or a more complex strategy like a Newtonian root appraisal methodology. This can be seen in chapter 3 when evaluating the PRx, there is a window of data with which the correlation function between ABP and ICP is evaluated. Similarly the HMF has a window of data over which the

correlation with the HMF and cerebral perfusion pressure (CPP) is calculated. When this analysis is run it is shown that the length of that window with respect to time has a direct effect on the predictive accuracy and in this case a 66 minute window of data for the PRx and a 72 minute window for the HMF has been reported to give the best performance. For the models in question this represents a 278 percent and a 611 percent increase in predictive accuracy. This technique will not work with all models in the same way because the "parameter" space partitions are either different or used within the model in different ways. The Ursino model is a good example of this as the time based ranges it uses are already accounted for within the model so any attempt at parameter restriction will only result in a smoother output. This is due to the differential nature of how the model deals with time. All increases to the time range result in less data being used to calculate the model and thus a smoother output. So to attempt to optimise Ursino's or any model with a similar differential time-window issue, then other forms of parameter restriction techniques need to be sought.

Model Alteration can be thought of as augmenting the structure of the model to include other modelling techniques. This concept goes straight to the heart of the topological idea of homotopy where one function is related to another through a continuous deformation. In other words, although the functions may be different they all belong to the same family and therefore share similar properties. With this idea, models are systematically changed to make them more accurate not only through replacing like for like but also through altering sections of a model to locally increase precision. In chapter 2 swapping in a continuous asymmetric sigmoid curve to replace a case based asymmetric sigmoid is an example of a like for like model alteration and this was done only so that the model as a whole could be more easily inverted. This optimisation had no effect on the overall predictive accuracy of the model as it was within a 0.09 percent deviation of the original curve this was due to the numerical nature of the curve fitting technique. This however allows the model to be used in a form fit for comparison.

Another model alteration optimisation that has been proposed in chapter 5 is using fractal characterisation of the physiological signal as a noise estimate for wavelet noise reduction. This uses the fractal nature of physiological signals in that if there is an underlying self similarity in any signal, it will be caused by a physiological response and not due to some artifact or noise. It relies on wavelets in two stages: firstly to estimate how much of the recorded signal is related to the fractal component from which a noise estimate is created. Then a simple wavelet smoothing technique is used to remove those time-frequencies which are not related to the physiological signal. When the Ursino model with the wavelet smoothed output signal is compared to the non smoothed version it shows a 350 percent gain in predictive accuracy. This fractal characterisation technique is not a panacea for all physiological wave form analysis however. For example, when summarising the fractal content of stable and unstable systems was attempted the Hölder exponent histograms show little or no difference between them suggesting that the underlying physiology wasn't playing an active role in causing the instability observed. This interpretation of results is less important when considering using this approach only as a noise estimate as it is only a measure of content that is required not if that content can be differentiated from any other.

Parameter Alteration is the inclusion of parameters in a model to add missing or increase the precision of the domain knowledge in the model. The creation of any model is a complex process and the goal of which is the creation of something which mimics a real world situation. One of the key principles in model creation is simplifying the situation to make it easier to model. The problem with starting simple is that to make the model more realistic, parts of the model need to be augmented. The issue balances at that point between making the model less simplistic but not too complex as to be obscure. Starting with the basic Ursino model there are a number of parameters that can not easily be measured and have to be simulated in some way. The arterial-arteriolar compliance is one such parameter. There are a number of attempts throughout this work at modelling this parameter: The compliance can be estimated

by using an averaged measurement of the diameter of the blood vessels then using a venturi flow effect to simulate the pressure differentials through the system. Or by using the ICP pulse amplitude methodology and estimate it via the area under the inverse of that curve. If nothing else can be used, then the peak to peak ICP to ABP relationship can be used as an estimate of the full system compliance which will at least track the arterial-arteriolar compliance. This is a much less accurate estimation but is at least one step up from setting it to be a constant and assuming it does not change.

The last approach investigated may have the most promise for traumatic brain injury management as a whole and that is the inclusion of a non invasive impedance measurement as an independent surrogate measure of compliance or ICP. The body's cell structure can be modelled as a simple electrical circuit containing two paths, one which is only resistive and the other which is both resistive and also capacitive. One could consider this structure fractal in nature where a small part of the whole has the same electrical properties of the whole itself. Or to think about that another way the impedance measurements that can be, and routinely are clinically, applied to the whole body should be applicable to a small part of the body such as the cranial space. The previously mentioned circuit is used already in the calculation of whole body water readings which is considered a measurement of a subject's overall level of health. When this technique is applied to the head the measurement will be of the water content contained within that container and it has been shown that it is linked to the measurement of compliance. A number of experiments were carried out where the relationship between impedance and ICP was studied, the normative ranges in human volunteers were defined and finally its inclusion as a new parameter in the Ursino model.

Each of the above techniques yield some gains in predictive ability of the overall Ursino model, however to fully understand all of these adjustments in context the techniques

have to be combined into a cohesive model and to be executed on the data. When this is done it can be seen that there is a gain in predictive accuracy of 52.6 percent over a non optimised version of the model.

The usefulness of such a model even with all the optimisation and improvements only becomes apparent when it is assessed in the context of the clinical environment and not just as a research tool for advancing the knowledge of autoregulatory modelling. It is to this end that a study of outcome using the optimised Ursino model was devised. This was tested in two stages firstly measured directly against outcome and then secondly as part of a more complex model incorporating other known prognostic factors, where it could be studied to determine if it increased the predictive nature of the model. The outcome measure in both arms of this study was a dichotomised 8-point extended Glasgow outcome scale, measured at 6 months after injury and split into "good" and "poor" groups around category scale point four (upper severe disability). The data for this study came from the BrainIT database [73] on a sample of 12 patients in whom the ICP signal contained both systolic and diastolic components. The results showed that there was no direct statistical relationship between the first 48 hours of autoregulatory status and clinical outcome. This is may in part be due to the small sample size. It was then decided to augment the model with known clinical parameters known to have prognostic factors on clinical outcome, such as age, sex, Glasgow motor and pupil scores on admission and then re-run the analysis which proved to be more fruitful as this model yielded a good relation ship with clinical outcome. Of course this leaves the question does the autoregulatory prediction variable add any value to the model. To attempt to assess this the full model was evaluated using an automated parameter reduction technique in which Akaike's Information Criterion was used as a measure of change between subsequent reduced models. Even though this ultimately showed the autoregulatory prediction value did not increase this model's ability to correlate with outcome it was better in general and remained in the model being reduced for longer than any other term which was automatically reduced.

All of this work has really only scratched the surface of the techniques that can be applied and the models that can be developed and tested in the cerebral autoregulatory domain. It has also begun to highlight some of the inadequacies with the literature in this area especially with model comparison and optimisation. One major issue is the lack of readily available data which meets the criteria, set out in chapter 3, that of high quality data with a high enough sampling rate and containing estimates of the state of autoregulation. The lack of such data means that any study of models or modelling is impeded by requiring data to be collected prospectively. This seems counter productive because every model that has been compared in this work has already been evaluated on a collected dataset for their original paper by their author, so clearly such data does exist even if not readily available. Another issue in this area is related to the idea of the autoregulatory space and the problem of choice, to ease inter-comparison there should be some agreed standard of what this space should be. This lack of agreement between investigators hampers all studies from simple optimisation questions such as: "what is the end point to optimise against?". Without adherence to an agreed standard of what is an autoregulation output, is one prediction of intact autoregulation equivalent to another models prediction?

These issues affect the full cerebral autoregulation research domain, so any solution should ideally involve the wider research community. To address the lack of consensus researchers in this domain need to come together to foster more collaboration and in particular to agree on standards of measurement and definition and to address the main issue of lack of "good" data. Ideally such a group should administer a store of donated datasets which would help drive open collaboration and research into defining standards. The idea of large research networks which are focused on a research area are not a new one: BrainIT (www.brainit.org), EBIC (www.ebic.nl), ABIC (www.abic.vcu.edu), COSBID (www.cosbid.org) to name a few of these networks. However no network exists in the specific domain of cerebral autoregulation or cerebral haemodynamics.

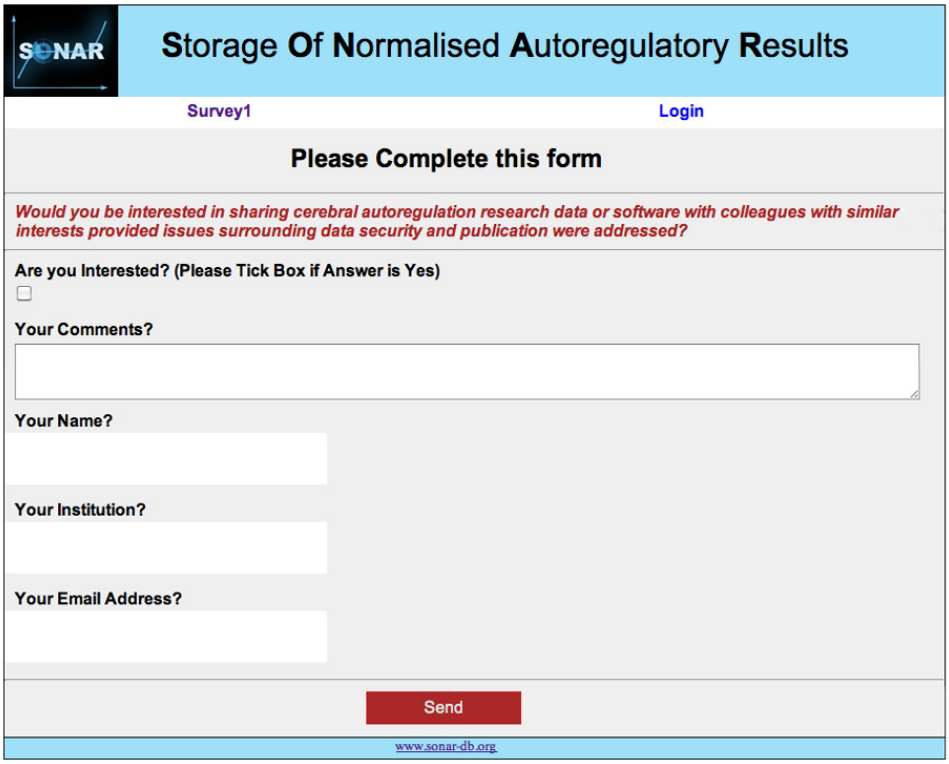


Figure 8.1: Questionnaire form from the SONAR website.

This is a great "ideal" of course which can so easily fall at the first hurdle if no one else in the wider research community feels that sharing data and fostering collaboration is the best path forward to drive the future of studies and projects within the autoregulation domain. To gauge this feeling a small meeting was organised between a small group of leading UK researchers in the area. This included Tony Birch (Clinical Physics University of Southampton) , Ronney Pannerai (Clinical Physics, University of Leicester), Ian Piper (Clinical Physics, Greater Glasgow Health board), David Simpson(Clinical Phyiscs, University of Southampton) and myself. At this meeting I proposed the question of whether such a collaboration was a good idea and was met with resounding agreement. From here, under the working title of Storage Of Normalised Autoregulatory Results (SONAR), a web site was designed with a polling form, figure 8.1, asking the question, "Do you think creating a larger research network for sharing data and developing standards is practical and if so would you participate". The link to the web site was then emailed out to the research community based on email lists supplied from the other attendees of the original meeting. Out of the 45 emails sent, 60 percent


Figure 8.2: Group photograph of the attendees to the inaugural CARNet meeting.

responded and all of those were positive and agreed that it was worth pursuing.

The interim steering group for the project, made up of the original meeting participants and now included Marek Czosnyka from Cambridge. Having reviewed this survey response, we set about organising an initial meeting of this network inpotentia. Our aim being to not only discuss the concept of collaboration but also discussing specifically technical solutions to sharing not just data but also methods, models and research. This inaugural meeting was held on the 6th of July 2011 at Imperial College London where 30 researchers, see figure 8.2 and table 8.1, participated and the name for the new network was agreed to be Cerebral Autoregulation Research Network or CARNet and the main goals were to be those that were initially laid out in the first proposal and are repeated below, table 8.2. A formal steering group was formed (shown in Table 8.3 below), a web site has been created (www.car-net.org) and currently funding is being sought.

| Photo Key | Attendee Name | Location |
|---|---|---|
| 1 | Emmanuel Katsogridakis | Leicester, UK |
| 2 | Bernardo Yelich | Uruguay |
| 3 | Liu Jia | China |
| 4 | Johannes van Lieshout | Netherlands |
| 5 | Corina Puppo | Uruguay |
| 6 | Ian Piper | Glasgow, UK |
| 7 | Stephen Hobson | York, UK |
| 8 | Ronney Panerai | Leicester, UK |
| 9 | Bart Depreitere | Belgium |
| 10 | Stephen Payne | Oxford, UK |
| 11 | Vera Novak | USA |
| 12 | Thomas Heldt | USA |
| 13 | Erik Gommer | Netherlands |
| 14 | David Simpson | Southampton, UK |
| 15 | Jurgen Claassen | Netherlands |
| 16 | Tony Birch | Southampton, UK |
| 17 | Caroline Rickards | USA |
| 18 | Christina Aubrich | Germany |
| 19 | Tom Robinson | Leicester, UK |
| 20 | Elsa Azevedo | Portugal |
| 21 | John Potter | Norfolk, UK |
| 22 | Astrid Hoedemaekers | Netherlands |
| 23 | Karol Budohoski | Cambridge, UK |
| 24 | Andrew Robertson | Canada |
| 25 | Jorge Serrador | USA |
| 26 | Marcel Aries | Netherlands |
| 27 | Rong Zhang | USA |
| 28 | Kenichi Iwasaki | USA |
| 29 | Matthias Reinhard | Germany |
| 30 | Georgios Mitsis | Cyprus |
| 31 | Richard Hughson | Canada |
| 32 | Shieak Tzeng | New Zealand |

Table 8.1: List of the attendees to the inaugural CARNet meeting.

| Number | Goal |
|---|---|
| 1 | Sharing data |
| 2 | Sharing methods for experimental set-ups and data analysis |
| 3 | Sharing results, experiences and ideas |

Table 8.2: The main goals for the CARNet group. As agreed at the first meeting.

| Member Name | Title |
|---|---|
| David Simpson | Chairman |
| Stephen Payne | Secretary |
| Vera Novak | Funding coordinator |
| Martin Shaw | Technical coordinator |
| Jurgen Claassen | Projects coordinator |
| Erik Gommer | Ordinary member |

Table 8.3: The steering group members for the CARNet group.

This network is extremely young and has not had a chance to fully attempt to address these goals but now that it exists it suggests that there is a more hopeful future for better collaboration of researchers within this important clinical area and the major problems facing the domain can now start to be tackled as a group.

The four main goals set out at the end of chapter 1 have been met with varying degrees of success throughout this work. Firstly the assessment of the reworked Ursino model has shown that it has a predictive power which is equal to if not better than the other models which were tested, that is not to say the predictive power found would be classed as good by any means. An effective one in three chance of correctly predicting the autoregulatory state is only acceptable when assessing the second main aim of the work, that is comparison of this new index of autoregulation against the other more widely accepted autoregulatory models of the PRx and the HMF which demonstrate only a one in ten chance of predicting correctly.

This comparison of models has a number of challenges to keep it fair between all the models included in the test. The major problem, which has been mentioned before, is collecting a “clean” dataset which can be used in the comparison, every dataset used in this work had noise or missing data issues which needed to be addressed. It is the need to address the limitations which naturally leads to the creation of a framework to perform these comparison operations in a structured way and to also improve upon any of the models through a series of optimisation steps. However, this approach was not a universal solution as all optimisation strategies do not apply in all situations

which is well illustrated by the fact that even a simple optimisation strategy can not work on the reworked Ursino model. The rest of the framework and its improvements and applications have been explored quite thoroughly earlier in this chapter, however because of its abstract and ubiquitous nature it is one of the most important outcomes from this work as it reveals some of the issues with autoregulatory research as a whole such as a lack of a standard for defining how autoregulation should be defined. Should it be dichotomous, categorical or a continuous function? This naturally leads to the last aim from chapter 1, the proposal for creating a multi centre collaboration for the assessment of this model within the wider autoregulatory community.

Cerebral autoregulation has wide reaching clinical implications if a robust and practical clinical methodology can be developed and validated. Key to this is a structured approach to compare and optimise models of autoregulation, both those that already exist and when new ones are developed. I believe that tackling this fundamental lack of scientific comparison is one of the key ways to advance the knowledge of this research area. Abstracting the modelling process via topological concepts provides an easier means to visualise the overall process and to evaluate new functions for modelling and optimisation. To make this process efficient and to reduce the likelihood of duplication of effort, a sensible solution is to pool any existing resources and build a community driven to answer basic issues collectively.

# Appendix A

# Mathematical reworking of the Ursino Model

| Variable | Meaning |
|---|---|
| $P_a(t)$ | Arterial Blood Pressure |
| $P_{ICP}(t)$ | Intracranial pressure |
| $P_{CPP}(t)$ | Cerebral perfusion pressure |
| $C_a(t)$ | Arterial-arteriolar compliance |
| $R_f$ | Cerebrospinal fluid formation resistance |
| $R_{Pv}$ | Proximal venous resistance |
| $q_n$ | Basal cerebrospinal fluid flow rate |
| $\tau$ | Time constant of autoregulation |
| $\Delta C_a$ | Amplitude of sigmoidal curve |
| $C_{an}$ | Basal arterial compliance for the sigmoid curve |
| $k_r$ | Constant of proportion between arterial resistance and arterial-arteriolar volume |

Table A.1: Reworked Ursino model variables

## A.1 Introduction

The mathematical reworking for this model has been done both by hand as well as by the Maple computer algebra system [57] as a check to make sure that it is correct. The original mathematical model is based on the physiological model shown in figure 2.2 and is discussed in chapter 2. This electric equivalence circuit is used to compute a number of quantities in the original model.

## A.2 The original model

From the original paper [102] the mathematical model is defined by two aspects firstly a basic set of quantities that are defined in table A.1. These are in general secondary to the original model and can be considered state variables or constants which only play an auxiliary role overall. Then, secondly, the base equations that are derived from the physiological model and its equivalence need be considered.

In total there are seven main equations that are used to rearrange the original model. The strategy here is to combine the original equations into a cohesive mathematical

equation then to rearrange this to output the required cerebral autoregulatory state. To begin with the arterial-arteriolar volume and its relationship to arterial compliance is defined as

$$\begin{aligned} V_a(t) &= C_a(t)(P_a(t) - P_{ICP}(t)) \\ &= C_a(t)P_{CPP}(t) \end{aligned} \tag{A.1}$$

then the arterial resistance is shown to be

$$R_a(t) = \frac{k_r C_{an}^2}{V_a(t)^2} \tag{A.2}$$

The cerebral blood flow is derived in two ways directly from the equivalence diagram

$$q(t) = \frac{P_a(t) - P_c(t)}{R_a(t)} \tag{A.3}$$

$$= \frac{P_c(t) - P_{ICP}(t)}{R_f} + \frac{P_c(t) - P_{ICP}(t)}{R_{Pv}} \tag{A.4}$$

the flow rate was then normalised as follows

$$x(t) = \frac{q(t) - q_n}{q_n} \tag{A.5}$$

The capillary pressure is calculated by letting the flow rate formula A.3 equal to equation A.4 then rearranging to give

$$P_c(t) = \frac{P_a(t)R_f R_{Pv} + P_{ICP}(t)R_a(t)R_{Pv} + P_{ICP}(t)R_a(t)R_f}{R_f R_{Pv} + R_a(t)R_{Pv} + R_a(t)R_f} \tag{A.6}$$

Finally the rate of change of arterial compliance is calculated from the three processes for autoregulation

$$\frac{d}{dt}C_a(t) = \frac{-C_a(t) + \sigma(G(t)x(t))}{\tau} \tag{A.7}$$

where $\sigma()$ is the case based sigmoid function defining a part of the autoregulatory dynamics.

## A.3 Mathematical Reworking

From these equations we begin with equation A.1 and differentiate this to give

$$\frac{d}{dt}V_a(t) = C_a(t)\frac{d}{dt}P_{CPP}(t) + P_{CPP}(t)\frac{d}{dt}C_a(t) \tag{A.8}$$

Which when we rearrange equation A.8 for $\frac{d}{dt}C_a(t)$ we get

$$\frac{d}{dt}C_a(t) = \frac{\frac{d}{dt}V_a(t) - C_a(t)\frac{d}{dt}P_{CPP}(t)}{P_{CPP}(t)} \tag{A.9}$$

This new equation A.9 can then be equated with the original function A.7 for the rate of change of arterial compliance so that the main gain function can be assessed:

$$\begin{aligned}
\frac{-C_a(t) + \sigma(G(t)x(t))}{\tau} &= \frac{\frac{d}{dt}V_a(t) - C_a(t)\frac{d}{dt}P_{CPP}(t)}{P_{CPP}(t)} && \Rightarrow \\
\sigma(G(t)x(t)) &= \frac{\tau\frac{d}{dt}V_a(t) - \tau C_a(t)\frac{d}{dt}P_{CPP}(t)}{P_{CPP}(t)} + C_a(t) && \Rightarrow \\
G(t) &= \sigma^{-1}\left(\frac{\tau\frac{d}{dt}V_a(t) - \tau C_a(t)\frac{d}{dt}P_{CPP}(t)}{P_{CPP}(t)} + C_a(t)\right)\frac{1}{x(t)} && \text{(A.10)}
\end{aligned}$$

From this point if we proceed with the original sigmoid function the $G(t)$ function will also end up bifurcated, split by the same case as is used in the sigmoid function. What this means is there are two variations of the $\sigma()$ function dependent on the $x(t)$ value. Allowing an asymmetric curvature at the top and bottom of the sigmoid curve. This of course has the knock on effect of causing the $G(t)$ function to have two variations

also.

$$\sigma(z) = \frac{C_{an} + \frac{\Delta C_a}{2} + (C_{an} - \frac{\Delta C_a}{2}) \exp(\frac{4z}{\Delta C_a})}{1 + \exp(\frac{4z}{\Delta C_a})} \tag{A.11}$$

$$x(t) \begin{cases} < 0 \Rightarrow \Delta C_a = \Delta C_{a1} \\ > 0 \Rightarrow \Delta C_a = \Delta C_{a2} \end{cases} \tag{A.12}$$

To understand how to calculate $G(t)$ directly there are two main intermediate calculations that must be combined. The inverse of $\sigma()$ and the calculation of the normalised flow $x(t)$. To begin with take the sigmoid equation A.11 and multiply by the denominator and divide by $\sigma(z)$ to give

$$\sigma(z) = \frac{C_{an} + \frac{\Delta C_a}{2} + (C_{an} - \frac{\Delta C_a}{2}) \exp\left(\frac{4z}{\Delta C_a}\right)}{1 + \exp\left(\frac{4z}{\Delta C_a}\right)}$$

$$1 + \exp\left(\frac{4z}{\Delta C_a}\right) = \frac{C_{an} + \frac{\Delta C_a}{2}}{\sigma(z)} + \left(\frac{C_{an} - \frac{\Delta C_a}{2}}{\sigma(z)}\right) \exp\left(\frac{4z}{\Delta C_a}\right)$$

If we then subtract $\exp\left(\frac{4z}{\Delta C_a}\right)$ from both sides and collect for the exponential terms

$$1 = \frac{C_{an} + \frac{\Delta C_a}{2}}{\sigma(z)} + \left(\frac{C_{an} - \frac{\Delta C_a}{2}}{\sigma(z)} - 1\right) \exp\left(\frac{4z}{\Delta C_a}\right)$$

then we can isolate the exponential

$$\frac{1 - \frac{C_{an} + \frac{\Delta C_a}{2}}{\sigma(z)}}{\frac{C_{an} - \frac{\Delta C_a}{2}}{\sigma(z)} - 1} = \exp\left(\frac{4z}{\Delta C_a}\right)$$

Next we simplify the left hand side and take the log of both sides

$$\log\left(\frac{\sigma(z) - C_{an} - \frac{\Delta C_a}{2}}{C_{an} - \frac{\Delta C_a}{2} - \sigma(z)}\right) = \frac{4z}{\Delta C_a}$$

Finally if we isolate $z$ we have

$$z = \frac{\Delta Ca}{4} \log \left( \frac{\sigma(z) - C_{an} - \frac{\Delta C_a}{2}}{C_{an} - \frac{\Delta C_a}{2} - \sigma(z)} \right) \tag{A.13}$$

If this is placed to one side and we now consider normalised flow and flow equations A.5 and A.4 respectively we can see that

$$\begin{aligned} x(t) &= \frac{q(t) - q_n}{q_n} \\ &= \frac{q(t)}{q_n} - 1 \end{aligned}$$

and

$$\begin{aligned} q(t) &= \frac{P_C(t) - P_{ICP}(t)}{R_f} + \frac{P_C(t) - P_{ICP}(t)}{R_{Pv}} \\ &= \frac{(R_{Pv} + R_f)(P_C(t) - P_{ICP}(t))}{R_f R_{Pv}} \end{aligned}$$

if we then combine these equations together we get

$$\begin{aligned} x(t) &= \frac{(R_{Pv} + R_f)(P_C(t) - P_{ICP}(t))}{q_n R_f R_{Pv}} - 1 \\ &= \frac{(R_{Pv} + R_f)(P_C(t) - P_{ICP}(t)) - q_n R_f R_{Pv}}{q_n R_f R_{Pv}} \end{aligned} \tag{A.14}$$

To complete this rearrangement we will let $z = G(t)x(t)$ and substitute this into equation A.13

$$G(t)x(t) = \frac{\Delta Ca}{4} \log \left( \frac{\sigma(G(t)x(t)) - C_{an} - \frac{\Delta C_a}{2}}{C_{an} - \frac{\Delta C_a}{2} - \sigma(G(t)x(t))} \right) \tag{A.15}$$

and we know from equation A.10 what $\sigma(G(t)x(t))$ is equal to

$$G(t)x(t) = \frac{\Delta Ca}{4} \log \left( \frac{\frac{\tau \frac{d}{dt} V_a(t) - \tau C_a(t) \frac{d}{dt} P_{CPP}(t)}{P_{CPP}(t)} + C_a(t) - C_{an} - \frac{\Delta C_a}{2}}{C_{an} - \frac{\Delta C_a}{2} - \frac{\tau \frac{d}{dt} V_a(t) - \tau C_a(t) \frac{d}{dt} P_{CPP}(t)}{P_{CPP}(t)} + C_a(t)} \right) \tag{A.16}$$

To simplify this slightly let us take the numerator and denominator into their own functions

$$= \frac{\Delta Ca}{4} \log \left( \frac{F_{num}(t)}{F_{den}(t)} \right) \tag{A.17}$$

This now allows us to look at $F_{num}(t)$ and $F_{den}(t)$ independently of one another

$$\begin{aligned} F_{num}(t) &= \frac{\tau \frac{d}{dt} V_a(t) - \tau C_a(t) \frac{d}{dt} P_{CPP}(t)}{P_{CPP}(t)} + C_a(t) - C_{an} - \frac{\Delta C_a}{2} \\ &= \frac{\tau \frac{d}{dt} V_a(t) - \tau C_a(t) \frac{d}{dt} P_{CPP}(t) + C_a(t) P_{CPP}(t) - C_{an} P_{CPP}(t) - \frac{\Delta C_a}{2} P_{CPP}(t)}{P_{CPP}(t)} \end{aligned} \tag{A.18}$$

From equation A.1 we can change the $C_a(t)$ into a function in $V_a(t)$

$$\begin{aligned} F_{num}(t) &= \frac{\tau \frac{d}{dt} V_a(t) - \tau \frac{V_a(t)}{P_{CPP}(t)} \frac{d}{dt} P_{CPP}(t) + \frac{V_a(t)}{P_{CPP}(t)} P_{CPP}(t) - C_{an} P_{CPP}(t) - \frac{\Delta C_a}{2} P_{CPP}(t)}{P_{CPP}(t)} \\ &= \frac{\tau \frac{d}{dt} V_a(t) - \tau \frac{V_a(t)}{P_{CPP}(t)} \frac{d}{dt} P_{CPP}(t) + V_a(t) - (C_{an} + \frac{\Delta C_a}{2}) P_{CPP}(t)}{P_{CPP}(t)} \\ &= \frac{\tau P_{CPP}(t) \frac{d}{dt} V_a(t) - \tau V_a(t) \frac{d}{dt} P_{CPP}(t) + V_a(t) P_{CPP}(t) - (C_{an} + \frac{\Delta C_a}{2}) (P_{CPP}(t))^2}{(P_{CPP}(t))^2} \\ &= \frac{\left(\tau \frac{d}{dt} V_a(t) + V_a(t)\right) P_{CPP}(t) - \tau V_a(t) \frac{d}{dt} P_{CPP}(t) - (C_{an} + \frac{\Delta C_a}{2}) (P_{CPP}(t))^2}{(P_{CPP}(t))^2} \\ &= \frac{2\left(\tau \frac{d}{dt} V_a(t) + V_a(t)\right) P_{CPP}(t) - 2\tau V_a(t) \frac{d}{dt} P_{CPP}(t) - (2C_{an} + \Delta C_a) (P_{CPP}(t))^2}{2(P_{CPP}(t))^2} \end{aligned} \tag{A.19}$$

If we now apply the same simplification technique we find that

$$F_{num}(t) = \frac{H_{num}(t)}{2(P_{CPP}(t))^2} \tag{A.20}$$

Then a set of similar steps can be carried out on $F_{den}(t)$ to show that

$$F_{den}(t) = \frac{-2\left(\tau\frac{d}{dt}V_a(t) + V_a(t)\right)P_{CPP}(t) + 2\tau V_a(t)\frac{d}{dt}P_{CPP}(t) + (2C_{an} - \Delta C_a)(P_{CPP}(t))^2}{2(P_{CPP}(t))^2} \tag{A.21}$$

$$= \frac{H_{den}(t)}{2(P_{CPP}(t))^2} \tag{A.22}$$

When we now take the numerator equation A.20 and the denominator equation A.22 back into equation A.17 we get

$$G(t)x(t) = \frac{\Delta C_a}{4}\log\left(\frac{\frac{H_{num}(t)}{2(P_{CPP}(t))^2}}{\frac{H_{den}(t)}{2(P_{CPP}(t))^2}}\right)$$

$$G(t) = \frac{\Delta C_a \log\left(\frac{H_{num}(t)}{H_{den}(t)}\right)}{4x(t)} \tag{A.23}$$

Finally if we substitute equation A.14 into equation A.23 we end up with equation A.24. With the case split as is shown in equation A.12 that is $\Delta C_a = \Delta C_{a1}$ when $x(t)$ is less than zero and $\Delta C_a = \Delta C_{a2}$ when the normalised flow rate is greater than zero.

$$G(t) = \frac{-\log\left(\frac{H_{num}(t)}{H_{dem}(t)}\right)\Delta C_a q_n R_f R_{Pv}}{4((R_{Pv} + R_f)(P_{ICP}(t) - P_C(t)) + q_n R_f R_{Pv})} \tag{A.24}$$

$$H_{num}(t) = -(2C_{an} + \Delta C_a)P_{CPP}(t)^2 + \left(2\tau\frac{d}{dt}V_a(t) + 2V_a(t)\right)P_{CPP}(t) - 2\tau V_a(t)\frac{d}{dt}P_{CPP}(t) \tag{A.25}$$

$$H_{dem}(t) = (2C_{an} - \Delta C_a)P_{CPP}(t)^2 - \left(2\tau\frac{d}{dt}V_a(t) + 2V_a(t)\right)P_{CPP}(t) + 2\tau V_a(t)\frac{d}{dt}P_{CPP}(t) \tag{A.26}$$

This is a relatively complex model however that can be simplified from equations A.25 and A.26 so that the main $G(t)$ function becomes

$$\begin{aligned} H_{dem}(t) + H_{num}(t) &= (2C_{an} - \Delta C_a)P_{CPP}(t)^2 - (2C_{an} + \Delta C_a)P_{CPP}(t)^2 \\ &= -2\Delta C_a P_{CPP}(t)^2 \\ H_{num}(t) &= -2\Delta C_a P_{CPP}(t)^2 - H_{dem}(t) \\ \frac{H_{num}(t)}{H_{den}(t)} &= \frac{-2\Delta C_a P_{CPP}(t)^2}{H_{den}(t)} - 1 \end{aligned} \tag{A.27}$$

substituting equation A.27 into function A.24 we finally get

$$G(t) = \frac{-\log\left(\frac{-2\Delta C_a P_{CPP}(t)^2}{H_{den}(t)} - 1\right)\Delta C_a q_n R_f R_{Pv}}{4((R_{Pv} + R_f)(P_{ICP}(t) - P_C(t)) + q_n R_f R_{Pv})} \tag{A.28}$$

where $\Delta C_a$ changes based on the original sigmoid case split as detailed above and $H_{den}(t)$ is described in equation A.26. This form (equation A.28) of the reworked Ursino model has a two main issues to direct use in most clinical situations. These issues are addressed in chapter 2.

# Appendix B

# Methodology to model an asymmetric sigmoid curve.

## B.1 Introduction

During the modelling of many processes in the medical arena there is a need for functions that are both continuous and differentiable at all points. This is to aid in the creation of medical models that are mathematically robust under transformations that may be applied to them. One such set of models that have frequently been used are the sigmoid family of curves. These are useful in many areas especially in pharmacokinetic modelling and physiological modelling. Normally the curves that are used will be symmetric in their curvature at the top and bottom but there is a call for more control in creation and fitting of these curves to data where the top and bottom curvature is distinct from each other.

In the past there have been at least two popular asymmetric sigmoid curves Richards [80] and Gompertz [34] both of which could be classed as proportionally asymmetric, that is the difference in curvature of one is proportional to the difference in the other. This is of course an advancement over purely symmetric functions however this may not go far enough to address the needs of some of the models currently in use today.

The classical symmetric sigmoid function has the form (equation B.1) which is easily recognised in figure B.1.

$$f(x) = \frac{A}{1 + Be^{-Cx}} \tag{B.1}$$

There needs to be more control over all the aspects of the function, both top and bottom curvature should be individually configurable as well as the various asymptotes.

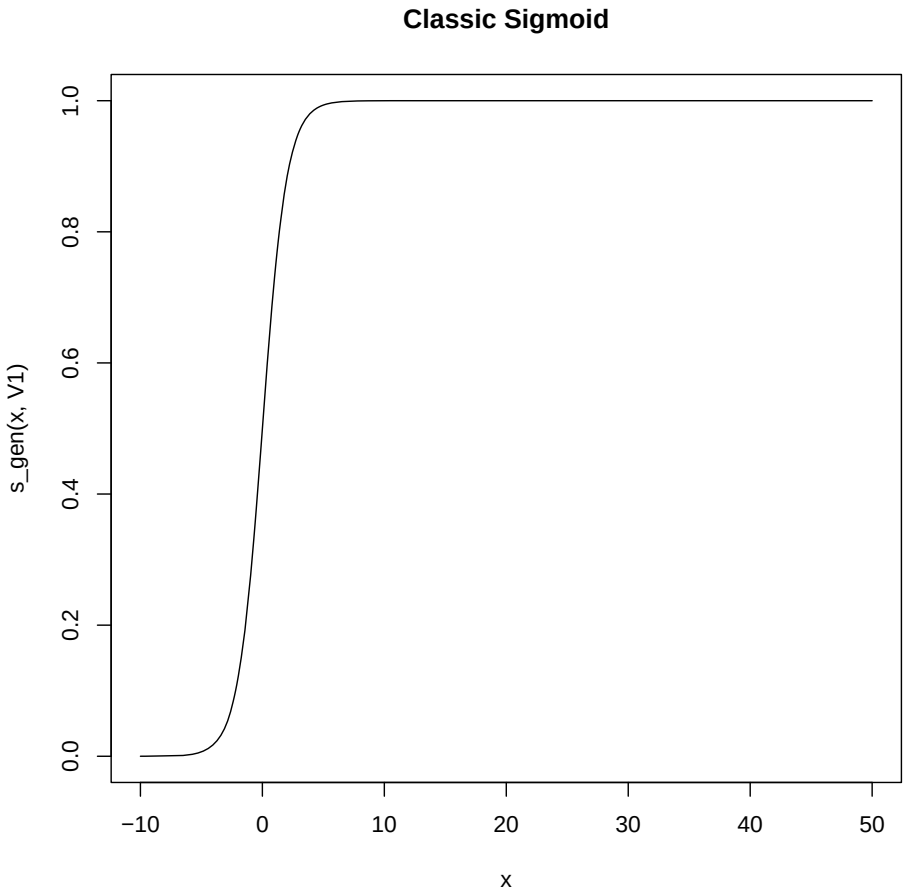


Figure B.1: Classic Sigmoid

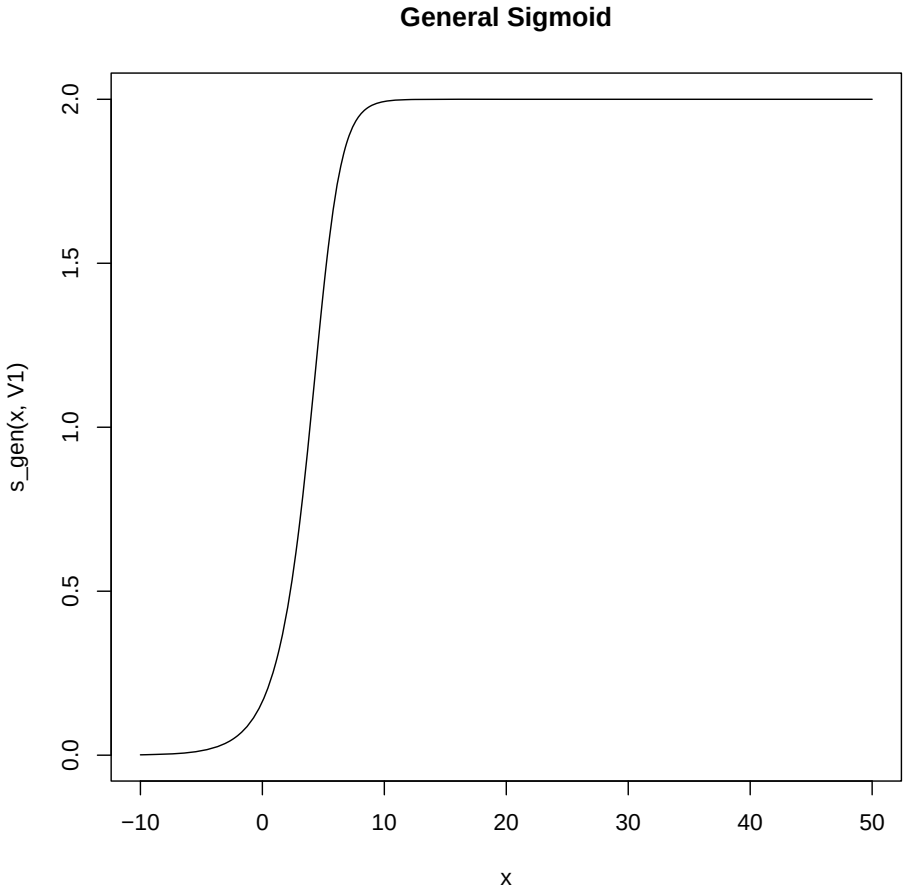


Figure B.2: General Asymmetric Sigmoid

## B.2 Asymmetric Sigmoids

### B.2.1 General Sigmoid Form

The classic generalised sigmoid function [80] has the form (equation B.2) and can be evaluated as both a standard sigmoid and as a proportional asymmetric sigmoid.

$$f(x) = A + \frac{B - A}{\left(1 + Ce^{-D(x-G)}\right)^{\frac{1}{H}}} \tag{B.2}$$

Where $\{A, B, C, D, G, H\}$ are all constants defining the shape of the sigmoid (see figure B.2) and $e$ is Euler's number 2.718. Notice in equation B.2 that variables $A$ and $B$ specify the lower and upper asymptote respectively, $C$ and $D$ giving the general

curvature of the upper and lower turning points and it is from these that the general limits of the width of the sigmoid can be derived. The variable $G$ defines a translation in the $x$ axis for the sigmoid. Lastly $H$ will specify the inflection point for the curve and hence how proportionally asymmetric it is.

The inflection point setting is misleading however as it only alters essentially where the upper and lower curves meet leaving the general slope of the sigmoid at the mercy of the width. To get a truly configurable sigmoid this minor problem need to be overcome.

### B.2.2 Gompertz Function

The second most widely used form of asymmetric sigmoid is the Gomperz function [34] and has the form

$$f(x) = A + Be^{-Ce^{-D(x-G)}} \tag{B.3}$$

this function is exponentially asymptotic at the lower asymptote hence as a sigmoid proportionally asymmetric. This can be seen if you compare the Gompertz function to a general symmetric sigmoid (figure B.3). Where the upper curve hardly changes and the lower curve is exponentially faster to reach the asymptote. However, a limitation of this is that the curves will always be exponentially proportional to each other.

### B.2.3 Case Based Asymmetry

The last asymmetric sigmoid in common use with good control over both the upper and lower curvature is through a basic case switch

$$f(x) = \begin{cases} \frac{A}{1+Be^{-Cx}} & x \leq 0 \\ \frac{D}{1+Ge^{-Hx}} & x > 0 \end{cases} \tag{B.4}$$

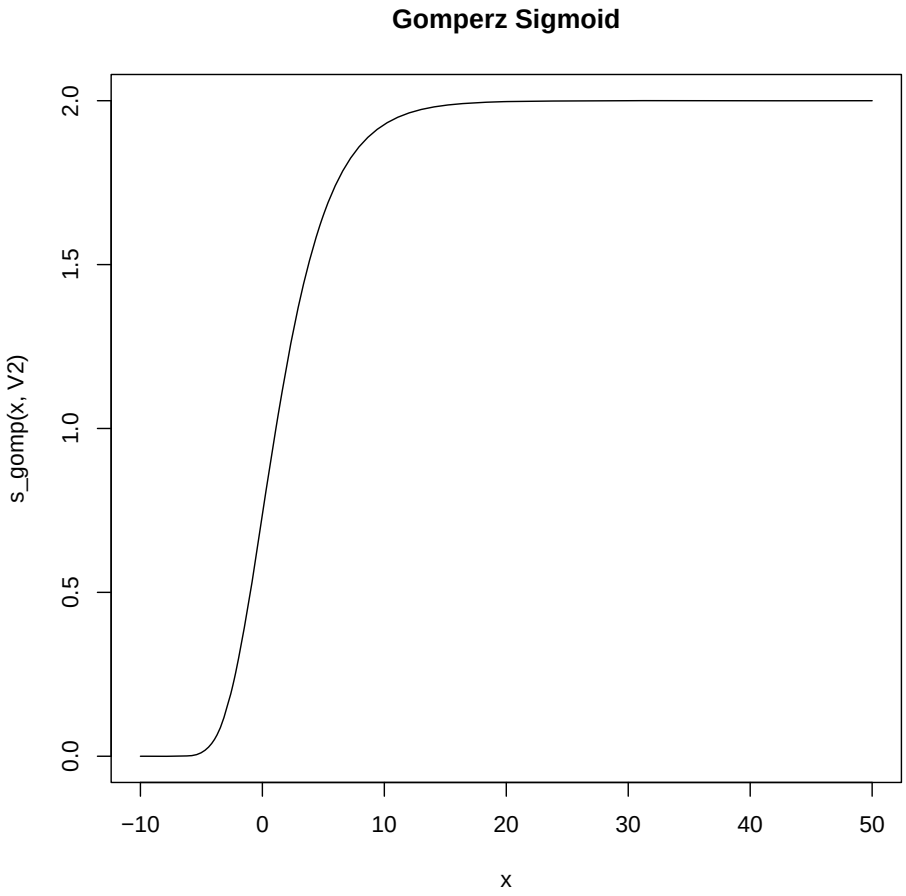


Figure B.3: Gomperz Sigmoid

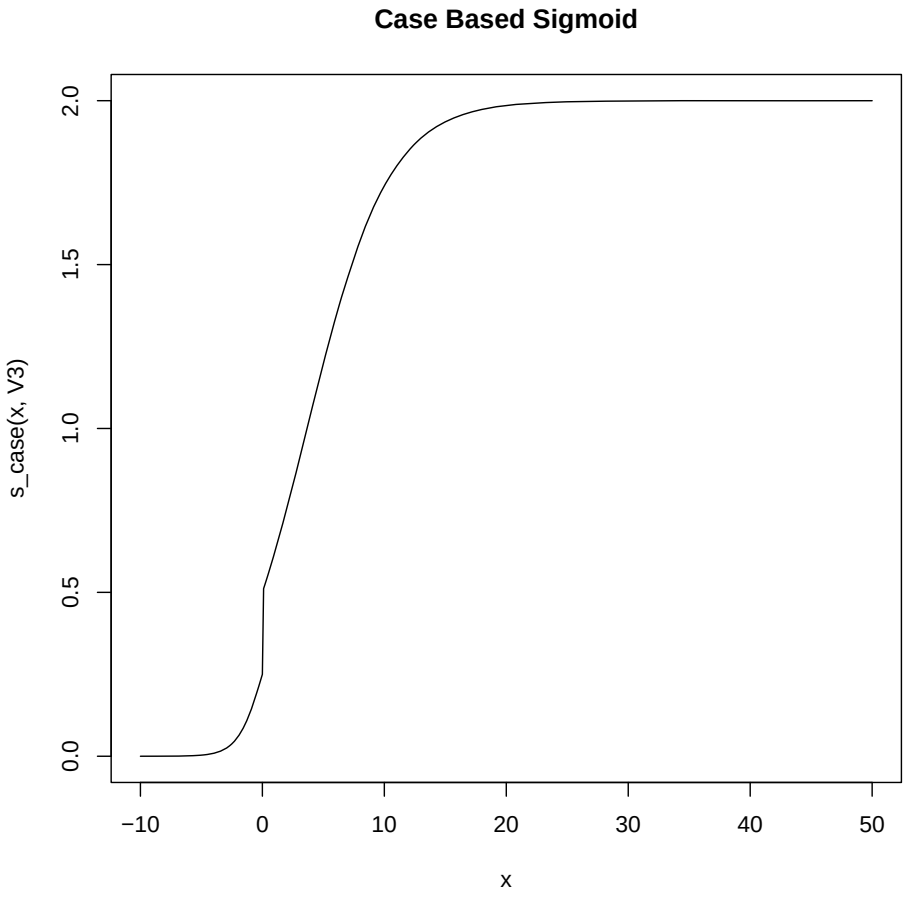


Figure B.4: Case Based Sigmoid

where the first case defines the lower curvature and the second case would affect the upper curvature (figure B.4). The main problem with this approach is it is not a continuously differentiable function and is discontinuous at the switch over point in this case 0. This if treated carefully isn't much of a problem however it can introduce issues, which have to be worked around, into any larger analysis that is being performed with the sigmoid function. A good example of such a problem is trying to statistically fit data to the inverse of the above sigmoid can often cause the discontinuity point to become a disassociation. That is the limits of each half of the function are not equal as $x$ tends to the discontinuity point or 0 in this case.

Each of these sigmoid curves have their uses however even with the most generic of the above functions, equation B.4, its not applicable in all situations.

## B.3 Methodology

The technique used to construct the new asymmetric sigmoid isn't a new one [99] however what is presented below does extend this methodology to give better handling of the asymptotic nature of the sigmoid. At the heart of this idea is modification of an existing symmetric sigmoid curve. This is via multiplication and addition of other curves on one half of the sigmoid.

The three main participating curves are a general sigmoid minus the asymmetry term $H$ which is shown in equation B.5.

$$f(x) = A + \frac{B - A}{1 + Ce^{-D(x-I)}} \tag{B.5}$$

The first additional function can be seen in equation B.6 which is a skewed Gaussian type curve that when matched properly with equation B.5 will allow the manipulation of the upper curve of the original sigmoid. Where $J$ defines the scaling of the function,

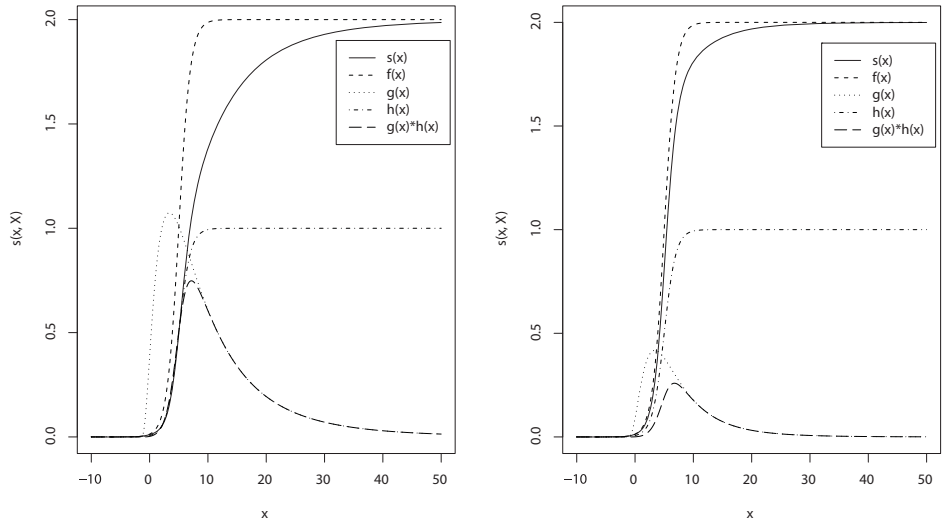


Figure B.5: New Asymmetric sigmoid curve examples.

$K$ defines the width of the function and $L$ defines its placement on the $x$ axis.

$$g(x) = Je^{-K\Re((log(-x-L))^2)} \tag{B.6}$$

The second additional sigmoid clamped between 1 and 0 will improve the tail of the additional function B.6, this can be seen in equation B.7.

$$h(x) = \frac{1}{1 + e^{-M(x-N)}} \tag{B.7}$$

The new sigmoid is a linear combination of these three functions. This is shown in equation B.8 and in figure B.5.

$$\begin{aligned} s(x) &= f(x) - g(x)h(x) \\ s(x) &= A + \frac{B-A}{1 + Ce^{-D(x-I)}} - \frac{Je^{-K\Re((log(-x-L))^2)}}{1 + e^{-M(x-N)}} \end{aligned} \tag{B.8}$$

This is only the general form of this equation and the parameter set

$$\mathbf{P} = \{A, B, C, D, I, J, K, L, M, N\}$$

can be simplified to $\mathbf{P_{Fin}} = \{A, B, C, D, I, J, K\}$ giving the final form of the sigmoid

in equation B.9.

$$s(x) = A + \frac{B - A}{1 + Ce^{-D(x-I)}} - \frac{Je^{-K\Re((log(-x-log(I))^2)}}{1 + e^{-D(x-I)}} \tag{B.9}$$

The set $\mathbf{P_{Fin}}$ should then be created through a non linear least squares fit to an original data set or original quasi-asymmetric curve.

## B.4 Discussion

With each new attempt at a fully asymmetric sigmoid curve the parameter set increases at the same time generally making the function more complex to use. This has to be balanced against the gains to the accuracy and the versatility of the new curve function. With this new function B.9 this balance has been achieved through the use of related parameters in the main parameter set. Also because the placement of each of the additional functions is based on the properties of the original base sigmoid (equation B.5) then each of the fitting variables are linked to the previous parameter set. So there exists a function $q(\mathbf{X})$ that given the subset $\mathbf{P_2} \cup \mathbf{P_3} = \{J, K, L, M, N\} \in \mathbf{P}$, where $\mathbf{P_2}$ and $\mathbf{P_3}$ are the parameter sets from functions B.6 and B.7 respectively, the function would generate a set based on $\mathbf{P_1} = \{A, B, C, D, I\} \in \mathbf{P}$.

Through general investigation of the combination of the three curves a number of rules can be found that satisfy this $q(\mathbf{X})$ criteria. Firstly only one of the curvatures should be affected. So to fix the lower curvature $h(x)$ should be as close to the main function $f(x)$ as possible. So $\mathbf{P}_3$ should be fixed to $\{D, I\}$. Secondly $g(x)$ should always be greater than both $f(x)$ and $h(x)$ at the start of the lower curvature this means $\{L\}$ needs to be specified so that it is always proportionally less than $\{I\}$ so in this case $log(I)$ has been chosen. Lastly to guarantee a smooth transition to and from 0 on $g(x)h(x)$ the parameter set $\{J, K\}$ should be limited to make sure where $g(x)$ and $h(x)$ cross happens on the slope of $h(x)$. This then fixes the function $q(\mathbf{X})$ as is shown in

| Variable | fitted value |
|---|---|
| $A$ | 0.113 |
| $B$ | 0.525 |
| $C$ | 54.598 |
| $D$ | 53.333 |
| $I$ | -0.075 |
| $J$ | -0.0001 |
| $K$ | 0.876 |

Table B.1: Fitted values for the asymmetric sigmoid parameters

equation B.10.

$$q(\{p : p \in \mathbf{P_2} \cup \mathbf{P_3}\}) = \begin{cases} log(I) & p = L \\ I & p = N \\ D & p = M \end{cases} \tag{B.10}$$

When this is then introduced into the generalised form B.8 this will create the more practical final form of the function B.9.

## B.5 Comparison of the new model to a case based sigmoid

For this new asymmetric sigmoid curve to be useful it needs to mimic any of the existing asymmetric strategies. To test this within the autoregulatory domain the case based curve from the Ursino paper was chosen and evaluated based on the static values in the paper. This creates the dashed curve in figure B.6. Then using a simple non linear least squares fitting technique on the new asymmetric sigmoid function to find the values for the unknown parameters this gives the curve shown by the solid line on figure B.6. The values of the parameters are shown in table B.1. The goodness of fit is measured by the comparison between the old model and the new which gives an $r$ value of 0.9991. This error is explained by the nature of the curve fitting algorithm used in generating the unknown parameters.

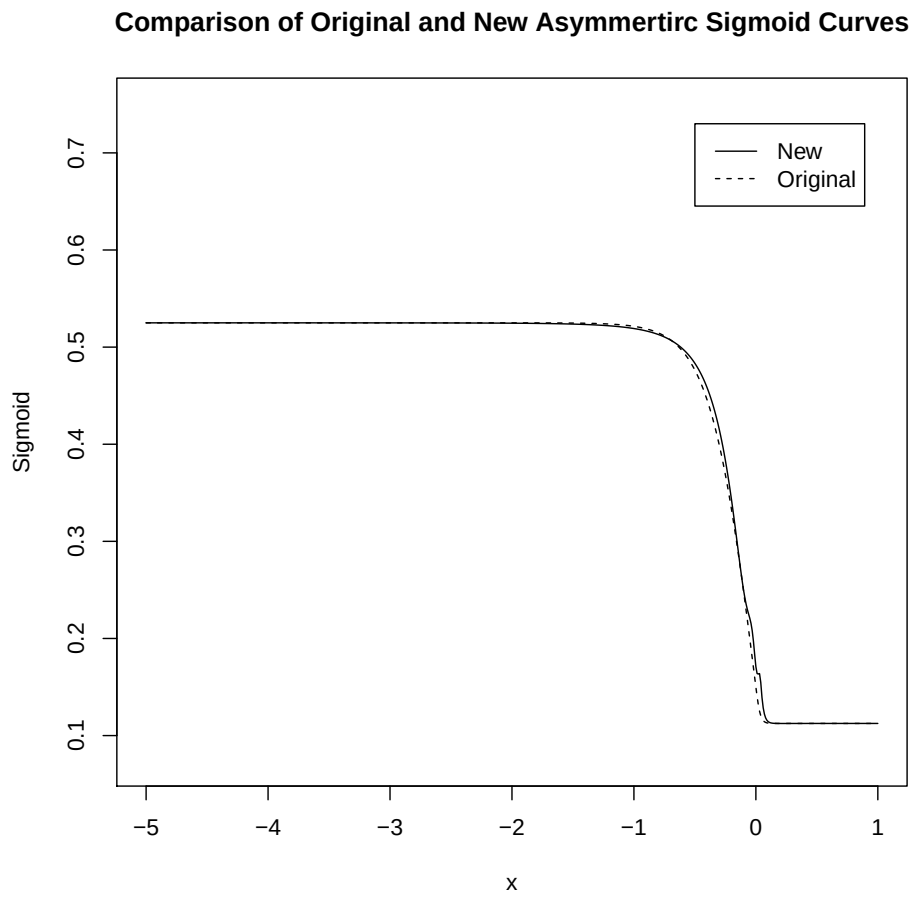


Figure B.6: Comparison of the original Ursino sigmoid to the new fitted asymetric sigmoid.

## B.6 Inversion of the new sigmoid function

It is often useful to be able to invert a function which can increase its utility in many situations. Firstly to fully understand how this can be achieved with the new asymmetric sigmoid it should be first stated that because there is an increase in mathematical complexity this adversely effects any simple algebraic solution. An algebraic solution to the inverse of each sub function that makes up the new sigmoid can be found. Even for function B.6 which makes use of $\Re()$. This function cant be inverted directly but because of apriori knowledge of the original sigmoid it is possible to create an inverse function. All of this, however, doesn't help in crafting a working inverse for the combined sigmoid.

The first thing to realise about the sigmoid is that any working inverse has a very restricted range of values for the independent variable which is because the asymmetric sigmoid is bound above and below by its asymptotes. This translates into two vertical bounds on the inverse function and this is a range restriction on the variable. Anything which are outside these bounds will be imaginary in nature. The second point that should be made about sigmoid's in general is that they have no oscillations, which means that when they are inverted there will be no ambiguity over which value to use as there will only ever be one value. This is not true, for example, with a sine wave and this can be seen with the arc sine function in its full form has an infinite number of values it can take for a single independent value. Then lastly the fact that multiple transcendental functions, that is a function whose value can not be represented as a set of polynomial equations, tend to make purely mathematical inverse solutions very difficult to construct.

Both of these points mean that an inverse solution should be achievable, especially since there is a one to one relationship with input and output. However the solution may not be as elegant as a purely algebraic one because of the fact the function has three

distinct bounded sections and $g(x)/h(x)$ is a non trivial combination of transcendental functions. From this the best strategy for creating the inverse is to simplify the model and attempt to invert it as far as possible to obtain a partial inverse. Then you would use a number of numerical techniques to solve what remained. This has its limitations of course but these are mostly in the implementation of the numeric algorithm in order for it to be able to accurately find all the values. This is made easer because of the one to one relationship with the function values as there should only ever be a single value to numerically find.

So by starting with the more general equation B.8, as this will allow us the greatest scope with simplification approaches, the simplest partial inverse that could be found is shown in equations B.12 and B.11.

$$\begin{aligned}\mathrm{ro}(z,y) =& yMe^{(Ne^z+NL-P)} - yCMe^{(Ne^z+NL-P+Fe^z+FL-E)} \\ &- AMe^{(Ne^z+NL-P)} + ACMe^{(Ne^z+NL-P+Fe^z+FL-E)} \\ &- BMe^{(Ne^z+NL-P)} - y + yCe^{(Fe^z+FL-E)} \\ &+ A - ACe^{(Fe^z+FL-E)} + B + Je^{(-Kz^2+K\arg^2(e^z))} \\ &- JCe^{(-Kz^2+K\arg^2(e^z)+Fe^z+FL-E)} \end{aligned} \tag{B.11}$$

$$\sigma_z^{-1}(y) = e^{(\mathrm{ro}(z,y))} - L \tag{B.12}$$

To then calculate the inverse value, the roots of $\mathrm{ro}(z,y) = 0$ should be found for the specific value of $y$. Then this singular root should be then used with equation B.12.

## B.7 Conclusion

This methodology for construction of an asymmetric sigmoid function has improved control over creating the asymmetry in the curve with only a slight increase in complexity of the equation which uses only one more parameter to fit that of the general sigmoid function. It has the property that it is continuous and differentiable at all points on the curve overcoming any problems that arise in a case based sigmoid approach. As such its use in the various clinical modelling applications would both be straight forward to implement and beneficial to the overall model.

# Appendix C

# Mathematical derivation of a model comparison method.

# C.1 Introduction

To be confident that the comparisons methodology used is adequate for use with the cerebral autoregulation models under test a study of the most common techniques was under taken.

# C.2 Methods

Firstly let $M$ be defined as the contingency table or confusion matrix of the autoregulation model comparison:

$$M = \begin{bmatrix} T_P & F_N \\ F_P & T_N \end{bmatrix}$$

Where $T_P, T_N, F_P, F_N$ are the usual number of true positives, true negatives, false positives and false negatives respectively this shall be the basis for most of the tests to work from. Each of the tests was addressed in turn:

The Fishers exact test needs a balanced number of positive and negatives tests to be performed and in the case of the data set used this is not the case, so any testing performed will be skewed. Most comparisons of this type would use the F-measure [81], from information theory, to assess how well a model corresponds to a given known response:

$$F_\beta = \frac{(1+\beta^2)T_P}{(1+\beta^2)T_P + \beta^2 F_N + F_P} \tag{C.1}$$

Where $\beta = \frac{FN}{(TP+FN)}$ is the false negative rate. The F-measure is normalised between the values of zero and one giving a contained range of model rating. However I feel this normalised value isn't as useful as the determinant of $M$ or in the more general

case the Matthew's correlation coefficient (MCC).

$$MCC = \frac{T_P T_N - F_P F_N}{\sqrt{(T_P + F_P)(T_p + F_N)(T_N + F_P)(T_N + F_N)}} \tag{C.2}$$

$$= \frac{\chi}{\sqrt{n}} \tag{C.3}$$

$$= \phi \tag{C.4}$$

The glsMCC [6] can be thought of as a normalised determinant of the comparisons contingency table $M$. It is also equivalent to the phi coefficient and in turn is related to Chi-squared testing, as such the Matthews correlation coefficient ranges, like the F-value, between zero and one.

One thing to note about the $MCC$ is if any of the sums in the denominator equals 0 then we assume $MCC = 0$. This is a consequence of:

$$\lim_{x \to 0} \frac{x}{\sqrt{x}} = 0 \tag{C.5}$$

The receiver operating characteristic (ROC) is a generally accepted methodology for assessing the accuracy or predictive ability of a model however in this case the ROC would not be appropriate. The ROC is usually calculated by running the experiment at different predictor levels and then plotting true positives against false negatives at each of these levels, however in this case there is only one set level for prediction per model so the ROC is not as useful in this context.

The area under the ROC curve (AUC) can be calculated via a trapezoid method for numerical integration. With a single point of interest on the ROC curve the AUC equation can be simplified to

$$AUC = \frac{(T_P F_P + F_N T_N + 2T_P T_N)}{2(T_P + F_N)(F_P + T_N)} \tag{C.6}$$

It can be shown mathematically that the one point AUC is bounded on either side by the $MCC$ and the F-measure:

$$MCC \leq AUC \leq F_\beta \leq 1 \tag{C.7}$$

Let $a \in \mathbb{N}$ then assume $MCC > AUC$ this implies:

$$\frac{T_P T_N - F_P F_N}{\sqrt{(T_P + F_P)(T_p + F_N)(T_N + F_P)(T_N + F_N)}} > \frac{(T_P F_P + F_N T_N + 2T_P T_N)}{2(T_P + F_N)(F_P + T_N)} \tag{C.8}$$

Then let $T_P, T_N, F_P, F_N = a$ so equation C.8 becomes:

$$\begin{aligned} \frac{a^2 - a^2}{\sqrt{(2a)(2a)(2a)(2a)}} &> \frac{(a^2 + a^2 + 2a^2)}{2(2a)(2a)} \\ \frac{0}{\sqrt{(16a^4)}} &> \frac{4a^2}{8a^2} \\ 0 &> \frac{1}{2} \end{aligned}$$

Hence $MCC > AUC$ can not be true so $MCC \leq AUC$. A similar argument can be constructed for $AUC \leq F_\beta$. From equation C.3 we can see the $MCC$ is proportional to the $\chi^2$ distribution which has a tendency to only over estimate the fit if the number of points are too small. Or put another way as $N$ increases the $MCC$ tends to the correct fit and from equation C.7 the $MCC$ will never give a goodness of fit estimate more than the $AUC$ as it is bounded by it and will always be at least as accurate in this situation. This implies that choosing the $MCC$ as the predictive accuracy measure, or goodness of fit, will always be a good compromise between all the tests available.

For a more numeric example of the applicability of this choice it can be argued thus: Consider if the model only ever predicts intact autoregulation, information theory would rate this model above average because at least half of the time it would be correct however in this case this is a problem because it is the ability to separate both

types (intact and non-intact) accurately, not just the ability to derive an answer which is important in classification of these models. So instead of using the F-measure, by using instead the $MCC$ this model would perform very poorly. The use of the $MCC$ also has the added advantage of assessing inverted models, that is models which still have a high degree of specificity and sensitivity but are predicting the exact opposite of what has initially been set out as its goal. In a general comparison of the equations C.2 and C.6 we can see that the argument above against the F-measure also still holds.

## C.3 Conclusion

As can be seen from the above analysis that the $MCC$ is a good all round fit for a general model comparison technique and will be useful when used with the different autoregulation models.

# Appendix D

# Differencing to Differentiable.

# D.1 Introduction

The algorithm used by Daley to calculate the highest modal frequency from his 2004 paper in stroke [27] can be summarised as follows. The original physiological model [22] assessed can be represented as a third order differentiable model relating the dynamic relationship of pressure transmission between intracrainial pressure (ICP) and arterial blood pressure (ABP) as shown in equation D.1. Where $Y(t)$ is ICP at time $t$ and $U(t)$ is ABP at time $t$.

$$\frac{\mathrm{d}^3}{\mathrm{d}t}Y(t) + \alpha_2\frac{\mathrm{d}^2}{\mathrm{d}t}Y(t) + \alpha_1\frac{\mathrm{d}}{\mathrm{d}t}Y(t) + \alpha_0 Y(t) = \beta_3\frac{\mathrm{d}^2}{\mathrm{d}t}U(t) + \beta_2\frac{\mathrm{d}}{\mathrm{d}t}U(t) + \beta_1 U(t) \quad \text{(D.1)}$$

Daley describes modal analysis as investigating the energy transaction between the pressure systems (ABP and ICP) by way of looking at the general dynamic characteristics, in particular focusing on the resonant frequencies. These frequencies are directly tied to the pressure transmission with the high frequencies being reduced by vasoconstriction and increased by vasodilation. So if the highest modal frequency is chosen for study the effects of these physiological changes in the system should be discernable. To calculate these frequencies the solution to equation D.2 needs to be found.

$$x^3 + \alpha_2 x^2 + \alpha_1 x + \alpha_0 = 0 \quad \text{(D.2)}$$

This will only give the radian modal frequencies, the highest of these will then be divided by $2\pi$ to find the highest modal frequency (HMF).

This is all still quite theoretical, as the data collected will not be a continuous signal so can not be considered directly differentiable. Using the recorded data the system would be defined more like equation D.3. Where $Y_{[n]}$ is the ICP value recorded at index $n$ and similar for $U_{[n]}$ is the ABP at index $n$. If $m$ is the total number of points in the

data set then $n \in [1, m]$.

$$Y_{[n]} + a_2 Y_{[n-1]} + a_1 Y_{[n-2]} + a_0 Y_{[n-3]} = b_3 U_{[n]} + b_2 U_{[n-1]} + b_1 U_{[n-2]} \tag{D.3}$$

Finding the constant values for D.3 can easily be achieved using an autoregressive moving average with exogenous inputs (ARMAX) technique. However going from equation D.3 to equation D.1 in [27] is performed using a black box software program. To understand the actual process required to transform the equation constants $a_1, a_2, a_3$ into the necessary $\alpha_1, \alpha_2, \alpha_3$ parameters, the basic relationship between the difference equation and its differential counterpart needs to be understood.

## D.2 Difference Equations.

The classical definition of a difference equation would be expressed as successive differences of a function applied to sequential values of a variable as can be seen in equation D.4. This can be extended to a second order difference equation D.5 and then more generally to D.6.

$$\Delta(Y_{[s]}) = Y_{[s+1]} - Y_{[s]} \tag{D.4}$$

$$\Delta^2(Y_{[s]}) = \Delta(Y_{[s+1]}) - \Delta(Y_{[s]}) \tag{D.5}$$

$$\Delta^r(Y_{[s]}) = \Delta^{r-1}(Y_{[s+1]}) - \Delta^{r-1}(Y_{[s]}) \tag{D.6}$$

Combining these above equations into a set

$$\Delta^3(Y_{[s]}) + p\Delta^2(Y_{[s]}) + q\Delta(Y_{[s]}) + rY_{[s]} \tag{D.7}$$

$$=\Delta^2(Y_{[s+1]}) - \Delta^2(Y_{[s]}) + p\Delta(Y_{[s+1]}) - p\Delta(Y_{[s]}) + qY_{[s+1]} - qY_{[s]} + rY_{[s]} \tag{D.8}$$

$$\begin{aligned}=&\Delta(Y_{[s+2]}) - \Delta(Y_{[s+1]}) - \Delta(Y_{[s+1]}) + \Delta(Y_{[s]}) + pY_{[s+2]} - pY_{[s+1]} \\ &- pY_{[s+1]} + pY_{[s]} + qY_{[s+1]} - qY_{[s]} + rY_{[s]}\end{aligned} \tag{D.9}$$

$$\begin{aligned}=&Y_{[s+3]} - Y_{[s+2]} - Y_{[s+2]} + Y_{[s+1]} - Y_{[s+2]} + Y_{[s+1]} + Y_{[s+1]} - Y_{[s]} \\ &+ pY_{[s+2]} - pY_{[s+1]} - pY_{[s+1]} + pY_{[s]} + qY_{[s+1]} - qY_{[s]} + rY_{[s]}\end{aligned} \tag{D.10}$$

$$=Y_{[s+3]} + (p-3)Y_{[s+2]} + (3-2p+q)Y_{[s+1]} + (p-q+r-1)Y_{[s]} \tag{D.11}$$

Then let $s = n - 3$ equation D.11 would then become

$$\Delta^3(Y_{[n-3]}) + p\Delta^2(Y_{[n-3]}) + q\Delta(Y_{[n-3]}) + rY_{[n-3]} = Y_{[n]} + a_2Y_{[n-1]} + a_1Y_{[n-2]} + a_0Y_{[n-3]} \tag{D.12}$$

It is now easy to see that D.3 is a difference equation of the form D.12.

## D.3 Taylor series expansions.

The Taylor series of a continuous complex valued function $f$ about a point $a$ is defined to be equation D.13.

$$f(x) = \sum_{n=0}^{\infty} \frac{f^{(n)}(a)}{n!}(x-a)^n \tag{D.13}$$

where $f^{(n)}(a)$ is the $n$-th differential with respect to $x$ evaluated at a point $a$.

Consider the finite expansion of three functions $f(t+x)$, $f(t-x)$ and $f(t-2x)$ up to

order 4 about a point $t$ which can be seen in equations D.14, D.15 and D.16.

$$f(t+x) = f(t) + x\frac{\mathrm{d}}{\mathrm{d}x}f(t) + \frac{x^2}{2}\frac{\mathrm{d}^2}{\mathrm{d}x}f(t) + \frac{x^3}{6}\frac{\mathrm{d}^3}{\mathrm{d}x}f(t) + O(x^4) \tag{D.14}$$

$$f(t-x) = f(t) - x\frac{\mathrm{d}}{\mathrm{d}x}f(t) + \frac{x^2}{2}\frac{\mathrm{d}^2}{\mathrm{d}x}f(t) - \frac{x^3}{6}\frac{\mathrm{d}^3}{\mathrm{d}x}f(t) + O(x^4) \tag{D.15}$$

$$f(t-2x) = f(t) - 2x\frac{\mathrm{d}}{\mathrm{d}x}f(t) + 2x^2\frac{\mathrm{d}^2}{\mathrm{d}x}f(t) - \frac{4x^3}{3}\frac{\mathrm{d}^3}{\mathrm{d}x}f(t) + O(x^4) \tag{D.16}$$

Then by performing a set of linear operations on the above equations each of the differential terms can be isolated. Firstly adding equations D.14 and D.15 we get

$$f(t+x) + f(t-x) = 2f(t) + x^2\frac{\mathrm{d}^2}{\mathrm{d}x}f(t) + O(x^4) \tag{D.17}$$

$$\frac{\mathrm{d}^2}{\mathrm{d}x}f(t) = \frac{f(t+x) + f(t-x) - 2f(t)}{x^2} + O(x^4) \tag{D.18}$$

then by subtracting equations D.14 and D.15 we get

$$\begin{aligned} f(t+x) - f(t-x) &= 2x\frac{\mathrm{d}}{\mathrm{d}x}f(t) + \frac{2x^3}{6}\frac{\mathrm{d}^3}{\mathrm{d}x}f(t) + O(x^4) \\ &= 2x\frac{\mathrm{d}}{\mathrm{d}x}f(t) + \frac{x^3}{3}\frac{\mathrm{d}^3}{\mathrm{d}x}f(t) + O(x^4) \end{aligned} \tag{D.19}$$

if we now add equation D.16 and two times equation D.14 we get

$$\begin{aligned} f(t-2x) + 2f(t+x) =& f(t) - 2x\frac{\mathrm{d}}{\mathrm{d}x}f(t) + 2x^2\frac{\mathrm{d}^2}{\mathrm{d}x}f(t) - \frac{4x^3}{3}\frac{\mathrm{d}^3}{\mathrm{d}x}f(t) \\ &+ 2(f(t) + x\frac{\mathrm{d}}{\mathrm{d}x}f(t) + \frac{x^2}{2}\frac{\mathrm{d}^2}{\mathrm{d}x}f(t) + \frac{x^3}{6}\frac{\mathrm{d}^3}{\mathrm{d}x}f(t)) + O(x^4) \\ =& 3f(t) + 3x^2\frac{\mathrm{d}^2}{\mathrm{d}x}f(t) - x^3\frac{\mathrm{d}^3}{\mathrm{d}x}f(t) + O(x^4) \end{aligned} \tag{D.20}$$

Then using a linear combinations of equations D.19, D.17 and D.20 we get

$$\begin{aligned}
&3(f(t+x)-f(t-x))\\
&+f(t-2x)+2f(t+x)\\
&-3(f(t+x)+f(t-x)) = f(t-2x)+2f(t+x)-6f(t-x)\\
&\qquad = -3f(t)+6x\frac{\mathrm{d}}{\mathrm{d}x}f(t)+O(x^4)\\
&\qquad \frac{\mathrm{d}}{\mathrm{d}x}f(t) = \frac{2f(t+x)+3f(t)-6f(t-x)+f(t-2x)}{6x}+O(x^4)
\end{aligned} \tag{D.21}$$

Using a similar combination for only equations D.17 and D.20

$$\begin{aligned}
&f(t-2x)+2f(t+x)\\
&-3(f(t+x)+f(t-x)) = f(t-2x)-f(t+x)-3f(t-x)\\
&\qquad = -3f(t)-x^3\frac{\mathrm{d}^3}{\mathrm{d}x}f(t)+O(x^4)\\
&\qquad \frac{\mathrm{d}^3}{\mathrm{d}x}f(t) = \frac{f(t+x)+3f(t)+3f(t-x)-f(t-2x)}{x^3}+O(x^4)
\end{aligned} \tag{D.22}$$

If $t$ is considered to be any given time point at which the function $f$ is evaluated at and $\delta$ is the difference between successive time points then $t+\delta$ will convert the continuous function into a discontinuous one, that is $f(t+\delta) \equiv f_{[n+1]}$. As this switch will cause the function to lose accuracy, especially in the points that would lie between $t$ and $t+\delta$, it will be safe to ignore the functions terms with orders higher than four. Taking all of this into account would give for equations D.21, D.18 and D.22:

$$\frac{\mathrm{d}}{\mathrm{d}x}f(t) = \frac{2f(t+\delta)+3f(t)-6f(t-\delta)+f(t-2\delta)}{6\delta} \tag{D.23}$$

$$\frac{\mathrm{d}^2}{\mathrm{d}x}f(t) = \frac{f(t+\delta)-2f(t)+f(t-\delta)}{\delta^2} \tag{D.24}$$

$$\frac{\mathrm{d}^3}{\mathrm{d}x}f(t) = \frac{f(t+\delta)+3f(t)+3f(t-\delta)-f(t-2\delta)}{\delta^3} \tag{D.25}$$

With the base work now done we can take these three equations and apply them as

shown below

$$\begin{aligned}
&\frac{\mathrm{d}^3}{\mathrm{d}x}f(t)+p\frac{\mathrm{d}^2}{\mathrm{d}x}f(t)+q\frac{\mathrm{d}}{\mathrm{d}x}f(t)+rf(t)\\
&\qquad=\frac{f(t+\delta)+3f(t)+3f(t-\delta)-f(t-2\delta)}{\delta^3}\\
&\qquad\quad+\frac{p}{\delta^2}(f(t+\delta)-2f(t)+f(t-\delta))\\
&\qquad\quad+\frac{q}{6\delta}(2f(t+\delta)+3f(t)-6f(t-\delta)+f(t-2\delta))+rf(t)\\
&\qquad=\frac{f(t+\delta)}{\delta^3}+\frac{3f(t)}{\delta^3}+\frac{3f(t-\delta)}{\delta^3}-\frac{f(t-2\delta)}{\delta^3}\\
&\qquad\quad+\frac{pf(t+\delta)}{\delta^2}-\frac{2pf(t)}{\delta^2}+\frac{pf(t-\delta)}{\delta^2}\\
&\qquad\quad+\frac{qf(t+\delta)}{3\delta}+\frac{qf(t)}{2\delta}-\frac{qf(t-\delta)}{\delta}+\frac{qf(t-2\delta)}{6\delta}+rf(t)\\
&\qquad=\left(\frac{1}{\delta^3}+\frac{p}{\delta^2}+\frac{q}{3\delta}\right)f(t+\delta)+\left(\frac{3}{\delta^3}-\frac{2p}{\delta^2}+\frac{q}{2\delta}+r\right)f(t)\\
&\qquad\quad+\left(\frac{3}{\delta^3}+\frac{p}{\delta^2}-\frac{q}{\delta}\right)f(t-\delta)+\left(\frac{q}{6\delta}-\frac{1}{\delta^3}\right)f(t-2\delta)
\end{aligned}\tag{D.26}$$

## D.4 Solving the original model

This is of course only the ICP side of equation D.1. To fully solve for equation D.2 the ABP side of the equation needs to be considered. As this is also a differencing equation the same theory will apply to it but it only needs a second order solution. This second order disparity between the ABP and ICP is a consequence of the solution of the physiological model on which the HMF methodology is based. The solution would then become equation D.27.

$$\begin{aligned}
&i\frac{\mathrm{d}^2}{\mathrm{d}x}g(t)+j\frac{\mathrm{d}}{\mathrm{d}x}g(t)+kg(t)\\
&\qquad=\left(-\frac{2i}{\delta^2}+k\right)g(t)+\left(\frac{i}{\delta^2}-\frac{1}{2}j\right)g(t-\delta)+\left(\frac{i}{\delta^2}+\frac{1}{2}j\right)g(t+\delta)
\end{aligned}\tag{D.27}$$

If equation D.27 is allowed to equal equation D.26 and it is then normalised for $f(t+\delta)$. We get equation D.28

$$\begin{aligned}\left(\frac{1}{\delta^3}+\frac{p}{\delta^2}+\frac{q}{3\delta}\right)f(t+\delta)+\left(\frac{3}{\delta^3}-\frac{2p}{\delta^2}+\frac{q}{2\delta}+r\right)f(t)&\\+\left(\frac{3}{\delta^3}+\frac{p}{\delta^2}-\frac{q}{\delta}\right)f(t-\delta)+\left(\frac{q}{6\delta}-\frac{1}{\delta^3}\right)f(t-2\delta)&\\=\left(-\frac{2i}{\delta^2}+k\right)g(t)+\left(\frac{i}{\delta^2}-\frac{1}{2}j\right)g(t-\delta)&\\+\left(\frac{i}{\delta^2}+\frac{1}{2}j\right)g(t+\delta)&\qquad\text{(D.28)}\end{aligned}$$

$$\begin{aligned}f(t+\delta)+\left(\frac{\frac{3}{\delta^3}-\frac{2p}{\delta^2}+\frac{q}{2\delta}+r}{\frac{1}{\delta^3}+\frac{p}{\delta^2}+\frac{q}{3\delta}}\right)f(t)+\left(\frac{\frac{3}{\delta^3}+\frac{p}{\delta^2}-\frac{q}{\delta}}{\frac{1}{\delta^3}+\frac{p}{\delta^2}+\frac{q}{3\delta}}\right)f(t-\delta)&\\+\left(\frac{\frac{q}{6\delta}-\frac{1}{\delta^3}}{\frac{1}{\delta^3}+\frac{p}{\delta^2}+\frac{q}{3\delta}}\right)f(t-2\delta)&\\=\left(\frac{-\frac{2i}{\delta^2}+k}{\frac{1}{\delta^3}+\frac{p}{\delta^2}+\frac{q}{3\delta}}\right)g(t)+\left(\frac{\frac{i}{\delta^2}-\frac{1}{2}j}{\frac{1}{\delta^3}+\frac{p}{\delta^2}+\frac{q}{3\delta}}\right)g(t-\delta)&\\+\left(\frac{\frac{i}{\delta^2}+\frac{1}{2}j}{\frac{1}{\delta^3}+\frac{p}{\delta^2}+\frac{q}{3\delta}}\right)g(t+\delta)&\qquad\text{(D.29)}\end{aligned}$$

Then equation D.29 gives six basic functions which contain the six unknowns $\{p,q,r,i,j,k\}$.

$$\begin{aligned}a_2&=\frac{\frac{3}{\delta^3}-\frac{2p}{\delta^2}+\frac{q}{2\delta}+r}{\frac{1}{\delta^3}+\frac{p}{\delta^2}+\frac{q}{3\delta}}\\a_1&=\frac{\frac{3}{\delta^3}+\frac{p}{\delta^2}-\frac{q}{\delta}}{\frac{1}{\delta^3}+\frac{p}{\delta^2}+\frac{q}{3\delta}}\\a_0&=\frac{\frac{q}{6\delta}-\frac{1}{\delta^3}}{\frac{1}{\delta^3}+\frac{p}{\delta^2}+\frac{q}{3\delta}}\\b_3&=\frac{\frac{i}{\delta^2}+\frac{1}{2}j}{\frac{1}{\delta^3}+\frac{p}{\delta^2}+\frac{q}{3\delta}}\\b_2&=\frac{\frac{i}{\delta^2}-\frac{1}{2}j}{\frac{1}{\delta^3}+\frac{p}{\delta^2}+\frac{q}{3\delta}}\\b_1&=\frac{-\frac{2i}{\delta^2}+k}{\frac{1}{\delta^3}+\frac{p}{\delta^2}+\frac{q}{3\delta}}\end{aligned}$$

Solving this linear set of equations yields

$$p = \frac{3 + 12a_0 + a_1}{(8a_0 + a_1 - 1)\delta} \tag{D.30}$$

$$q = \frac{12a_0 + 6a_1 - 1}{(8a_0 + a_1 - 1)\delta^2} \tag{D.31}$$

$$r = \frac{54a_0 + 12a_1 + a_2}{(8a_0 + a_1 - 1)\delta^3} \tag{D.32}$$

$$i = \frac{3b_1 + 3b_3}{(8a_0 + a_1 - 1)\delta} \tag{D.33}$$

$$j = \frac{6b_1 + 6_b 3}{(8a_0 + a_1 - 1)\delta^3} \tag{D.34}$$

$$k = \frac{6b_1 + 6b_2 + 6b_3}{(8a_0 + a_1 - 1)\delta^3} \tag{D.35}$$

It is then only a simple task of calculating the roots of the equation D.36

$$\lambda^3 + p\lambda^2 + q\lambda + r = 0 \tag{D.36}$$

These are then the radian modal frequencies which need to be converted via division by $2\pi$ to be come actual frequencies.

## D.5 Conclusion

When the solutions to the differential to differencing linear equations are known, the calculation of the modal frequencies becomes trivial. This technique of transforming between continuous differentials and a point set difference equation has also been shown to extend from second order to third order and will also extend to any order above that as well. This may be a useful tool to study any non linear dynamical system encountered in future autoregulatory models.

# Bibliography

[1] R. Aaslid, K. F. Lindegaard, W. Sorteberg, and H. Nornes. Cerebral autoregulation dynamics in humans. *Stroke*, 20(1):45–52, Jan 1989.

[2] H. Akaike. A new look at the statistical model identification. *IEEE Transactions on Automatic Control*, 19(6):716–723, 1974.

[3] M. E. Andersen. Development of physiologically based pharmacokinetic and physiologically based pharmacodynamic models for applications in toxicology and risk assessment. *Toxicol Lett*, 79(1-3):35–44, Sep 1995.

[4] C. J. Avezaat and J. H. van Eijndhoven. Clinical observations on the relationship between cerebrospinal fluid pulse pressure and intracranial pressure. *Acta Neurochir (Wien)*, 79(1):13–29, 1986.

[5] C. J. Avezaat, J. H. van Eijndhoven, and D. J. Wyper. Cerebrospinal fluid pulse pressure and intracranial volume-pressure relationships. *J Neurol Neurosurg Psychiatry*, 42(8):687–700, Aug 1979.

[6] P. Baldi, S. Brunak, Y. Chauvin, C. A. Andersen, and H. Nielsen. Assessing the accuracy of prediction algorithms for classification: an overview. *Bioinformatics*, 16(5):412–424, May 2000.

[7] Murad Banaji, Ilias Tachtsidis, David Delpy, and Stephen Baigent. A physiological model of cerebral blood flow control. *Math Biosci*, 194(2):125–173, Apr

2005.

[8] James B. Bassingthwaighte, Larry S. Liebovitch, and Bruce J. West. *Fractal Physiology (Methods in Physiology 2 An American Physiological Society Book).* An American Physiological Society Book, illustrated edition edition, October 1994.

[9] G. K. Batchelor. *An Introduction to Fluid Dynamics.* Cambridge University Press, new ed edition, February 2000.

[10] A. A. Birch, M. J. Dirnhuber, R. Hartley-Davies, F. Iannotti, and G. Neil-Dwyer. Assessment of autoregulation by means of periodic changes in blood pressure. *Stroke*, 26(5):834–837, May 1995.

[11] A. P. Blaber, R. L. Bondar, F. Stein, P. T. Dunphy, P. Moradshahi, M. S. Kassam, and R. Freeman. Transfer function analysis of cerebral autoregulation dynamics in autonomic failure patients. *Stroke*, 28(9):1686–1692, Sep 1997.

[12] G. J. Bouma, J. P. Muizelaar, K. Bandoh, and A. Marmarou. Blood pressure and intracranial pressure-volume dynamics in severe head injury: relationship with cerebral blood flow. *J Neurosurg*, 77(1):15–19, Jul 1992.

[13] BrainIT. http://www.brainit.org.

[14] Z Chen, K Hu, P C Ivanov, V Novk, and H E Stanley. Phase synchronization of pressure-flow fluctuations: A measure of cerebral autoregulation dynamics. *Phys. Rev. E*, 73(physics/0508102):031915. 8 p, Aug 2005.

[15] C. M. Chern, T. B. Kuo, W. Y. Sheng, W. J. Wong, Y. O. Luk, L. C. Hsu, and H. H. Hu. Spectral analysis of arterial blood pressure and cerebral blood flow velocity during supine rest and orthostasis. *J Cereb Blood Flow Metab*, 19(10):1136–1141, Oct 1999.

[16] Chang-Ming Chern, Terry B J Kuo, A-Ching Chao, Wen-Yung Sheng, and Han-Hwa Hu. Spectral analysis of cerebrovascular regulation in patients with autonomic dysfunction. *J Chin Med Assoc*, 66(7):393–399, Jul 2003.

[17] Arturo Chieregato, Alessandra Tanfani, Christian Compagnone, Claudia Turrini, Federica Sarpieri, Maurizio Ravaldini, Luigi Targa, and Enrico Fainardi. Global cerebral blood flow and CPP after severe head injury: a xenon-CT study. *Intensive Care Medicine*, 33(5):856–862, May 2007. PMID: 17384928.

[18] S. C. Choi. Sample size in clinical trials with dichotomous endpoints: use of covariables. *J Biopharm Stat*, 8(3):367–375, Jul 1998.

[19] Kenneth S. Cole and Robert H. Cole. Dispersion and absorption in dielectrics i. alternating current characteristics. *The Journal of Chemical Physics*, 9(4):341, 1941.

[20] Jonathan P Coles, Tim D Fryer, Peter G Bradley, Jurgens Nortje, Peter Smielewski, Kenneth Rice, John C Clark, John D Pickard, and David K Menon. Intersubject variability and reproducibility of 15o pet studies. *J Cereb Blood Flow Metab*, 26(1):48–57, Jan 2006.

[21] Alan Crockard, Richard Hayward, and Julian Hoff. *Neurosurgery: The Scientific Basis of Clinical Practice*. Wiley-Blackwell, 3 edition, January 2000.

[22] M. Czosnyka, S. Piechnik, H. K. Richards, P. Kirkpatrick, P. Smielewski, and J. D. Pickard. Contribution of mathematical modelling to the interpretation of bedside tests of cerebrovascular autoregulation. *J Neurol Neurosurg Psychiatry*, 63(6):721–731, Dec 1997.

[23] M. Czosnyka, P. Smielewski, P. Kirkpatrick, R. J. Laing, D. Menon, and J. D. Pickard. Continuous assessment of the cerebral vasomotor reactivity in head injury. *Neurosurgery*, 41(1):11–7; discussion 17–9, Jul 1997.

[24] M. Czosnyka, P. Smielewski, P. Kirkpatrick, D. K. Menon, and J. D. Pickard. Monitoring of cerebral autoregulation in head-injured patients. *Stroke*, 27(10):1829–1834, Oct 1996.

[25] M. Czosnyka, P. Smielewski, S. Piechnik, L. A. Steiner, and J. D. Pickard. Cerebral autoregulation following head injury. *J Neurosurg*, 95(5):756–763, Nov 2001.

[26] M. Daley. Dataset: Expermental model of autoregulation in piglets (n = 6), 2004. Dataset.

[27] Michael L Daley, Massroor Pourcyrous, Shelly D Timmons, and Charles W Lefler. Assessment of cerebrovascular autoregulation: changes of highest modal frequency of cerebrovascular pressure transmission with cerebral perfusion pressure. *Stroke*, 35(8):1952–1956, Aug 2004.

[28] Joseph F Dasta, Trent P McLaughlin, Samir H Mody, and Catherine Tak Piech. Daily cost of an intensive care unit day: the contribution of mechanical ventilation. *Crit Care Med*, 33(6):1266–1271, Jun 2005.

[29] D. L Donoho. De-noising by soft-thresholding. *IEEE Transactions on Information Theory*, 41(3):613–627, May 1995.

[30] DAVID L. DONOHO and JAIN M. JOHNSTONE. Ideal spatial adaptation by wavelet shrinkage. *Biometrika*, 81(3):425 –455, 1994.

[31] Koray S Erer. Adaptive usage of the butterworth digital filter. *J Biomech*, 40(13):2934–2943, 2007.

[32] Erzhen Gao, William L. Young, John Pile-Spellman, Eugene Ornstein, and Qiyuan Ma. Mathematical considerations for modeling cerebral blood flow autoregulation to systemic arterial pressure. *Am J Physiol Heart Circ Physiol*, 274(3):H1023–1031, March 1998.

[33] L. A. Geddes and L. E. Baker. *Principles of Applied Biomedical Instrumentation*. Wiley-Interscience, 3 edition, August 1989.

[34] Benjamin Gompertz. On the nature of the function expressive of the law of human mortality, and on a new mode of determining the value of life contingencies. *Philosophical Transactions of the Royal Society of London*, 115:513–583, 1825. ArticleType: primary_article / Full publication date: 1825 / Copyright 1825 The Royal Society.

[35] Marvin J. Greenberg and John R. Harper. *Algebraic Topology: A First Course*. Westview Press, January 1981.

[36] L Hacein-Bey, R Nour, J Pile-Spellman, R Van Heertum, P D Esser, and W L Young. Adaptive changes of autoregulation in chronic cerebral hypotension with arteriovenous malformations: an acetazolamide-enhanced single-photon emission CT study. *AJNR. American Journal of Neuroradiology*, 16(9):1865–1874, October 1995. PMID: 8693988.

[37] Roman Hlatky, Yu Furuya, Alex B Valadka, Jorge Gonzalez, Ari Chacko, Yasu Mizutani, Charles F Contant, and Claudia S Robertson. Dynamic autoregulatory response after severe head injury. *J Neurosurg*, 97(5):1054–1061, Nov 2002.

[38] D. W. Hosmer, T. Hosmer, S. Le Cessie, and S. Lemeshow. A comparison of goodness-of-fit tests for the logistic regression model. *Stat Med*, 16(9):965–980, May 1997.

[39] Tim Howells, Kristin Elf, Patricia A Jones, Elisabeth Ronne-Engstrm, Ian Piper, Pelle Nilsson, Peter Andrews, and Per Enblad. Pressure reactivity as a guide in the treatment of cerebral perfusion pressure in patients with brain trauma. *J Neurosurg*, 102(2):311–317, Feb 2005.

[40] Chantal W P M Hukkelhoven, Anneke J J Rampen, Andrew I R Maas, Elana

Farace, J Dik F Habbema, Anthony Marmarou, Lawrence F Marshall, Gordon D Murray, and Ewout W Steyerberg. Some prognostic models for traumatic brain injury were not valid. *Journal of Clinical Epidemiology*, 59(2):132–143, February 2006. PMID: 16426948.

[41] Chantal W P M Hukkelhoven, Ewout W Steyerberg, J. Dik F Habbema, Elana Farace, Anthony Marmarou, Gordon D Murray, Lawrence F Marshall, and Andrew I R Maas. Predicting outcome after traumatic brain injury: development and validation of a prognostic score based on admission characteristics. *J Neurotrauma*, 22(10):1025–1039, Oct 2005.

[42] Chantal W P M Hukkelhoven, Ewout W Steyerberg, Anneke J J Rampen, Elana Farace, J. Dik F Habbema, Lawrence F Marshall, Gordon D Murray, and Andrew I R Maas. Patient age and outcome following severe traumatic brain injury: an analysis of 5600 patients. *J Neurosurg*, 99(4):666–673, Oct 2003.

[43] Impedimed. http://www.impedimed.com/products/sfb7-for-body-composition/.

[44] B. Jennett and M. Bond. Assessment of outcome after severe brain damage. *Lancet*, 1(7905):480–484, Mar 1975.

[45] B. Jennett, J. Snoek, M. R. Bond, and N. Brooks. Disability after severe head injury: observations on the use of the glasgow outcome scale. *J Neurol Neurosurg Psychiatry*, 44(4):285–293, Apr 1981.

[46] G. Jorch and N. Jorch. Failure of autoregulation of cerebral blood flow in neonates studied by pulsed doppler ultrasound of the internal carotid artery. *Eur J Pediatr*, 146(5):468–472, Sep 1987.

[47] Z. M. Kadas, W. D. Lakin, J. Yu, and P. L. Penar. A mathematical model of the intracranial system including autoregulation. *Neurol Res*, 19(4):441–450, Aug 1997.

[48] C. J. Kirkness, P. H. Mitchell, R. L. Burr, and D. W. Newell. Cerebral autoregulation and outcome in acute brain injury. *Biol Res Nurs*, 2(3):175–185, Jan 2001.

[49] Richard E. Klabunde. *Cardiovascular Physiology Concepts*. Lippincott Williams & Wilkins, July 2004.

[50] T. B. Kuo, C. M. Chern, W. Y. Sheng, W. J. Wong, and H. H. Hu. Frequency domain analysis of cerebral blood flow velocity and its correlation with arterial blood pressure. *J Cereb Blood Flow Metab*, 18(3):311–318, Mar 1998.

[51] J. M. Lam, J. N. Hsiang, and W. S. Poon. Monitoring of autoregulation using laser doppler flowmetry in patients with head injury. *J Neurosurg*, 86(3):438–445, Mar 1997.

[52] H. S. Levin, C. Boake, J. Song, S. Mccauley, C. Contant, P. Diaz-Marchan, S. Brundage, H. Goodman, and K. J. Kotrla. Validity and sensitivity to change of the extended glasgow outcome scale in mild to moderate traumatic brain injury. *J Neurotrauma*, 18(6):575–584, Jun 2001.

[53] Barbara E Lingwood, Kimble R Dunster, Paul B Colditz, and Leigh C Ward. Noninvasive measurement of cerebral bioimpedance for detection of cerebral edema in the neonatal piglet. *Brain Res*, 945(1):97–105, Jul 2002.

[54] Andrew I R Maas, Anthony Marmarou, Gordon D Murray, Sir Graham M Teasdale, and Ewout W Steyerberg. Prognosis and clinical trial design in traumatic brain injury: the impact study. *J Neurotrauma*, 24(2):232–238, Feb 2007.

[55] Maltron. http://www.maltronint.com/popup%5fpages/bioscan916.htm.

[56] Benoit B. Mandelbrot. *The Fractal Geometry of Nature*. W. H. Freeman, 1 edition, 1983.

[57] MapleSoft. http://www.maplesoft.com/.

[58] A. Marmarou, K. Shulman, and R. M. Rosende. A nonlinear analysis of the cerebrospinal fluid system and intracranial pressure dynamics. *J Neurosurg*, 48(3):332–344, Mar 1978.

[59] Anthony Marmarou, Juan Lu, Isabella Butcher, Gillian S McHugh, Nino A Mushkudiani, Gordon D Murray, Ewout W Steyerberg, and Andrew I R Maas. Impact database of traumatic brain injury: design and description. *J Neurotrauma*, 24(2):239–250, Feb 2007.

[60] Frederic H. Martini and Judi L. Nath. *Fundamentals of Anatomy & Physiology*. Benjamin Cummings, 8th edition, January 2008.

[61] J. P. Muizelaar, H. A. Lutz, and D. P. Becker. Effect of mannitol on icp and cbf and correlation with pressure autoregulation in severely head-injured patients. *J Neurosurg*, 61(4):700–706, Oct 1984.

[62] Sunil Mukhi and N. Mukunda. *Introduction to topology, differential geometry and group theory for physicists*. Wiley Eastern, 1990.

[63] J. F. Muzy, E. Bacry, and A. Arneodo. Wavelets and multifractal formalism for singular signals: Application to turbulence data. *Physical Review Letters*, 67(25):3515, December 1991.

[64] J Nocedal and SJ Wright. *Numerical Optimization*. Berlin, New York: Springer-Verlag, ISBN 978-0-387-30303-1, 2nd edition, 2006.

[65] J. Olesen and M. Leonardi. The burden of brain diseases in europe. *Eur J Neurol*, 10(5):471–477, Sep 2003.

[66] R. B. Panerai. Assessment of cerebral pressure autoregulation in humans–a review of measurement methods. *Physiol Meas*, 19(3):305–338, Aug 1998.

[67] R. B. Panerai, M. Chacon, R. Pereira, and D. H. Evans. Neural network modelling of dynamic cerebral autoregulation: assessment and comparison with established methods. *Med Eng Phys*, 26(1):43–52, Jan 2004.

[68] R. B. Panerai, S. L. Dawson, P. J. Eames, and J. F. Potter. Cerebral blood flow velocity response to induced and spontaneous sudden changes in arterial blood pressure. *Am J Physiol Heart Circ Physiol*, 280(5):H2162–H2174, May 2001.

[69] R. B. Panerai, S. L. Dawson, and J. F. Potter. Linear and nonlinear analysis of human dynamic cerebral autoregulation. *Am J Physiol*, 277(3 Pt 2):H1089–H1099, Sep 1999.

[70] R. B. Panerai, S. T. Deverson, P. Mahony, P. Hayes, and D. H. Evans. Effects of co2 on dynamic cerebral autoregulation measurement. *Physiol Meas*, 20(3):265–275, Aug 1999.

[71] R. B. Panerai, A. W. Kelsall, J. M. Rennie, and D. H. Evans. Cerebral autoregulation dynamics in premature newborns. *Stroke*, 26(1):74–80, Jan 1995.

[72] S. J. Payne and L. Tarassenko. Combined transfer function analysis and modelling of cerebral autoregulation. *Ann Biomed Eng*, 34(5):847–858, May 2006.

[73] I. Piper, G. Citerio, I. Chambers, C. Contant, P. Enblad, H. Fiddes, T. Howells, K. Kiening, P. Nilsson, Y. H. Yau, and BrainI. T. Group. The brainit group: concept and core dataset definition. *Acta Neurochir (Wien)*, 145(8):615–28; discussion 628–9, Aug 2003.

[74] Ian Piper, Iain Chambers, Giuseppe Citerio, Per Enblad, Barbara Gregson, Tim Howells, Karl Kiening, Julia Mattern, Pelle Nilsson, Arminas Ragauskas, Juan Sahuquillo, Rob Donald, Richard Sinnott, Anthony Stell, and BrainI. T. Group. The brain monitoring with information technology (brainit) collaborative network: Ec feasibility study results and future direction. *Acta Neurochir (Wien)*,

152(11):1859–1871, Nov 2010.

[75] R Development Core Team. *R: A language and environment for statistical computing*. R Foundation for Statistical Computing, Vienna, Austria. ISBN 3-900051-07-0, 2008.

[76] Kalyan Raman. A stochastic differential equation analysis of cerebrospinal fluid dynamics. *Fluids Barriers CNS*, 8(1):9, 2011.

[77] Peter Reilly and Ross Bullock. *Head Injury: Pathophysiology and Management*. A Hodder Arnold Publication, 2 edition, July 2005.

[78] M. Reinhard, A. Hetzel, M. Lauk, and C. H. Lcking. Dynamic cerebral autoregulation testing as a diagnostic tool in patients with carotid artery stenosis. *Neurol Res*, 23(1):55–63, Jan 2001.

[79] M. Reinhard, T. Mller, B. Guschlbauer, J. Timmer, and A. Hetzel. Transfer function analysis for clinical evaluation of dynamic cerebral autoregulation–a comparison between spontaneous and respiratory-induced oscillations. *Physiol Meas*, 24(1):27–43, Feb 2003.

[80] F. J. Richards. A flexible growth function for empirical use. *J. Exp. Bot.*, 10(2):290–301, June 1959.

[81] C. J. Van Rijsbergen. *Information Retrieval*. Butterworth-Heinemann, 2nd edition, March 1979.

[82] C. Britton Rorabaugh. *Notes on Digital Signal Processing: Practical Recipes for Design, Analysis and Implementation*. Prentice Hall, 1 edition, November 2010.

[83] Professor Wilson Rugh II. *Nonlinear System Theory: The Volterra / Wiener Approach*. The Johns Hopkins University Press, August 1981.

[84] N. Scafetta, L. Griffin, and B. J. West. Hölder exponent spectra for human gait. *Physica A: Statistical Mechanics and its Applications*, 328(3-4):561–583, October 2003.

[85] M. Shaw and I. R. Piper. Structured search methodology for reviewing autoregulatory modelling literature. In *British Neurosurgical Research Group Proceedings*, 2005.

[86] M. Shaw and I. R. Piper. Improving comparison of models of pressure autoregulation by adaption of existing models to provide normalised outputs. *British Journal of Neurosurgery*, 21(1):73–80, February 2007.

[87] M. Shaw and IR. Piper. Comparison of two models of cerebral pressure autoregulation. *J Neurotrauma*, 23(5):798, 2006.

[88] M. Shibata, S. Einhaus, J. B. Schweitzer, S. Zuckerman, and C. W. Leffler. Cerebral blood flow decreased by adrenergic stimulation of cerebral vessels in anesthetized newborn pigs with traumatic brain injury. *J Neurosurg*, 79(5):696–704, Nov 1993.

[89] Allan J. Sieradski. *An Introduction to Topology & Homotopy*. P W S Publishers, August 1996.

[90] D. F. Signorini, P. J. Andrews, P. A. Jones, J. M. Wardlaw, and J. D. Miller. Predicting survival using simple clinical variables: a case study in traumatic brain injury. *J Neurol Neurosurg Psychiatry*, 66(1):20–25, Jan 1999.

[91] Luzius A Steiner, Jonathan P Coles, Andrew J Johnston, Doris A Chatfield, Peter Smielewski, Tim D Fryer, Franklin I Aigbirhio, John C Clark, John D Pickard, David K Menon, and Marek Czosnyka. Assessment of cerebrovascular autoregulation in head-injured patients: a validation study. *Stroke*, 34(10):2404–2409, Oct 2003.

[92] Ewout W Steyerberg, Nino Mushkudiani, Pablo Perel, Isabella Butcher, Juan Lu, Gillian S McHugh, Gordon D Murray, Anthony Marmarou, Ian Roberts, J. Dik F Habbema, and Andrew I R Maas. Predicting outcome after traumatic brain injury: development and international validation of prognostic scores based on admission characteristics. *PLoS Med*, 5(8):e165; discussion e165, Aug 2008.

[93] Z. R Struzik. Determining local singularity strengths and their spectra with the wavelet transform. *Fractals*, 8(2), January 2000.

[94] T. Teorell. Kinetics of distribution of substances administered to the body. i. the extravascular mode of administration. *Arch. Int. Pharmacodyn.*, 57:205, 1937.

[95] T. Teorell. Kinetics of distribution of substances administered to the body. ii . the extravascular mode of administration. *Arch. Int. Pharmacodyn.*, 57:226, 1937.

[96] F. P. Tiecks, C. Douville, S. Byrd, A. M. Lam, and D. W. Newell. Evaluation of impaired cerebral autoregulation by the valsalva maneuver. *Stroke*, 27(7):1177–1182, Jul 1996.

[97] F. P. Tiecks, A. M. Lam, R. Aaslid, and D. W. Newell. Comparison of static and dynamic cerebral autoregulation measurements. *Stroke*, 26(6):1014–1019, Jun 1995.

[98] Gerard J. Tortora and Bryan H. Derrickson. *Principles of Anatomy and Physiology*. Wiley, 12 edition, April 2008.

[99] Gerardo Tusman, Adriana Scandurra, Stephan H Bhm, Fernando Suarez-Sipmann, and Fernando Clara. Model fitting of volumetric capnograms improves calculations of airway dead space and slope of phase iii. *J Clin Monit Comput*, 23(4):197–206, Aug 2009.

[100] M. Ursino. A mathematical study of human intracranial hydrodynamics. part 1–the cerebrospinal fluid pulse pressure. *Ann Biomed Eng*, 16(4):379–401, 1988.

[101] M. Ursino. A mathematical study of human intracranial hydrodynamics. part 2–simulation of clinical tests. *Ann Biomed Eng*, 16(4):403–416, 1988.

[102] M. Ursino and C. A. Lodi. A simple mathematical model of the interaction between intracranial pressure and cerebral hemodynamics. *J Appl Physiol*, 82(4):1256–1269, Apr 1997.

[103] M. Ursino and C. A. Lodi. Interaction among autoregulation, co2 reactivity, and intracranial pressure: a mathematical model. *Am J Physiol*, 274(5 Pt 2):H1715–H1728, May 1998.

[104] W.N. Venables and B.D. Ripley. *Modern Applied Statistics with S*. Springer, 4th ed. 2002. corr. 2nd printing edition, October 2003.

[105] G. N. Wilkinson and C. E. Rogers. Symbolic description of factorial models for analysis of variance. *Journal of the Royal Statistical Society. Series C (Applied Statistics)*, 22(3):pp. 392–399, 1973.

[106] J. T. Wilson, L. E. Pettigrew, and G. M. Teasdale. Structured interviews for the glasgow outcome scale and the extended glasgow outcome scale: guidelines for their use. *J Neurotrauma*, 15(8):573–585, Aug 1998.

[107] J. T. Wilson, L. E. Pettigrew, and G. M. Teasdale. Emotional and cognitive consequences of head injury in relation to the glasgow outcome scale. *J Neurol Neurosurg Psychiatry*, 69(2):204–209, Aug 2000.

[108] Allyson R Zazulia, Tom O Videen, John C Morris, and William J Powers. Autoregulation of cerebral blood flow to changes in arterial pressure in mild alzheimer's disease. *Journal of Cerebral Blood Flow and Metabolism: Official*

*Journal of the International Society of Cerebral Blood Flow and Metabolism*, 30(11):1883–1889, November 2010. PMID: 20736966.

[109] R. Zhang, J. H. Zuckerman, C. A. Giller, and B. D. Levine. Transfer function analysis of dynamic cerebral autoregulation in humans. *Am J Physiol*, 274(1 Pt 2):H233–H241, Jan 1998.